NASA/CR—2007-214676

Use of Plasma Actuators as a Moving-Wake Generator

Thomas C. Corke, Flint O. Thomas, and Michael J. Klapetzky
University of Notre Dame, Notre Dame, Indiana

January 2007

NASA STI Program . . . in Profile

Since its founding, NASA has been dedicated to the advancement of aeronautics and space science. The NASA Scientific and Technical Information (STI) program plays a key part in helping NASA maintain this important role.

The NASA STI Program operates under the auspices of the Agency Chief Information Officer. It collects, organizes, provides for archiving, and disseminates NASA's STI. The NASA STI program provides access to the NASA Aeronautics and Space Database and its public interface, the NASA Technical Reports Server, thus providing one of the largest collections of aeronautical and space science STI in the world. Results are published in both non-NASA channels and by NASA in the NASA STI Report Series, which includes the following report types:

- TECHNICAL PUBLICATION. Reports of completed research or a major significant phase of research that present the results of NASA programs and include extensive data or theoretical analysis. Includes compilations of significant scientific and technical data and information deemed to be of continuing reference value. NASA counterpart of peer-reviewed formal professional papers but has less stringent limitations on manuscript length and extent of graphic presentations.

- TECHNICAL MEMORANDUM. Scientific and technical findings that are preliminary or of specialized interest, e.g., quick release reports, working papers, and bibliographies that contain minimal annotation. Does not contain extensive analysis.

- CONTRACTOR REPORT. Scientific and technical findings by NASA-sponsored contractors and grantees.

- CONFERENCE PUBLICATION. Collected papers from scientific and technical conferences, symposia, seminars, or other meetings sponsored or cosponsored by NASA.

- SPECIAL PUBLICATION. Scientific, technical, or historical information from NASA programs, projects, and missions, often concerned with subjects having substantial public interest.

- TECHNICAL TRANSLATION. English-language translations of foreign scientific and technical material pertinent to NASA's mission.

Specialized services also include creating custom thesauri, building customized databases, organizing and publishing research results.

For more information about the NASA STI program, see the following:

- Access the NASA STI program home page at *http://www.sti.nasa.gov*

- E-mail your question via the Internet to *help@sti.nasa.gov*

- Fax your question to the NASA STI Help Desk at 301–621–0134

- Telephone the NASA STI Help Desk at 301–621–0390

- Write to:
  NASA Center for AeroSpace Information (CASI)
  7115 Standard Drive
  Hanover, MD 21076–1320

NASA/CR—2007-214676

Use of Plasma Actuators as a Moving-Wake Generator

Thomas C. Corke, Flint O. Thomas, and Michael J. Klapetzky
University of Notre Dame, Notre Dame, Indiana

Prepared under Cooperative Agreement NCC3–935

National Aeronautics and
Space Administration

Glenn Research Center
Cleveland, Ohio 44135

January 2007

Acknowledgments

The authors gratefully acknowledge the valuable help and advice of the technical monitor Dr. David Ashpis and the funding from NASA Glenn Research Center that made this work possible.

This work was sponsored by the Fundamental Aeronautics Program at the NASA Glenn Research Center.

Level of Review: This material has been technically reviewed by NASA technical management.

Available from

NASA Center for Aerospace Information
7115 Standard Drive
Hanover, MD 21076–1320

National Technical Information Service
5285 Port Royal Road
Springfield, VA 22161

Available electronically at http://gltrs.grc.nasa.gov

Executive Summary

The work documented in this report tests the concept of using plasma actuators as a simple and easy way to generate a simulated moving-wake and the disturbances associated with it in turbines. This wake is caused by the blades of the upstream stages of the turbine. Two types of devices, one constructed of arrays of NACA 0018 airfoils, and the one constructed of flat plates were studied. The airfoils or plates were equipped with surface mounted dielectric barrier discharge (DBD) plasma actuators, which were used to generate flow disturbances resembling moving-wakes. CTA hot-wire anemometry and flow visualization using a smoke-wire were used to investigate the wake independence at various spacings and downstream locations. The flat plates were found to produce better results than the airfoils in creating large velocity fluctuations in the free-stream flow. Different dielectric materials, plasma actuator locations, leading edge contours, angles of attack and plate spacings were investigated, some with positive results. The magnitudes of the velocity fluctuations were found to be comparable to existing mechanical moving-wake generators, thus proving the feasibility of using plasma actuators as a moving-wake generator.

CONTENTS

LIST OF FIGURES

LIST OF TABLES

LIST OF SYMBOLS

English symbols

AC	alternating current
CNC	computer numerically controlled
DC	direct current
RMS	root-mean-square of fluctuating velocity
St	Strouhal number
T_{exp}	recored temperature during experiment $[^oF]$
T_{ref}	reference temperature during experiment $[^oF]$
V_{hw}	converted velocity from hot-wire [ft/s]
$V_{hw_{cor}}$	converted velocity from hot-wire [ft/s]
b	wake half-width [in.]
c	chord [in.]
f	frequency [Hz]
or	hot-wire overheat parameter
u_{inf}	free-stream velocity
u_{min}	minimum velocity
u_{inf}	free-stream velocity
x	streamwise coordinate [in.]
y	spanwise coordinate [in.]
z	vertical coordinate [in.]

Greek symbols

α	thermal resistivity
Ω	ohms

CHAPTER 1

INTRODUCTION

1.1 Motivation

Turbines consist of many stages of stators and rotors. Each stage encounters a moving wake that was created by the blade passing of the immediate upstream turbine stage. In addition to the wake, the stage encounters a higher level of stochastic turbulence. The wake passing causes a velocity deficit and a variation of the inlet flow angle to the cascade [15, 5]. Turbine research is continuously being done to improving the thrust capabilities and efficiencies of turbine engines. Some of the areas researchers concentrate on are separation control of the mean flow, heat transfer, and tip flow efficiencies.

Many different test facilities are used for this research. The types of experimental facilities range from full scale rotating test beds, capable of high mass flow rates and shock formation, to stationary linear cascade arrangements of airfoils in low-speed draw-through wind tunnels. Each type of facility has advantages and disadvantages over the others. For example, full scale test apparatuses are good in that they produce realistic test conditions but have limitations in where probes can be placed and are not well suited for flow visualization techniques. Also in these setups, there is little flexibility in the parameters that can be varied which in turn make if difficult or impossible to isolate the different causes and components of the flow field[7]. Also, these test rigs can be rather expensive to build, use, and maintain.

Wind tunnels have an advantage in that they can support a wide range of experimental techniques and test configurations, while also being able to be arranged to focus on only a particular facet of the flow. They are ideally suited for experiments with steady flow conditions because the incoming flow can be conditioned by the use of flow straighteners, mesh screens, and turbulence grids. This is done to first reduce the turbulence levels and then to raise it to a chosen level. In general they are more widely available and less expensive than full test rigs. The choice of the test setup ultimately depends on what part of the flow the researcher is most interested in and the conditions required to produce it.

The importance of the role that the unsteady disturbance plays in the dynamics of the flow through a turbine has been researched by many scientists. Dibelius and Ahlers[5] have shown that the unsteady disturbances, caused by blade passing, has a stabilizing effect on the channel flow between the downstream blades, which is caused by a downshift of the separation zone on the suction side of the blade. Doorly[6] has shown that the upstream wakes can significantly effect the turbine blade surface heat flux. Given this importance, it is necessary to be able to simulate the turbulence so that wind tunnels can be used for research on turbine blades in a controllable environment with more realistic test conditions.

Current mechanical means have proved to be very useful in simulating the upstream turbulence. Some of these setups will be discussed in Section 1.2. Though useful, existing setups have limitations and can be difficult to implement. For example, the test section must be modified to allow access for the moving-wake generating device, typically thin rods or cylinders. The slots that allow the cylinders to pass through have the potential of creating undesired disturbances in the test section. There also has to be some way to support the rotating device without obstructing the view of the researchers or vibrating the test section.

This is the motivation of trying to use plasma actuators as a moving-wake generator. The goal is to use the plasma actuators to simulate a moving wake by contiguously firing a series of actuators mounted on thin airfoils or flat plates spanning the test section. The plasma actuated moving-wake generator should allow much more flexibility than current mechanical means and should be easier to implement. The benefits of this include versatility in that it will be a self contained device that would simply be placed inside the test section, upstream of the airfoils. Because it would be self contained, it could be easily moved to other similar sized test sections without having to perform any modifications. The only hole(s) that might be needed in the test section would be to allow passing of the electrical leads for the plasma actuators out of the tunnel. Depending on the tunnel design, the leads could be passed between two adjoining sections, instead of having to drill a hole. This is much simpler than having to cut slots.

Another benefit is that, there are no moving parts to worry about flying apart or hitting anything. Also, there should be no restriction on how fast the disturbances can be created and propagated across the test section, at least from an electronics point of view, meaning that frequencies used will be limited to stay within real applications. This should be much less than any electronic limitation. An illustration of the concept is shown in Figure 1.1. This figure shows the intended orientation of the series of actuator bearing supports relative to a linear cascade of turbine blades. The vector diagram shows the intended propagated disturbance direction and the resulting apparent flow direction.

Section 1.2 gives a more detailed discussion of some of the other methods used in the past.

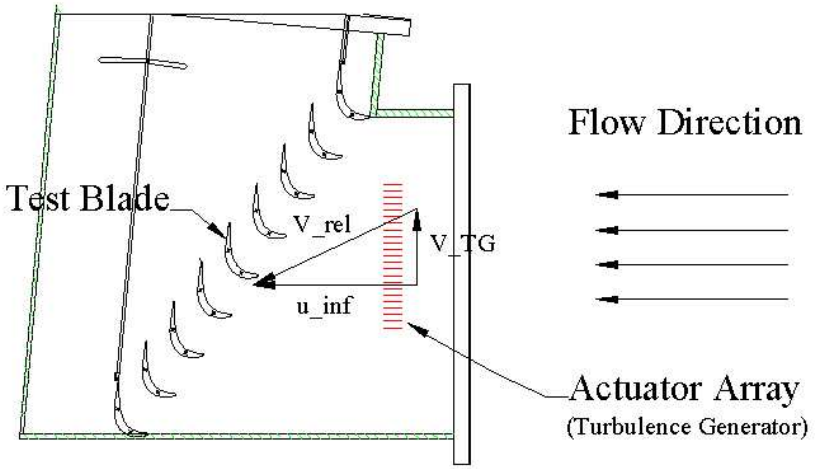

Figure 1.1. Illustration of concept of the moving-wake generator.

1.2 Background

Over the past few decades there have been many different methods used for simulating the upstream turbulence in a turbine or compressor. Some of these methods will be discussed in this section to help illustrate the need for an improved system.

The first experimental setup to be discussed was built by Doorly[6] at the University of Oxford. This setup used a rotating disk with radially mounted cylinders. The apparatus was designed to simulate upstream turbulence for heat transfer studies. The rods were held radially outward by the centrifugal force caused by the rotation of the disk. A figure from the work of Doorly and Oldfield[7] was included to help illustrate the geometry of the setup and is shown in Figure 1.2. As pointed out by Doorly[6], the design allowed for different cylinder diameters and spacings to simulate different turbine conditions, for instance blade passing frequency. His apparatus is versatile in the free-stream velocities that it can be used with. For some of Doorly's research[6], the free-stream wind tunnel velocity was 0.3 Mach. The velocity of the cylinder, relative to the flow, was on the order of 0.95 Mach. Doorly estimates the maximum amplitudes of the periodic incidence change of the inlet angle to be 10 to

15 percent, for the 35.8 mil (0.91 mm) and 67.3 mil (1.71 mm) diameter bars used. The peak turbulence level caused by the wakes, 100 bar diameters downstream in the wake path, was estimated to be 10 to 20 percent. This system maybe limited in lower-speed applications because the bars are held radially outward by the centrifugal force caused by the high rotational velocity of the disk. Another drawback of this design is that the bars are generally not parallel to the leading edges of the turbine blades. Doorly points out that ideally some sort of shuttle of parallel bars, like a ladder, would be fed through the test section just upstream, and parallel to the test blade[6]. This setup, though possible, has limitations in the cylinder velocity due to difficulties in recycling the cylinders for multiple passes. Otherwise, the experiment is limited to a short time based on a single pass of the cylinder apparatus. One team to implement such a setup was Murawski and Vafai[15].

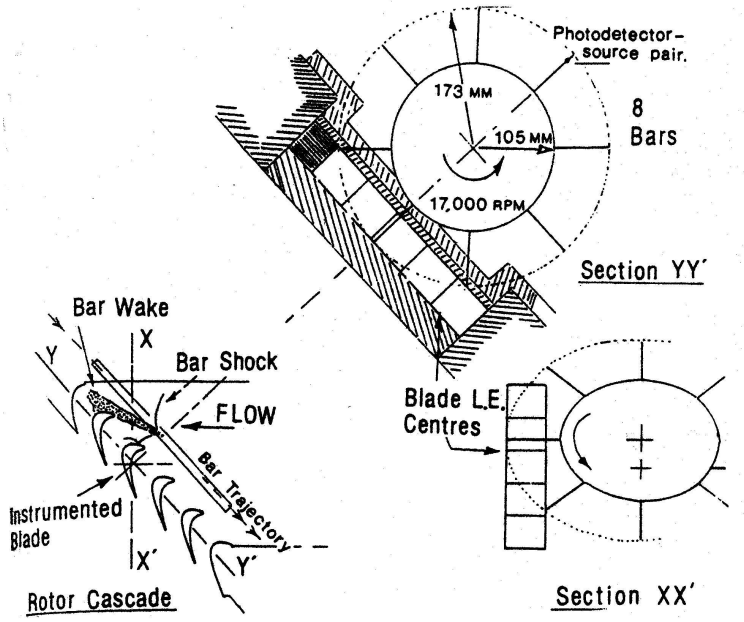

Figure 1.2. Schematic of the rotating bar wake generator used by Doorly. [7]

A 1.64 ft/s (0.5 m/s) to 16.4 ft/s (5 m/s) cylinder velocity could be achieved by Murawski and Vafai[15] with their test setup. They used a moving shuttle positioned in the floor and ceiling of the test section. This setup is shown in Figure 1.3 A. The shuttles could accept 0.374 in. (9.5 mm) diameter cylinders, at a 3.61 in. (91.7 mm) pitch and were positioned such that they located the cylinders 2.5 in. (6.35 cm) upstream of the test blades. Measurements at different, but constant, cylinder velocities showed that increasing the cylinder velocity, and thus the wake velocity, decreases the relative inlet flow angle[15]. According to there results, the inlet flow angle varied from approximately 4^o at the highest cylinder and free stream velocity to 36^o at the lowest conditions. This variation in inlet angle helps to illustrate the importance of using moving-wake generators in turbine research. Based on results of Halstead et al.[12], Murawski and Vafai estimated the wake width at the leading edge of the test blade to be 0.75 in. (1.905 cm) with a total velocity deficit of 25 percent. Also they estimated the peak turbulence intensity in the cylinder wake to be 14 percent with a wake width of 1.22 in. (3.096 cm). Blade passing frequencies from 12 Hz to 52 Hz could be achieved. Murawski and Vafai found that the secondary flow vortex structure is dependent on the the blade passing to axial chord flow frequency. Thus it is important to have flexibility in the rate of the disturbance propagation(generation) or blade passing frequency.

Some researchers have used cylinders mounted on conveyor belts. This cylinder/conveyor setup would then be passed through the test section, upstream of the test cascade, to produce the unsteady disturbance and because of the conveyor system experiments could easily be run for longer periods of time. Schobeiri and Pappu took this type of approach for their research and could achieve cylinder velocities of up to 20 ft/s (6 m/s)[19]. In their case, the cylinders passed close to the leading edge of the blades on the forward pass and then were routed outside of the test section, to

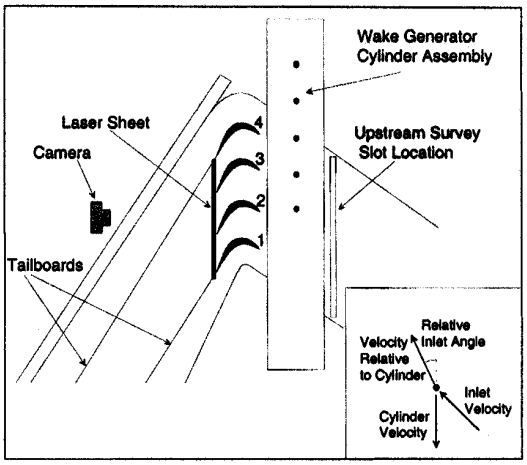

A: Passing shuttle of cylinders.[15]

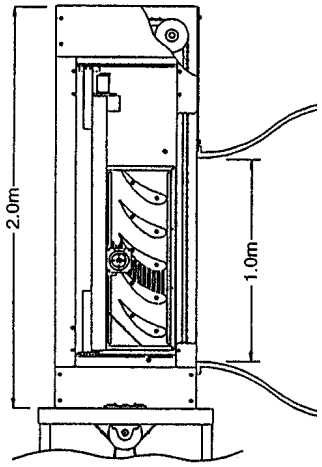

B: Cylinders mounted on belt.[19]

Figure 1.3. Additional examples of cylinder setups.

wrap around the outside of the test section. This setup is shown in Figure 1.3 B.

So far all of the apparatuses mentioned have been similar in that the plain in which the cylinders pass are parallel to the plain of the blade cascade. Work done by Pfeil et al.[16] on laminar to turbulent boundary layer transition caused by unsteady wakes on a flat plate, used what is considered a squirrel cage design as the disturbance generator. For their work, cylinders were mounted near the edge of a 23.6 in. (0.6 m) diameter rotatable disk, parallel to the axis of rotation[16]. The disk was then positioned inside the tunnel, just upstream of the flat plate being investigated. Like the others, this setup had the flexibility of different and controllable cylinder velocities based on the rotational velocity of the disk. The blade passing frequency could also be adjusted by changing the cylinder spacing. In this design, all of the cylinders are in the wind tunnel at all times. Variations in the rotational velocity of the disk alter both the plate Reynolds number and frequency of the velocity fluctuations. Whereas changes in the free-stream velocity alter the magnitude of the velocity fluctuation and the pressure gradient over the plate. There was no data given on the capabilities of the setup in terms of velocity fluctuations at the leading edge of the plate.

In terms of design, the most similar to the proposed plasma actuator design under investigation, was done by Dibelius and Ahlers[5]. Their design consisted of series of 5 individually rotatable flat plates. A figure from their work was included for illustrative purposes[5] and is shown as Figure 1.4. The plates were set at different angles of attack and then coupled together such that the turning of one plate would result in the turning of the other four plates. The angles that the plates were set at, relative to one another, were chosen to maintain a constant projected area as the plates were rotated. This system could achieve perturbation frequencies of up to 60 Hz. In addition to the moving-wake generator, they used a turbulence grid to simulate the stochastic turbulence and raise the turbulence level of the average 32.8 ft/s (10 m/s) free-stream velocity up to 6.5 percent. There was no indication of the magnitude of the unsteady velocity fluctuation possible.

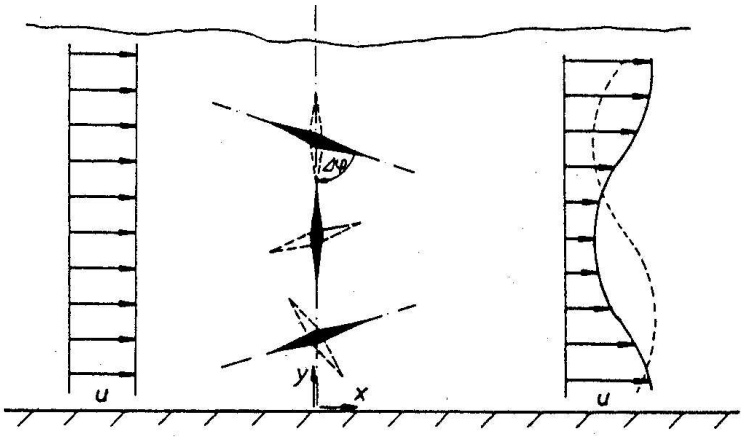

Figure 1.4. Principle of Dibelius and Ahlers wake generator. [5]

The Dibelius and Ahlers setup is similar to the plasma design in that at all times wakes from the generating apparatus exist. For their setup, the plates will generate a narrow wake when parallel to the flow and a larger wake when perpendicular to it. The plasma setup will always have narrow wakes caused by the plates and larger ones caused by the use of the plasma. Both systems rely on the free-stream flow to

carry the unsteady disturbances downstream. Also, both are designed to be oriented perpendicular to the free-stream flow Dibelius and Ahlers showed the ability of their configuration to be able to simulate the unsteady wake flow of a moving blade row by the use of a similarity plot of wake profiles at various downstream positions, with the theoretical Gaussian far wake profile, and a comparison of the magnitudes of the velocity deficits to real test cases.[5]

1.3 Objectives

The main objective is a proof of concept of a simple and efficient method for simulating a moving wake using plasma actuators. This concept could then be used to build an apparatus that will simulate the disturbances caused by the stators or rotors of a turbine over a more versatile and realistic range of velocities and blade passing frequencies than current mechanical means. This moving-wake generator could then be used for turbine research.

To achieve this objective, different types of setups, starting with airfoils will be tested along with different types of plasma actuators. The concept has the design constraint that the apparatus can not be placed any closer than 10 in. (25.4 cm) to the turbine test blade. Thus, it is desired to obtain results comparable to what can be achieved by mechanical means at this distance. The results of these tests will be summarized and where possible, compared to the mechanical models.

Lastly, the pros and cons of the setups will be discussed to pick the most viable direction for the practical application. Once this is done, the results can be used as a phase two starting point to start testing a full array of actuators and actually propagate a disturbance across a test section.

CHAPTER 2

EXPERIMENTAL SETUP

The experiments and results described in this thesis were all performed in the Plasma Flow Control Laboratory at the University of Notre Dame's Hessert Laboratory for Aerospace Research. This chapter discusses the experimental setup that was implemented for this research. One side note, more depth of the setup is given in this chapter than normal because the author of this thesis was responsible for and performed most of the construction required for the facility.

2.1 Wind Tunnel

The wind tunnel used is a new facility that was designed and constructed for the use of the research presented in this thesis. It is a general purpose wind tunnel that will be available for future research and as a test-bed to aid in the setup of experiments that will use other facilities in the Hessert Laboratory which have more stringent scheduling constraints.

Work on this particular facility started the summer of 2000 in the form of drawings[1]. Over that summer, refinements were made to the design, construction materials were located, ordered, and purchased. Due to the construction of another wind tunnel for the Hessert Laboratory, actual construction of this wind tunnel did not start until the autumn of 2001, and was completed in the spring of 2002. The summer of 2002

[1]Original drawings were done by Catherine Corke

was spent instrumenting and setting up the experimental equipment, such as, the traversing system, hot-wire anemometer, and pressure transducer that were needed for the experiments.

Similar to the other wind tunnels at the Hessert Laboratories, the new wind tunnel is an open-return design. But unlike most of the other wind tunnels this tunnel is a pusher-type as opposed to a typical draw-down type. The primary difference is that the fan is the first stage, and thus it is located upstream of the test section. In this configuration, the fan pushes air through the tunnel. The advantage of the pusher design is that the tunnel operates at a pressure higher than that of the surrounding atmosphere. This is beneficial in that if the tunnel should have or develop an air leak, the higher pressure will force the air out of the tunnel. This is preferred because it will tend to thin the boundary layer, reducing the possibility of causing a flow separation. In a typical draw-down tunnel, air leaks tend to thicken the boundary layer and cause unwanted disturbances in the test section.

An 18.25 in. (46.355 cm) diameter Chicago Blower Design 47 adjustable-pitch vane axial fan was chosen based on previous experience with this model and a cost savings as it was bought in conjunction with another Chicago Blower fan. The fan is rated for 6000 CFM (170 CMM), a total pressure of 8.681 inWG (2160 Pa), and has a maximum rotational speed of 3500 RPM. The variable pitch airfoils can be adjusted manually from a pitch setting of -2 to 8 degrees. The fan is driven by an electric 15 HP, 3 phase, Duty Master AC-motor made by Reliance Electric. The fan unit was purchased through Industrial Air Solutions, Inc at a net cost of $4270. This includes the price of the Baldor $\#ID15H210 - E$ variable frequency drive and the shipping costs. The fan is shown in Figure 2.1.

Following the fan comes a circular-to-square transition section. This was made by Troeger & Co. metal fabrication specialists from 16 gauge CRS(cold-rolled-steel)

Figure 2.1. Wind tunnel fan before final assembly.

at a cost of $465. Due to an oversight after a design change, this transition section went from an 18.00 in. (45.72 cm) interior dimension (ID) circle, instead of the 18.25 in. (46.36 cm) ID of the fan, to a 29.50 in. (74.93 cm) ID square. To fix this a 3/4 in. (1.90 cm) thick wood spacer ring was added in the joint between the fan and transition section to blend the two diameters. Silicon caulk was then used to seal the joint.

The next stage in the wind tunnel is the flow conditioning section. This conditioning element consists of a honeycomb section and 5 screens. The honeycomb section was purchased from Plascore Inc. at a cost of $172 plus shipping. It is a 29.5 in. (74.93 cm) square made up of 1/4 in. (6.35 mm) diameter straws that are 5.0 in. (12.7 cm) long. The honeycomb section is used as a flow straightener to remove any swirl from the flow caused by the fan. The screen material used was purchased from Albany International at a cost of $316. The screens are made up of 7.5 mil (0.191 mm) 316 stainless steel wire with a mesh of 28 by 28 wires per 1.0 in. (2.54 cm). This diameter wire and spacing gives a solidity of approximately 38 percent. Based

on the work of Loehrke[14], it was decided that only five screens were needed. Given the wire diameter of the screens, the optimum distance for the turbulence produced by the screens to decay to its minimum level was 9.00 in. (22.7 cm)[14]. To maintain this spacing, five 29.5 in. (74.93 cm) square box sections 9.00 in. (22.7 cm) deep were built out of 3/4 in. (1.905 cm) birch veneered plywood. The box sections can be seen in Figure 1. This figure also shows the 1.0 in. (2.54 cm) equal-leg angle iron flanges which were drilled and bolted to the plywood to provide a means of bolting the sections together. Strips of 1/8 in. (3.175 mm) DURO 60 black commercial neoprene rubber, purchased from the Royal Rubber Company, were glued to the angle iron flanges to seal the screen box sections and to aid in maintaining the tension in the screens.

Figure 2.2. The screen boxes before final assembly.

Prior to assembly of the flow conditioning section of the tunnel, the inside of the screen boxes were painted and the corners were sealed with silicon caulk. For assembly, the screens were stretched on a specially made rack and while under tension, the screen boxes were bolted together around the screens. The screen tensioning rack

was then removed and the screens were trimmed to the size of the screen box sections. One screen was placed in between each screen box, and one between the last screen box and the contraction. The honeycomb was placed in the first screen box and was pushed flat up against the first screen.

The next wind tunnel element in the series is the contraction section. A 5^{th} order polynomial curve was chosen for the contraction shape. A very gradual length-to-diameter ratio of 2:1 was originally chosen however, due to space limitations in the laboratory, this number was reduced to 1:1. The contraction was fabricated in-house and is not symmetric.

The inlet is a 29.5 in. (74.93 cm) ID square that reduces to an 18.0 in. (45.72 cm) ID wide by 12.0 in. (30.48 cm) ID tall rectangular outlet. This gives an area reduction ratio of 4:1. Based on these boundary conditions, the equation for the 5^{th} order polynomial curve for the top and bottom contour can be seen as Equation 2.1 and as Equation 2.2 for the sides.

$$z = -2.350 \times 10^{-6}x^5 + 1.733 \times 10^{-4}x^4 - 3.408 \times 10^{-3}x^3 + 14.75 \qquad (2.1)$$

$$z = -1.544 \times 10^{-6}x^5 + 1.139 \times 10^{-4}x^4 - 2.240 \times 10^{-6}x^3 + 14.75 \qquad (2.2)$$

To set the contraction shape, points calculated using Equations 2.1 and 2.2 were laid out on yellow pine 2x4's. These were cut, sanded, and used for the ribs of the contraction. A picture of the partially completed contraction can be seen in Figure 2.3. In order to lay out the shape of the top, bottom, and side panels, the three dimensional intersection, of the two dimensional 5^{th} order polynomial plains had to be found and transformed into two dimensions. Once this was done, the coordinates could be laid out on a piece 1/4 in. (6.35 mm) thick tempered hardboard, which was used as the paneling. The hardboard intersections, on the outside corners of the contraction, were first screwed together and then reinforced with fiber glass cloth

and resin. As with the screen sections, the inside of the contraction was painted and silicon caulk was used to seal the corners. Angle iron flanges were attached to the ends of the contraction walls for joining the contraction to the neighboring wind tunnel pieces.

Figure 2.3. The contraction during construction.

Just downstream of the contraction comes the test section. It has a rectangular cross section of 18.0 in. (45.72 cm) ID wide by 12.0 in. (30.48 cm) ID high and is 3.0 ft. (91.44 cm) long. It is made from 1/2 in. (12.7 mm) Plexiglas. Again, angle iron was used for the connecting flanges. A 30 in. (76.20 cm) section of the top panel is removable to allow access to the models. This section, along with the following two sections, were all placed on an easily movable wheeled bench. Having all the downstream elements of the wind tunnel mounted on the wheeled bench, and because the test section can easily be detached from the contraction, made access to the models quick and easy either through the front or the top of the test section. Located in the bottom panel of the test section is a 1/2 in (12.7 mm) by 23.5 in. (59.69 cm) slot. The slot starts 9.50 in. (24.13 cm) from the front of the test section

(upstream side) and runs along the center line of the test section. The slot allows access for the stream-wise traverse system.

Following the test section, the flow encounters a 90^o turn. The turn was designed into the tunnel to conserve lab space and to minimize the local air disturbance in the lab. The turn enables the air to be diffused towards the ceiling of the laboratory. The birch veneer plywood was again used for this section along with 26 gauge, galvanized steel, sheet metal to make the turning vanes. The vanes have a gap to cord ratio of 1:3. This was chosen to minimize the drag and thus the pressure drop through the section[3]. A picture of this section can be seen in Figure 2.4.

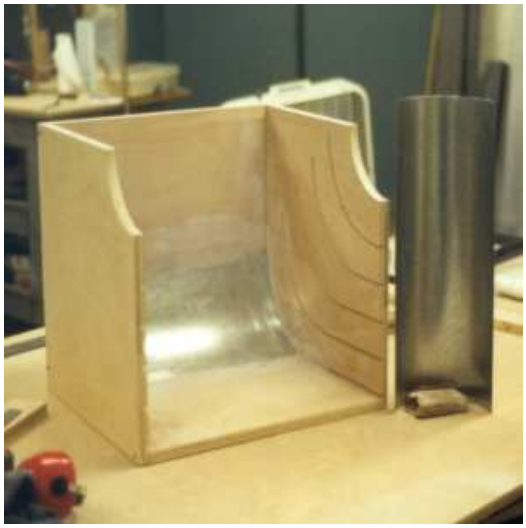

Figure 2.4. Flow turning section during construction.

The final piece of the tunnel is the diffuser. This is also made from birch veneer plywood. As mentioned earlier, this is directed towards the ceiling. It has a total interior angle of 12 degrees to maximize the pressure recovery while trying to avoid separation and thus a stalled diffuser. A picture of the finished tunnel is shown in Figure 2.5.

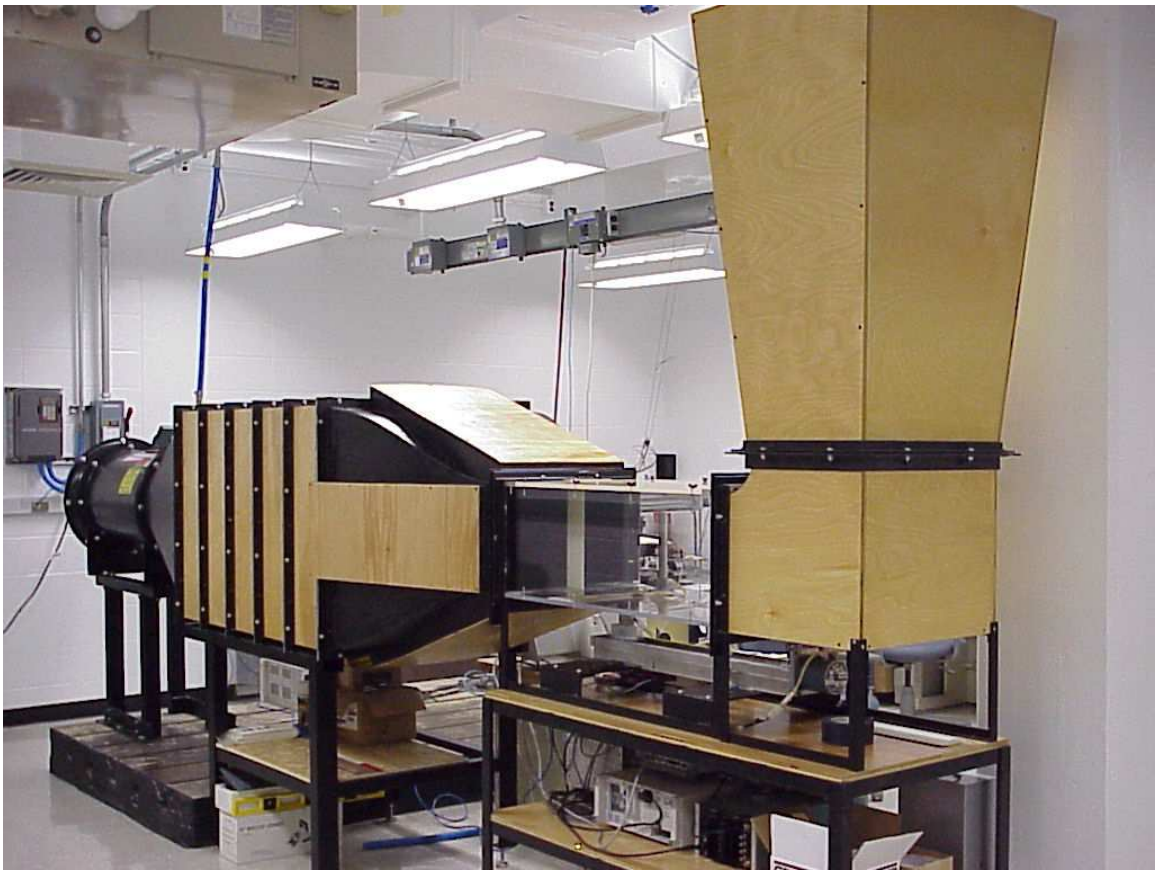

Figure 2.5. The fully completed wind tunnel.

Most of the building materials, such as the plywood, hardboard, screws, bolts, and etc. can be found at most home improvement warehouses. The steel used was purchased in South Bend from Alro Steel and the Plexiglas was purchased from Alro Plastics. The wood costs were approximately $140, the steel costs were approximately $100, and the Plexiglas was also $140. Miscellaneous expenses including a special steel cold-cutting saw blade($270 alone), screws, bolts, paint, and etc. came to about $850 dollars. This brings the grand total for building the tunnel to roughly $6500, excluding labor.

2.2 Traverse

After completion of the physical wind tunnel, two traversing systems were added. These allowed motion in both the streamwise and spanwise direction of any probe(s) added to the traversing pod. The streamwise system is a commercial aluminum traverse whose drive screw has 20 threads per inch. This drive screw is driven by a MO92-FD08 Superior Electric Slo-Sync stepper motor with 200 steps per revolution and drives an aluminum slider. This gives 1000 steps per inch (2.54 cm) of linear motion. A Velmex controller, which receives the signals sent from the computer, is used to control the motor and perform the desired motion. The stream-wise travel is 20 inches (50.8 cm). The Velmex controller can also be used manually to position the aluminum slider.

Mounted to the aluminum slider of the streamwise traverse is the spanwise traverse system. This traverse was designed and built by the author of this thesis. It uses a Micro Mo Electronics, Inc AM1524-V-6-35-07 micro-motor with a 158 housing parameter and a built-in 76:1 gear box. The stepper motor itself has 24 steps per revolution, but with the 76:1 gearbox, this provides 1824 steps per revolution. To change this rotary motion into a linear spanwise motion for the probe, a standard

US rack and pinion gear system was used. The rack was chosen to have a pitch of 48. The drive gear, that is the gear attached to the micro-motor, has a pitch diameter of 0.5625 in. (1.429 cm). This diameter was chosen to be close to that of the micro-motor in order to minimize the size of the traversing pod, see Figure 2.6. This, along with the 48 pitch, means that there are 27 teeth on the drive gear with a pitch circumference of 1.767 in. (4.488 cm). Because the drive gear was chosen to be close to the size of the motor, an idler gear was needed to transfer the motion of the drive gear to the rack. The idler gear has a pitch diameter of 0.3750 in. (9.525 mm) which results in 18 teeth and a pitch circumference of 1.178 in. (2.992 cm). All of this combines to give 1032 steps per inch (2.54 cm). The spanwise traverse allows for 16 inches (40.64 cm) of motion. The traversing pod is attached to a Nippon Bearing Co.(NB Corporation) SEBS-9A1-435 linear slide. The parts alone for this traverse, excluding the micro-motor, totaled $250 dollars.

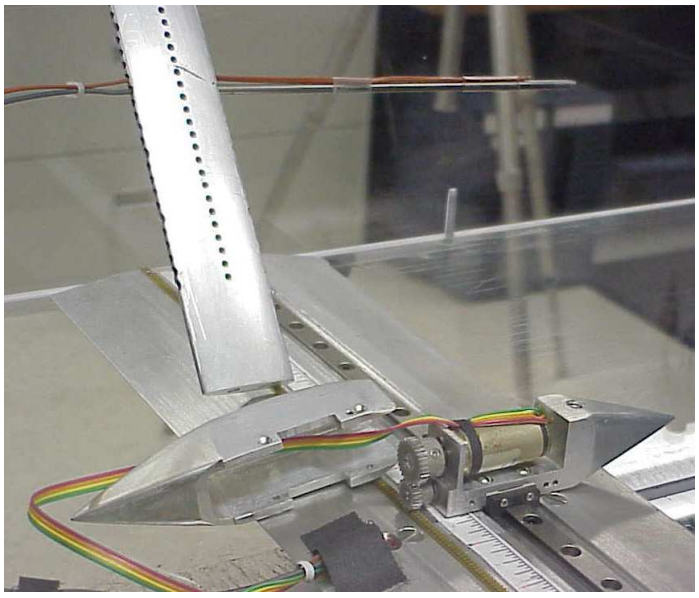

Figure 2.6. The spanwise traversing system.

2.3 Data Acquisition

An in-house fabricated computer running Linux was used for data acquisition and control. It utilizes an ECS L7S7A2 (sis 746 chip-set) mother board with an AMD Athlon XP 2.8 GHz 333 processor with 512MB RAM. For the Analog-to-Digital conversion, a PowerDAQ II PCI simultaneous-sampling multi-function PD2-MFS-4-1M/12 board was used. This is a 12 bit board that gives a maximum resolution of 2.44 mV/bit. Three of the four available channels were used in the single ended input configuration, and all other analog inputs on the STP-9616 connector board where grounded.

The single-ended acquisition mode is set using the software of the data acquisition programs. Using Linux, the programs[2], written in the C programming language, were modified to control the stepper motors for the traverses and to acquire the signals from the hot-wire, Pitot probe, and thermocouple.

A Dantec CTA(Constant-Temperature-Anemometer) 56C17 Bridge was used with a Dantec a CTA 56C01 Main Frame as the hot-wire anemometer. This sent the voltage fluctuations from the bridge, caused by the heat transfer from the hot-wire, first to a Hewlett Packard(now Agilent) 34401A multi-meter, then to a voltage-gain circuit, and lastly to the Power-DAQ card.

Two circuits built by the author of this thesis were used in the data-acquisition setup. The first was a gain circuit for the hot-wire to better utilize the full range of AD board. The circuit used four LM741 operational amplifiers. One op-amp was placed on both ends of the circuit to serve as unity-gain followers, in order to isolate the circuit from the other electronics. The first of the remaining two op-amps, along with resistors, were used to offset the DC signal component such that the signal from the

[2]The original programs were written by Junhui Huang and used the PowerDAQ libraries

hot-wire, with the wind tunnel off, was close to the minimum range of the AD board, which was -5.0 V. The last op-amp was used to gain the signal. The combination of resistors were chosen to give a gain of 6.33, the highest possible signal gain for upper range of the AD board, which is 5.0 V, at the maximum wind velocity used during the calibration of the hot-wire. A schematic of the circuit can be seen in Figure 2.7.

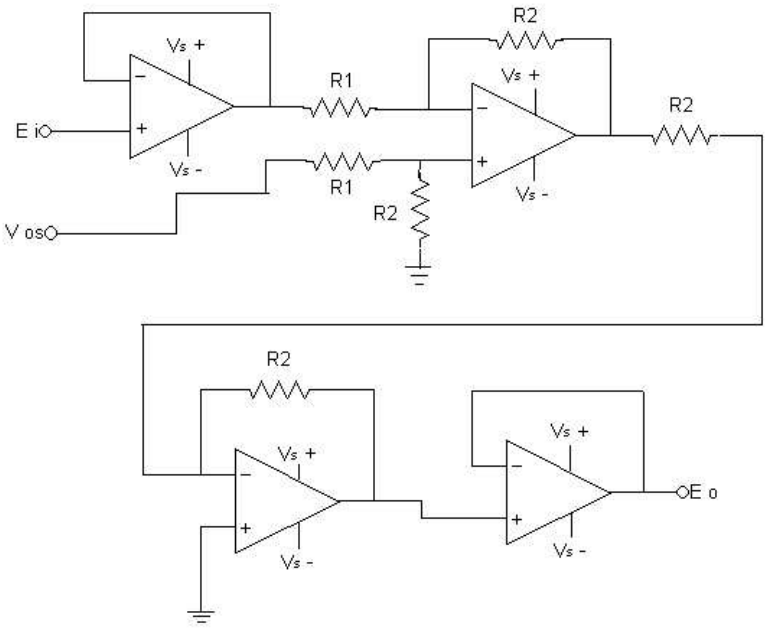

Figure 2.7. Circuit diagram of the gain circuit used.

The second circuit used served as a simple RC low-pass filter. The cut off frequency for the filter is controlled by the choice of resistor and capacitor. This frequency was chosen to be 135 KHz, using an 11.75 KΩ resistor and a 0.10 μF capacitor. An illustration of this circuit is shown in Figure 2.8.

The three signals were passed through the low-pass filter and acquired through three single-ended channels of the AD board. The signals were all referenced to the same instrument ground.

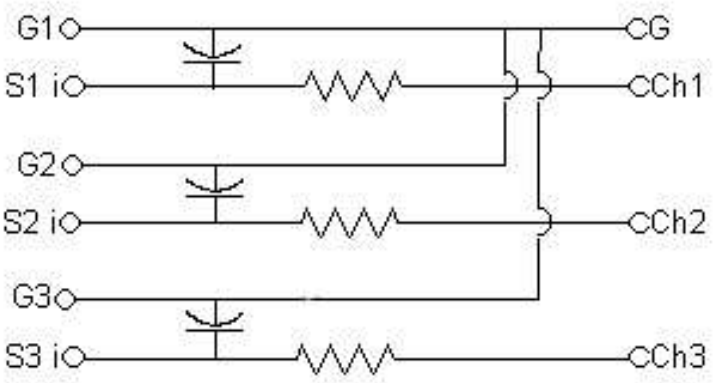

Figure 2.8. Circuit diagram of the filter circuit used.

A Validyne DP103-18 differential pressure transducer was used with a Validyne CD23 digital transducer indicator for the pressure measurements. The diaphragm used in the pressure transducer was a #18 and is rated for a maximum differential pressure of 2.22 inH_2O (550 Pa). This was chosen to cover the full range of the wind tunnel, which was a maximum wind velocity of approximately 85 ft/s (26 m/s). A Pitot static tube with a 0.120 in. (3.05 mm) outside diameter was connected to the differential pressure transducer thus allowing the dynamic pressure to be measured directly. A Dwyer 1430 Micro-manometer was used for the calibration of the pressure transducer. Once this was done, the tunnel velocity could be calculated, based on the voltage recorded by the computer from the pressure transducer.

It was discovered early on that the AC-motor that drives the fan for the wind tunnel generates enough heat to affect the readings of the hot-wire. To investigate and correct for this effect, an Omega 5TC-TT-T-24-72 type T thermocouple made from 20 mil (0.508 mm) diameter copper and constantan wire was used. Including the Teflon insulation on both the wires, the probe was elliptical in shape with major axis of 95 mil (2.413 mm) and a minor axis of 55 mil (1.397 mm). A DP116-TF2

miniature panel thermometer was used to relate the reading of the thermocouple to a temperature. This combination had a range of $\pm 200^o F$. The thermocouple was placed close to the hot-wire to record the local temperature. With the local temperature known, the hot-wire voltages could be corrected. The equation for the temperature correction that was used is presented as Equation 2.3.

$$v_{hw_{cor}} = \frac{1}{\sqrt{1 - \frac{\alpha}{or-1}(T_{exp} - T_{ref})}} v_{hw} \tag{2.3}$$

To summarize and better illustrate the complete setup, a flow chart is presented in Figure 2.9. This shows a basic sketch of the test section with the instrumentation.

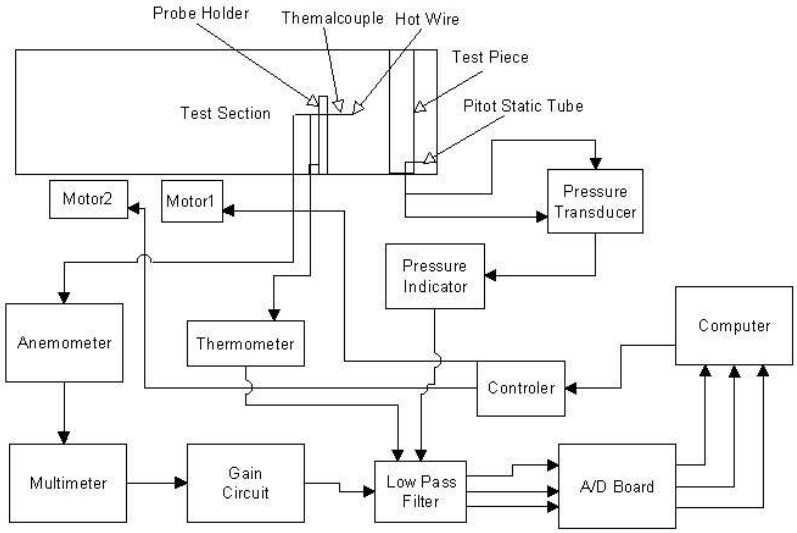

Figure 2.9. Flow chart of data acquisition setup.

During the experiments, only mean and RMS voltage data were of interest to the investigators. It was therefore decided to take longer sampling periods at lower sampling rates. A sampling rate of 2.0 KHz was chosen, and only 6 seconds of contiguous data was taken, although longer sampling periods would have been better. However, due to the large number spanwise locations tested, which ranged from 60 to 90 points

per wake profile, and the 2 second settling time, chosen to allow the flow and probe to adjust to the new probe location, longer sampling periods were not practical. For example, each additional second added 1 to 1.5 minutes to each profile measurement. This meant that over a full set of profile measurements, 12 to 18 minutes were added to the existing 1.8 to 2.6 hours needed to complete the measurements. Another factor that influenced the run times was the actuator longevity, which was a major issue in the early stages of the work. The plasma Kapton actuators had a short and finite life span.

2.4 Plasma Actuators

This section contains a brief description of how the plasma actuator system works, including the basics of the dynamics of the plasma actuator itself. For a more detailed explanation of the electronic system and the dynamics of the plasma actuator investigate the work of Thomas Corke and Post[17, 18].

Two separate systems were used over the course of this work. The first system was developed by Thomas Corke at the Illinois Institute of Technology. The second system used a PA04A high power linear operational amplifier in an EK04 evaluation kit available through APEX Microtechnology[3]. Though the designs of the systems are different, the principle is the same.

The plasma actuator system is basically nothing more than an AC-amplifier. It takes a low voltage AC signal from a function generator and amplifies it. For the two systems used the signal could be gained up to approximately 95 volts for Corke's system and at most approximately 75 volts for the Apex system. Any type of AC-signal could be sent through the amplifiers including sinusoidal, saw-tooth, and triangular waves. For the experiments performed in this thesis, a 5.0 KHz triangle wave was

[3]www.apexmicrotech.com

used. Potentiometers controlled the amount of the gain, which was monitored with an oscilloscope. After the signal leaves the first gain circuit, it is sent to a transformer to be gained further. Some initial experiments used transformers with a winding ratio of 30:1, but most of the experiments used transformers that had 140 windings. This means a gain of 140, which for translates to an AC-signal up to 13.3 KVpp for the first system. The plasma systems were comprised of multiple op-amps and transformers so that the AC-signals could be supplied to multiple electrodes.

This signal was then sent to the plasma actuator. An illustration of one is shown in Figure 2.10. Basically, it is two electrodes, that slightly overlap, separated by a dielectric material. As with any circuit, the voltage potential at any given point depends on where that point is referenced to. One electrode of the actuator can either be grounded or attached to another channel of the plasma system. If one electrode is grounded, the highest voltage potential across the actuator is half of the voltage supplied to the opposite electrode. This is because the AC-signal has no DC component and the furthest away from zero(ground) the signal gets is half of its peak-to-peak amplitude. If however, the opposite electrode is attached to a second channel from the plasma system, then the full potential, in this case up to 13.3 KV, can be achieved. This is because the second channel can be sent the same AC-signal but 180^o out of phase. This way, the signals reference each and the difference between them is the voltage potential across the actuator. The two channel setup was used for most of the experiments presented. Unfortunately, the power of the plasma actuator could not be obtained because the voltage potential across the actuator and the current through it could not be directly measured. However, the voltage potential across the actuator could be estimated by multiplying the voltage sent to the transformers by the number of windings of the transformer.

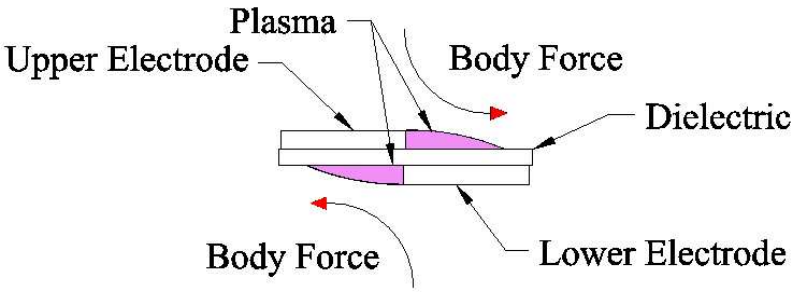

Figure 2.10. Illustration of a plasma actuator.

Also shown in Figure 2.10 is an indication of the direction of the body force that the plasma actuator produces. Some additional comments and figures will be presented during the discussion of the test setups in Section 2.5.

2.5 Test and Actuator Configurations

Due to the large number of experimental configurations tested and variations of each, the configurations were broken down into three main areas. These areas were designated as Airfoils, Flat Plates and Uniform Flat Plates and will be discussed in their respective chapters. With in these three main areas, there are 6 basic configurations. These will be denoted by configurations 1-6 and will be discussed in this section. The configuration designation and a short description of the respective setup is summarized at the end of this section in Table 2.1.

Other than the flow visualization, all of the experiments that were conducted involved wake profiles at different downstream locations of the test piece(s). Two main experiments were performed in the wakes of the different configurations. The first is referred to as stream profiles and the second is referred to as power profiles. Initially there were two sets of free-stream conditions being used as a check of the diversity of the moving-wake generator in terms of its application. Normally the wind

tunnels free-stream velocity would be set based on a desired Reynolds number for the test piece under investigation. Initially this was the case here as well but because the idea behind the moving-wake generator is to use it as an experimental tool in other research applications, the free-stream velocities were of more importance then the Reynolds number of the airfoil(s) or flat plate(s) being tested. The free-stream velocity used in the different stages of this work will be discussed in their respective configuration setups.

The stream profiles were the first experiments conducted. These consisted of wake profiles at the following cord lengths downstream of the trailing edge of the test piece: 0.5, 1, 2, 3, 4 and 5. They are called stream profiles because the main variable, other than having the actuator 'off' or 'on', is the streamwise position. When the effect of the actuator was tested, a wake profile at a particular downstream location was first conducted with the actuator 'off', with the probe transversing towards one side of the test section. Immediately following this profile, the actuator would be turned 'on' and another wake profile would be performed with the probe now traversing in the opposite direction. This would return the probe to the original starting position. Following this, the streamwise traverse would be manually adjusted to position the probe at the next downstream location.

What is being referred to as power profiles were all conducted 5 cord lengths downstream of the trailing edge of the test piece. These tests were an investigation into the effects of varying the voltage potential across the actuator, which is equivalent to varying the power of the actuator and is where the designation 'power profile' came from. In these cases, the hot-wire probe would be moved in one direction for one dial setting and then be moved in the opposite direction for the next dial setting. In all the cases, the voltage potential always started at zero and was increased. These tests were interchanged with the stream profiles for comparison.

In addition to these, a few experiments were done to investigate the position dependence of the flat plates. These cases were conducted in a similar manner to the power profiles, but instead of changing the voltage potential, the relative position of the plates was changed. The main purpose of doing this was to chose the plate arrangement that gave the most uniform wakes in terms of width and velocity deficit.

2.5.1 Configuration 1

The first configuration to be discussed is Configuration 1. The experiments performed under this configuration used one or two NACA_0018 airfoil(s) with a 3.1 in. (7.87 cm) chord, with two mounting holes, 2 in. (5.08 cm) apart and centered along the mean chord line in either end of the airfoil. Holding the airfoil were two, one on each side, 95 mil. (2.41 mm) thick aluminum plates that could be attached with screws to the test section to ensure consistent placement of the airfoil(s). One of these plates can be seen in the top of Figure 2.11[4]. Two series of holes, 2.0 in. (5.08 cm) apart from one another, were made in the aluminum plates. The holes had a spacing of 0.5 in. (1.27 cm) with the center hole on the center line of the test section when the plates were attached to the test section. The series of holes were offset from the front edge of the plate such that when the airfoil(s) was attached, it's leading edge was 0.5 in. (1.27 cm) downstream of the beginning edge of the test section. The series of holes allowed for the space between two airfoils to varied in 0.50 in. (cm) increments. One additional set of holes was added 0.25 in. (cm) from the center hole to allow for 0.25 in. (cm) space increase to the 0.50 in. (cm) space increments.

In the case when only one airfoil was tested, it was oriented vertically along the

[4]Also shown in this figure is a clear Plexiglas replacement plate, used for the flow visualization, and different mounting brackets, used for the flat plates, which will be discussed in later sections concerning the flat plates.

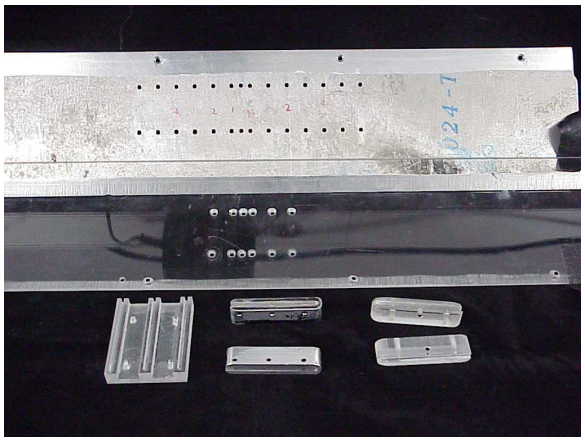

Figure 2.11. The various test specimen holders used.

centerline of the test section. For the two-airfoil cases, when possible, the airfoils were positioned such that the center line of the two airfoil combination was in line with the center line of the test section. For any case where the space between the airfoils was not an integer multiple of 1.0 in. (2.54 cm), the center line of the two airfoil combination was positioned as close to the center line of the test section as possible. The plate mounting holes were staggered such that the airfoil(s) were oriented at zero angle of attack. Examples of the single and dual airfoil setup can be seen in Figure 2.12. The experimental results are presented in Chapter 3.

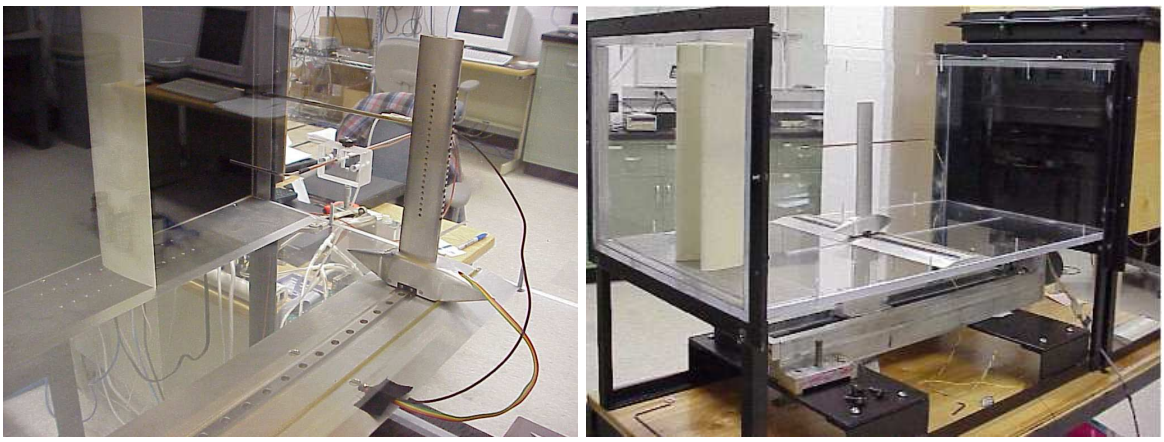

Single Airfoil Dual Airfoils

Figure 2.12. Example of single and dual airfoil setups.

As mentioned before, to investigate the utility of the moving-wake generator being developed, two free-stream velocities were chosen for the experiments. These were chosen to be within the range of Reynolds numbers that corresponded to the turbine research that was being done by another experimentalist[5]. In that research, plasma actuators are being used to control flow separation in a cascade of Pratt & Whitney Pack-B low pressure turbine blades. Blades with an axial of chord 6.28 in. (15.95 cm) are being tested. The first free-stream velocity was chosen to be 31 ft/s (9.45 m/s). This corresponds to a Reynolds number of 100K for the turbine blade in air at typical atmospheric conditions which were 29.5 in-Hg (749.3 mm-Hg) and 70^oF (21^oC). The second velocity used was 54 ft/s (16.5 m/s) which corresponds to a Reynolds number of 175K for the Pack-B blades.

Four cases, other than the non-actuated case, were investigated. These cases had the same actuator design but different actuator placements. The active edge of the actuator was placed in one of the following locations: at the leading edge, just before the maximum thickness point, at the point of maximum thickness, and just after the point of maximum thickness. A picture of the airfoil with an actuator placed at the leading edge can be seen in Figure 2.13, and the results for this configuration are presented in Chapter 3. Also shown in Figure 2.13 is an inverse mold casting of the airfoil. This was used as a template for positioning the actuators.

2.5.2 Configuration 2

After the investigations using Configuration 1, flat plates were tested. These tests encompass Configurations 2-6. Shown in Figure 2.14 is an overhead view of this experimental setup. This setup used the same mounting plates as the airfoils, but

[5]PhD work of Junhui Huang, being performed in the Hessert Laboratories at the University of Notre Dame.

Figure 2.13. Airfoil with Kapton actuator at leading edge and template.

with the addition of some mounting brackets, because the flat plates were too thin to accept the screws. The plates could be set at angles of attack by removing the rear mounting screw and pivoting the mounting bracket around the front screw. This is indicated by the upper most plate in Figure 2.14. The plate angle was set using a protractor. This was used, referencing the front edge of the aluminum mounting plate, to set the angle of the mounting brackets.

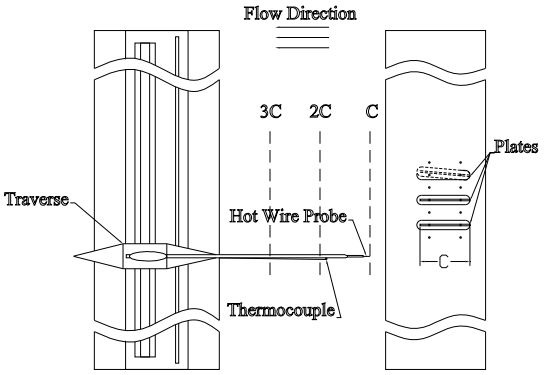

Figure 2.14. A sketch of an overhead view of the experimental test setup.

Configuration 2 used two flat plates with with a 2.0 in. (5.08 cm)chord and the Kapton type actuator. The actuator was positioned such that the flow induced by

the plasma would cause the oncoming flow to separate from the leading edge of the plate on the side closest to the neighboring plate. Due to problems keeping the copper tape attached to the surface at the leading edge while taking the wake profiles, two different plates were tried. The first had a thickness of 92 mil (2.34 mm) and the second was a slightly thicker plate, with a thickness of 132 mil (3.35 mm). The idea was that the thicker plate would provide a larger radius of curvature at the leading edge. This would reduce the bending of the Kapton tape thus making it easier for the adhesive to maintain attachment of the Kapton. A sketch showing the flat plate can be seen in Figure 2.15.

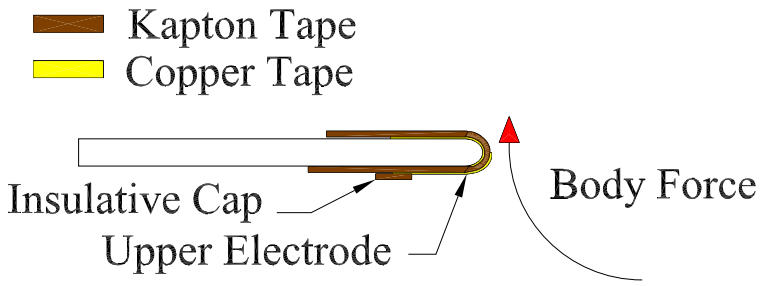

Figure 2.15. Configuration 2, Kapton actuator flat plate setup.

The results for this configuration are presented in Section 4.1. In Section 4.1.2, when the plates are set at an angle of attack, the direction the plates are rotated is counter clockwise in Figure 2.15. This would mean a positive angle of attack for a flow approaching from the right.

2.5.3 Configuration 3

The biggest difference between Configurations 2 and 3 was the type of actuator used. The third configuration was the first to use the printed circuit board type of actuator. This actuator was made using a LPKF computer numerically controlled

(CNC) milling machine. The LPKF milling machine is prototyping machine designed to manufacture prototype circuit boards. For these cases, the plate orientation was such that the induced velocity was in the channel between the two adjacent plates and directed upstream. The aim was to separate the flow from the plate to reduce or block the flow between the plates, essentially creating a larger body.

During these tests, two different actuator electrode setups were investigated. The first setup had an 8.00 in. (20.32 cm) lower electrode and the second had a 4.75 in. (12.07 cm) lower electrode. Both of these lengths had an upper and lower electrode width of 1.0 in. (2.54 cm) and the upper electrodes were 0.25 in. (6.35 mm) longer than the lower electrode. This enabled both sides of the upper electrode to extend 0.125 in. (3.18 mm) past the edges of the lower electrode. Also, the upper electrode overlapped the lower by 62 mil (1.59 mm) and the active actuator edge of the actuator was moved 1.0 in. (2.54 cm) from the leading edge to the mid-chord of the plate.

One other difference between this configuration and Configuration 2 is the leading edge contour. Because what is considered the lower electrode extended to the leading edge of the plate, the leading edge was shaped to a 1/4 ellipse. The leading edge is shown in Figure 2.16. It can be seen that the direction of the velocity component induced by the plasma actuator is upstream on one side of the plate and downstream on the other. In the case of the Kapton actuators, the second component of forcing is suppressed by being pressed against the airfoil or plate and being covered by Kapton.

The results for this configuration are presented in Section 4.2. It is important to note here that the results presented in that section refer to negative angles of attack. As with Configuration 2, this angle is referenced to a flow approaching from the right as shown in Figure 2.16. This is important due to the asymmetric leading edge. At the negative angle the flow is less likely to separate than if the plates were at positive angles relative to the flow.

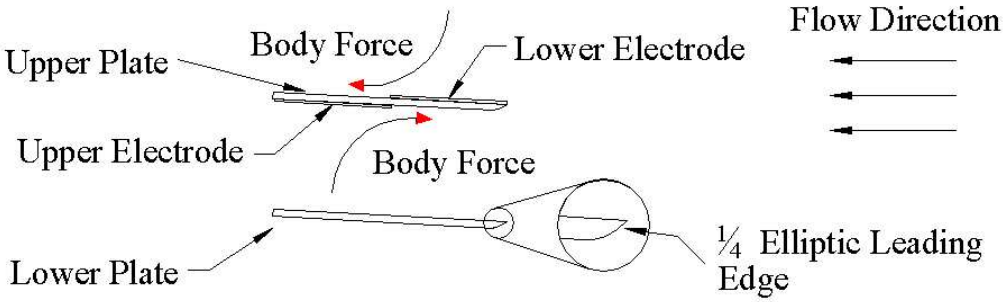

Figure 2.16. Configuration 3, setup for flat plate with PC type actuator.

2.5.4 Configuration 4

The third plate added to Configuration 3 to make Configuration 4 did not have the same leading edge contour as the other two, and was slightly thicker. Close inspection of the leading edges of the plates in Figure 2.17 shows the difference. The leading edges of the top two plates are not symmetrical. They have the previously mentioned 1/4 ellipse contour sloping away from the lower plasma electrode. The bottom plate in Figure 2.17 had a rounded leading edge. The experimental results for Configurations 2-4 are presented in Chapter 4.

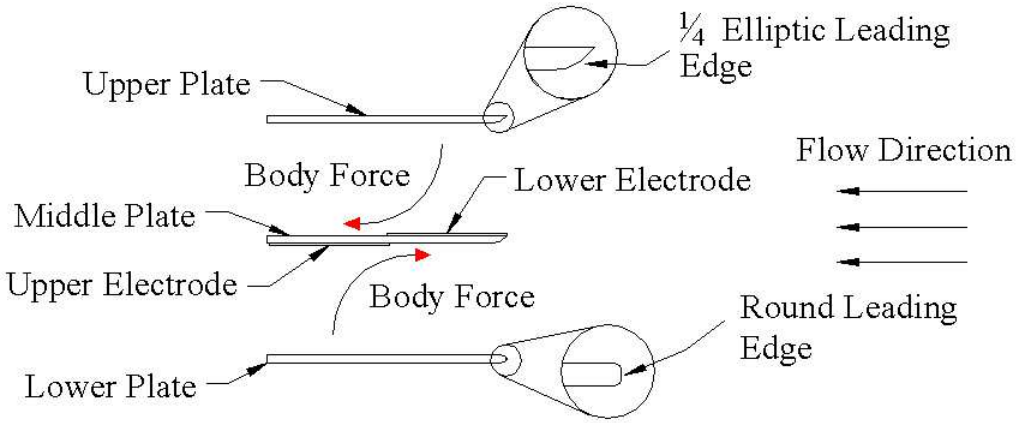

Figure 2.17. Configuration 4, setup for flat plate with PC type actuator.

2.5.5 Configuration 5

The 5^{th} configuration was basically a repeat of Configuration 4, but with uniform plates manufactured on the LPKF CNC milling machine. A 12 in. x 12 in. x 1/8 in. (30.38 cm x 30.48 cm x 3.18 mm), double sided copper-clad piece of FR-4 circuit board material was secured to the milling bed so that the 3 plates could be machined simultaneously. The copper was first machined off one side, leaving the electrode and a small extension for a wire lead, and then the board was flipped. After flipping the PC-board, the opposite electrode could be machined, and then the LPKF machine would cut out the plates. The leading edges of the plate were then lightly hand sanded to round the corners. This setup is shown in Figure 2.18.

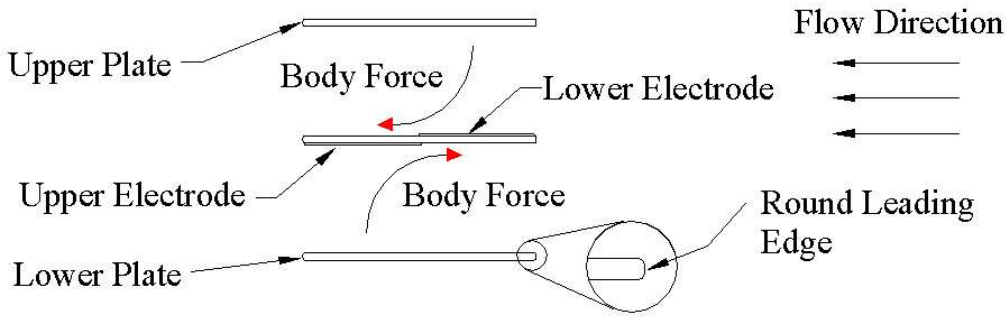

Figure 2.18. Configuration 5, setup for flat plate with PC type actuator.

Also new to Configurations 5 and 6 was a set of mounting brackets for the flat plates. These brackets, one of which is shown in the lower left of Figure 2.11, were machined on an end mill out of a solid piece of Plexiglas. They were designed to have the slots for the plates 3 mil (0.076 mm) larger than the thickness of the plates. This was done to ensure consistency and straightness of the placement of the plates with respect to each other.

2.5.6 Configuration 6

The 6^{th} and final configuration used three plates, but with a sandwiched electrode configuration. These plates were also made using the prototyping machine, so that they were as uniform as possible . The actuator configuration of these plates consisted of a lower electrode sandwiched between two upper electrodes. These were fabricated by machining 62.5 mil (1.588 mm) PC boards that were copper clad on one side. A 1.00 in. (2.54 cm) wide piece of copper foil tape was applied to the non-copper-clad side of one the boards. The copper tape was offset 31 mil (0.794 mm) from the leading edge. This piece of copper tape acted as the lower electrode. The two PC-boards were then epoxied together using 6 minute epoxy such that the electrodes on the copper clad side were aligned. The leading edges were then hand sanded to round the corners. The results for Configurations 5 and 6 are presented in Chapter 5.

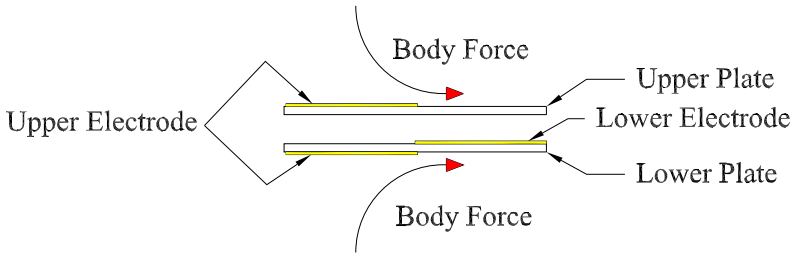

Figure 2.19. Configuration 6, sandwich type actuator setup.

To help summarize the configurations just described, a visual and tabular summary were included. The visual summary is shown in Figure 2.20 and a descriptive summary is provided in Table 2.1. Note that in some cases there are various sub-configurations. For example, configuration 1 denotes the airfoil(s) tests but different spacings were investigated along with different plasma actuator locations. The particular features of the tests will be discussed when the results are presented.

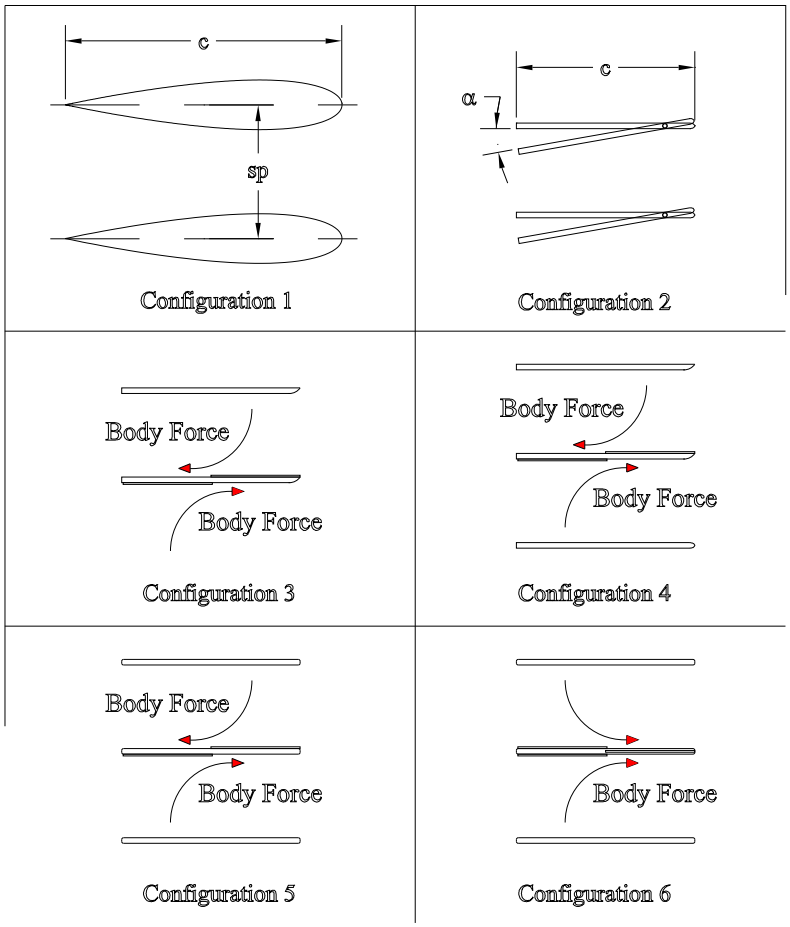

Figure 2.20. Image summary of the different configuration.

Table 2.1. Reference list of different configurations.

Configuration	Description
Configuration 1	NACA_0018 airfoil(s)
Configuration 2	Two flat plates, Kapton type of actuator
Configuration 3	Two flat plates, PC type of actuator
Configuration 4	Three flat plates, PC type of actuator
Configuration 5	Three uniform flat plates, PC type of actuator
Configuration 6	Three uniform flat plates, sandwiched PC type of actuator

2.6 Flow Visualization

Due to the vertical positioning of the airfoils and flat plates, a horizontal smoke-wire setup could be used. Initially the smoke-wire was placed downstream of the test pieces. During the experiments involving the flat plates this was changed. The flat plates were moved so that the smoke-wire was upstream of them. This allowed more of a wake distinction because the smoke was not being generated directly in the wake and in the free-stream at the same time.

Early test showed that the test velocities used for the hot-wire measurements were too fast for flow visualization using a smoke-wire. There was too much mixing of the smoke and the traces were drawn too thin, thus making the density of the smoke concentration too small. So lower wind tunnel velocities were tried and the wind velocity of 15.4 ft/s (4.69 m/s) was chosen. Even though velocities lower than the 15.4 ft/s (4.69 m/s) did give better visualization results, the desire was to keep the flow conditions as applicable to a real case as possible. This velocity corresponded to a Reynolds number of 50K for the Pack-B turbine blades previously mentioned. This was the most investigated Reynolds number in those experiments.

The smoke-wire setup consisted of two 'L' shaped copper tubes having an approximately 1.0 in. (2.54cm) piece of a hypodermic needle epoxied into either end. On one leg of the 'L', there was a coupler that allowed the copper tube to be separated so that the smoke-wire could be threaded through the hypodermic needles. On top of each of the copper tubes was a small reservoir for the model train smoke fluid/soap mix. The reservoir kept the copper tubes filled with the fluid/soap mixture. One of the copper tubes is shown in Figure 2.21. Adding soap to the smoke fluid helped reduce the surface tension of the smoke fluid thus allowing more fluid to collect and bead up on the smoke-wire. This allowed for hotter and longer burns with the smoke-wire, which made imaging better. The soap that was added was blue in color. It was found that this coloring resulted in a denser smoke that also had a blueish color, which the camera was better able to capture. The smoke fluid/soap mixture used 10 to 15 percent soap by volume.

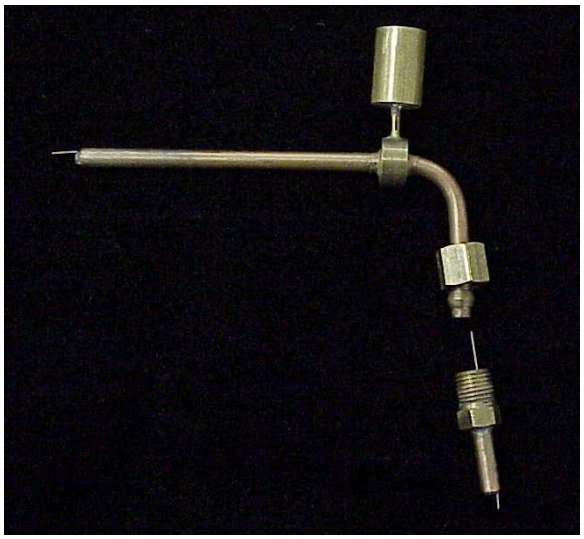

Figure 2.21. 'L' shaped smoke-wire holder/fluid applicator.

The smoke-wire, was a 2.7 mil (69 μm) diameter Nickel-Chromium wire. Its diameter was small enough to easily pass through the hypodermic needles but large

enough so that the surface tension of the smoke fluid prevented the fluid from significantly leaking. When the wire was slid through the hypodermic tubes, it was coated with a thin layer of fluid. The smoke fluid then formed into droplets due to a surface tension instability. The tension of the smoke-wire itself was maintained by the weight of two large nuts, attached to either end of the smoke-wire. Another advantage of the use of the copper tubes is that the electrodes, that provide the current though the smoke-wire, could be attached to the copper tubes. This prevents the tangling of wires while the smoke-wire is used and prevents having to pass current through the entire length of the smoke-wire.

Many different lighting setups with different backgrounds were employed in order to obtain reasonable images. These setups ranged from using a constant light source to using two high-powered strobe lights. It was found that the dual strode light configuration produced the best results. It consisted of two 1540-P2 Strobolume lamps powered by two 1540 Strobolume power supplies and controlled by two 1540-P1 Strobolume oscillators. The controllers had the ability to send and receive a trigger pulse. This feature was used to synchronize the two strobe lamps by having one controller send a pulse to the adjacent controller. The two strobe lamps were mounted side-by-side, positioned 0.50 in. (1.27 cm) apart, on a 2.50 in. (6.35) cm by 20.0 in. (50.8 cm) and 0.25 in. (0.635 cm) thick steel plate. The steel mounting plate was then attached to a tripod which was positioned next to the test section such that the strobe lamps pointed at the side of the test section, which was completely covered with cardboard except for a 1.0 in. (2.54 cm) slit centered on the smoke-wire and running the length of the test section. This was done to reduce the addition of light that would be reflected inside of the test section, which would intern reduce the contrast of the illuminated smoke. The two strobes allowed for a very wide and bright illumination of the smoke generated by the smoke-wire. An illustration of the

setup is shown in Figure 2.22. Placed on the opposite side of the test section, across from the strobe lamps, centered in line with the cardboard slit and halogen filament of the lamps, was a 1.50 in. (3.81 cm) by 25.0 in. (63.5 cm) mirror. This was added to reflect light back into the smoke to help illuminate the smoke for the video camera.

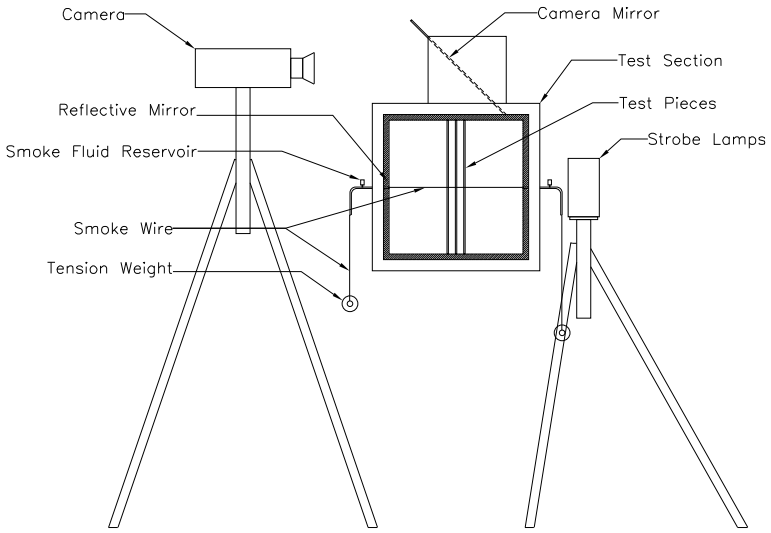

Figure 2.22. Flow visualization experimental setup.

The first tests were conducted having the side of the test section, opposite to the strobes, open to the light. The thought was to allow any light directed or reflected on that side of the test section to pass through. It was found however that covering the side with a dull black cloth[6] worked much better in reducing the amount of reflected light.

In addition to the tests of adding soap to the smoke fluid to improve the imaging, different strobe frequencies, cameras, and camera shutter speeds were tested. When some of these other configurations were used, the probability of the camera and the strobe being in phase was decreased, so that in some cases, the video footage was

[6]This cloth can be seen as the back drop in Figures 2.11, 2.13, and 2.21.

almost completely blank. The solution to this was to use a strobe frequency of 30 Hz, which was close to the frequency of the VHS video camera shutter.

A Panasonic AG-188 VHS camera was chosen over a Sony digital camera to record the images due to the superior imaging results. The orientation of the camera to the test section can be seen in Figure 2.22. Notice that the camera is recording the images from a mirror that was placed on top of the test section at a 45 degree angle. The bottom of the test section was also covered with the aforementioned black cloth to provide greater contrast and a uniform background. It is important to point out that because the camera was recording the images from the mirror, what the camera recored, was an inverted image of what is actually seen when looking down into the test section. After the video was acquired with the VHS camera, a software package called Main Actor was used on the Linux platform to capture and digitize the images in an uncompressed bit-map(*.bmp) format. This allowed for editing without the loss of quality that results from editing compressed formats such as jpeg's. To correct for some of the effects of the mirror, as a final step, the captured images were inverted using a program called Gimp. This was done so that the flow visualization images and the hot-wire data could be discussed with less confusion. Some of the imaging effects could not be corrected. For example, in some of the images presented for the flat plates, the plates appear as though they are set at opposite angles of attack. An example of this is shown in Figure 2.23. Note that the plates are in fact at the same angle of attack.

2.7 Data Reduction

This section is used to present a couple miscellaneous points about the data reduction.

A program called MATLAB©, developed by MathWorks, was used to fit the

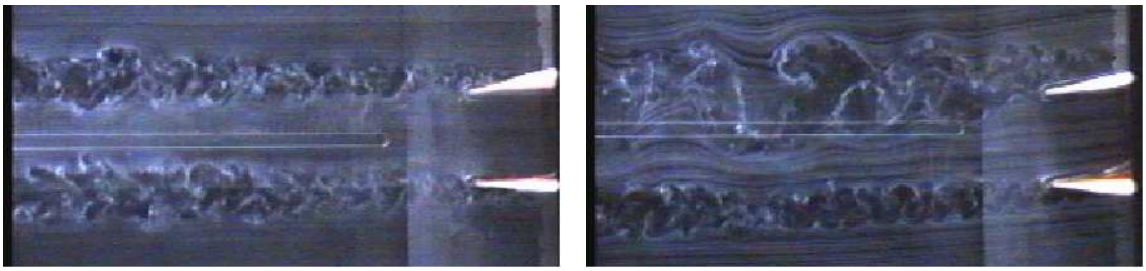

Zero angle of attack. 10 degree angle of attack.

Figure 2.23. Examples of imaging effects from flow visualization setup.

calibration data with a 5^{th} order polynomial, taking in to account the temperature correction. A FORTRAN program was used to then read in the constants and convert the raw data, using the temperature correction, to velocities. This program also calculated the mean and standard deviation, referred to as the RMS, of the converted data.

To illustrate the temperature dependence, Figure 2.24 was included. This figure shows the temperature variation during the pressure transducer calibration, along with an extended temperature investigation. The pressure transducer calibration comprises the first third of the time, i.e. the first 60 minutes. This large amount of time is due to the fact that a manual micrometer was used for the calibration and at each point, 3 readings were taken from it. After the calibration, the tunnel speed was reduced to approximately 29 ft/s (8.84 m/s) and held for 30 min. Then the speed was increased to approximately 43 ft/s (13.1 m/s) and held for 30 minutes, after which the tunnel was turned off. This test was done to check if the air temperature could be stabilized, which would mean that a temperature correction would not have to be made. From Figure 2.24 it is obvious that the air temperature is very dependent on the flow velocity. These temperature variations workout give velocity over estimates on the order of 5 percent at 30 ft/s (9.1 m/s) and 3.5 percent at 80 ft/s (24 m/s). As mentioned earlier, the thermocouple was added to be able to correct for the

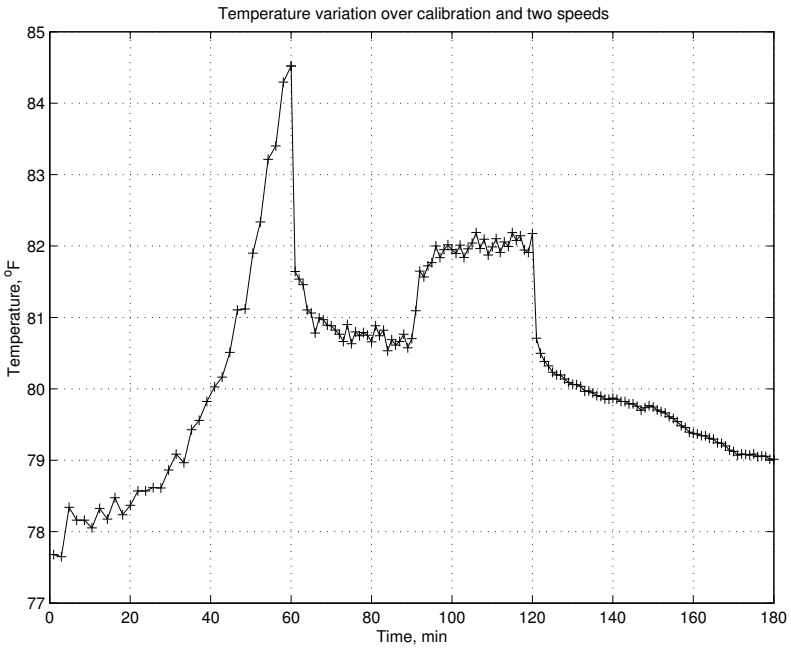

Figure 2.24. Air temperature dependence relative to time and free-stream velocity. t=0:60 for calibration(max. velocity 85 ft/s (25.9 m/s)), t=60:90 v=29 ft/s (8.84 m/s), t=90:120 v=43 ft/s (13.1 m/s)

temperature effect.

Once the voltages were converted, MATLAB©was again used. Programs were written to do all of the data handling and plotting for the various Figures presented in this thesis. Some particulars of how the data was reduced for the different figures are discussed as they are presented. One thing to draw attention to is the how the points used for comparison were chosen from the hot-wire measurements when the plate was at an angle of attack. The issue is that the location of the maximum deficit is not directly in line with the plate, nor is it in the same location for the both the plasma actuator 'off' and 'on' cases. When the plates are at zero angle of attack, the points line up so the minimum velocities for the 'off' and 'on' cases were just taken as the minimum velocities of each peak behind the plate. However, the angle of attack cases had to be treated differently.

To help illustrate this problem, Figure 2.25 from Chapter 6 is presented. This shows three select stream profiles with actuator 'off', 'on', and the difference between them, shifted by 1. Because the moving-wake generator is going to be placed in a fixed location, it is important to know exactly what the variation in the free-stream is going to be relative to a fixed spanwise location. The way that this was handled was to find the minimum velocity value for the plasma 'off' case behind the plate with the plasma actuator. This then fixed the spanwise location. The value used for comparison was taken from the actuator 'on' case at the same spanwise location. This is justified because upon setup, the moving-wake generator could be shifted to have the spanwise location, where the velocity fluctuation of interest is occurring, coincide with the desired downstream spanwise location, maybe the stagnation point on the test blade. In the first subplot is a sketch reflecting the plate orientation and location that the data was taken. The horizontal line indicated by the letter 'A' is the location of minimum velocity of the actuator 'off' case, and thus the y-location where the data was taken for comparison. The horizontal line indicated by the letter 'B' is in line with the center of the plate. The line indicated by the letter 'C' represents the angle of attack of the plate and the projected area. The vertical distance between the ends of this line are drawn to scale with the actual width of the projected area of the plate. The length, angle, or the location of the line in no other way represent the actual location of the plate.

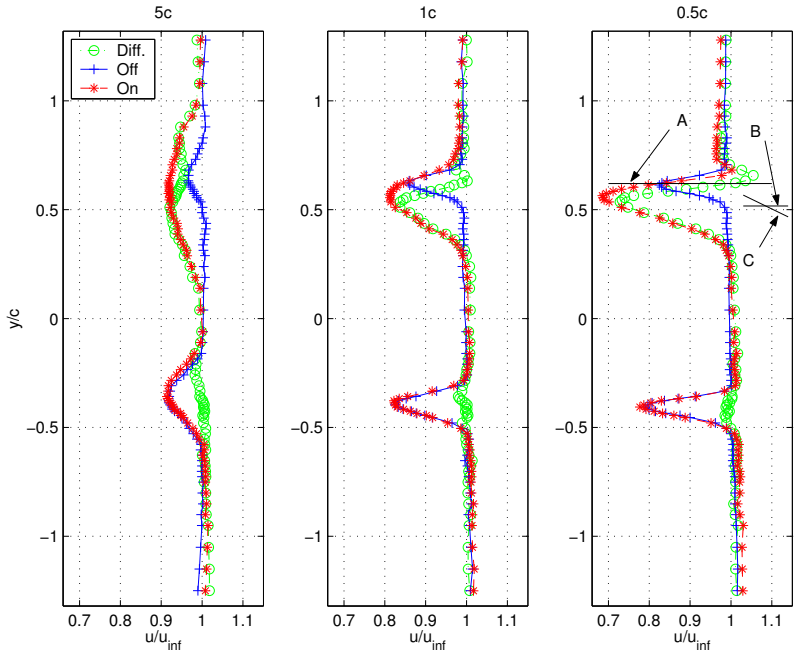

Figure 2.25. Select stream profiles of an actuator 'off' and 'on' case plotted with difference between them. A-Location minimum velocity of the actuator 'off' case. B-Indication of center of the plate area blockage. C-Represents the angle of attack of the plate and projected area.

CHAPTER 3

RESULTS: AIRFOIL

This chapter presents all off the results from the airfoil testing for Configuration 1. This includes hot-wire measurements and flow visualization. The hot-wire measurements for the single airfoil are presented first, followed the twin airfoils, and lastly the flow visualization results are presented. This follows the test order in which the results were obtained.

3.1 Single Airfoil

The initial design idea for the moving-wake generator was to use symmetric airfoils set at zero angle of attack. For this a NACA_0018 airfoil with a 3.1 in. (7.87 cm) chord was chosen as the first test specimen. Ideally, a NACA_0009 or NACA_0012 of similar chord length would have been chosen but molds for these airfoils were not available at the start of the testing. However, the mold for the NACA_0018 was available from previous research and was deemed a reasonable starting point for the tests. The reason for choosing an airfoil was that of practicality. A thin symmetric airfoil at zero angle of attack will produce a small wake relative to its maximum thickness. The thickness of the airfoil would add strength to the blade and make it easier to mount. This would be beneficial to larger test sections in that the larger spans could be easily bridged. Under the aerodynamic loads, the added thickness, in contrast to simply using a flat plate, would add strength making the airfoil less likely

to deflect, vibrate, or twist. Another advantage of the airfoil is the round leading edge. A sharp leading edge or flat plate is very sensitive to positioning relative to the flow. The slightest angle can cause flow separation to occur, where as a round leading edge reduces this sensitivity.

3.1.1 Wake Profiles

The first experiments conducted on the airfoil were hot-wire measurements. The type of measurements performed were streamwise velocity profiles behind the unactuated, single airfoil. A detailed explanation of the test setup can be seen in Section 2.5.1 of this thesis. The stream profiles were performed to establish the basic characteristics and downstream structure of the airfoils' wake. The intent was to obtain a base or control case to have as a datum. This case could then be used for comparison when the actuator(s) were attached to the airfoil, and when an additional airfoil was added to the test section. This was intended to make any effects produced by adding an actuator(s) or airfoil more apparent. Recall from Section 2.5.1 that two different free-stream velocities were used, namely 31 ft/s (9.45 m/s), which corresponds to a Reynolds number of 100K and is referred to as the low Reynolds number case, and 54 ft/s (16.5 m/s), which corresponds to a Reynolds number of 175K and is referred to as the high Reynolds number case. Recall that these Reynolds numbers are based on the setup for the Pack-B turbine blades.

The first figure presented, Figure 3.1, shows the mean velocity profiles for the low Reynolds number velocity case. The corresponding RMS profile is presented in Figure 3.2. Other than at the 1/2 chord downstream location, the profiles appear as expected. The 1/2 chord location shows some velocity variations close to the airfoil and some instrumentation drift, reflected in the variation of the free-stream velocity at either end of the profile. In these figures, and all of the profiles to be presented, the

distance from the probe location to the center line of the test section is normalized by the chord length of the airfoil. The mean velocity values in the profiles are normalized by their respective average free-stream velocities, taken to be the average of the first five data points in the profile. Similarly, the RMS values corresponding to the mean velocities are normalized by an average of the first five RMS values in their respective velocity wake profiles.

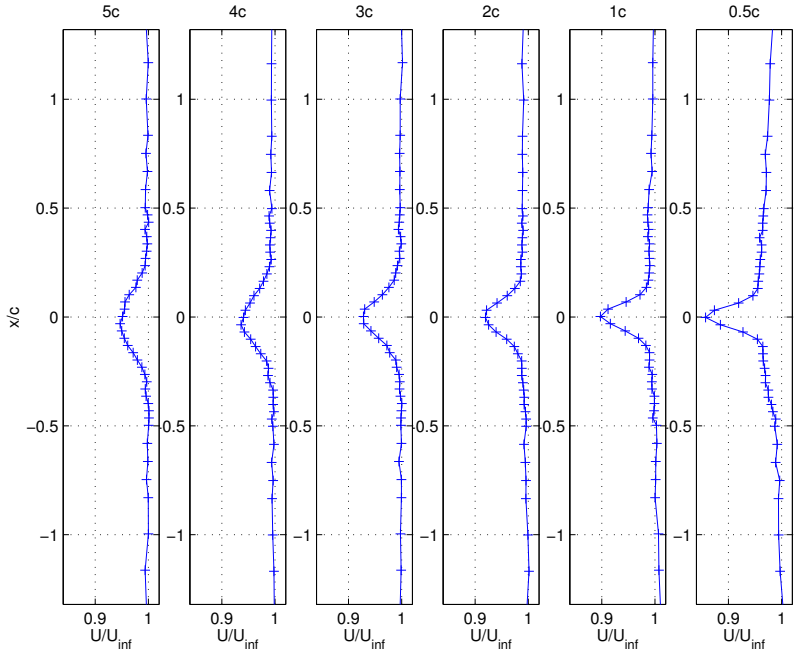

Figure 3.1. Wake profile behind a single NACA_0018 airfoil, low Reynolds number case.

Following the low Reynolds number tests, the higher Reynolds number tests were performed on the single plate. The results for the mean velocity and RMS profiles are shown in Figure 3.3 and 3.4, respectively. These results were very similar to the low Reynolds number case.

3.1.2 Similarity Plot

This section shows a more common representation of the previously presented mean velocity profiles, which is a similarity plot.

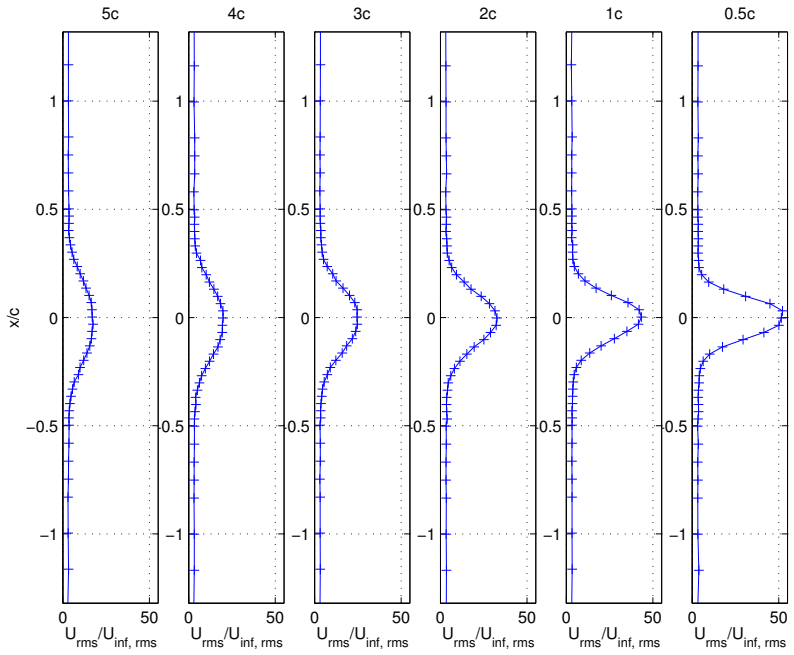

Figure 3.2. Corresponding RMS profile behind a single NACA_0018 airfoil, low Reynolds number case.

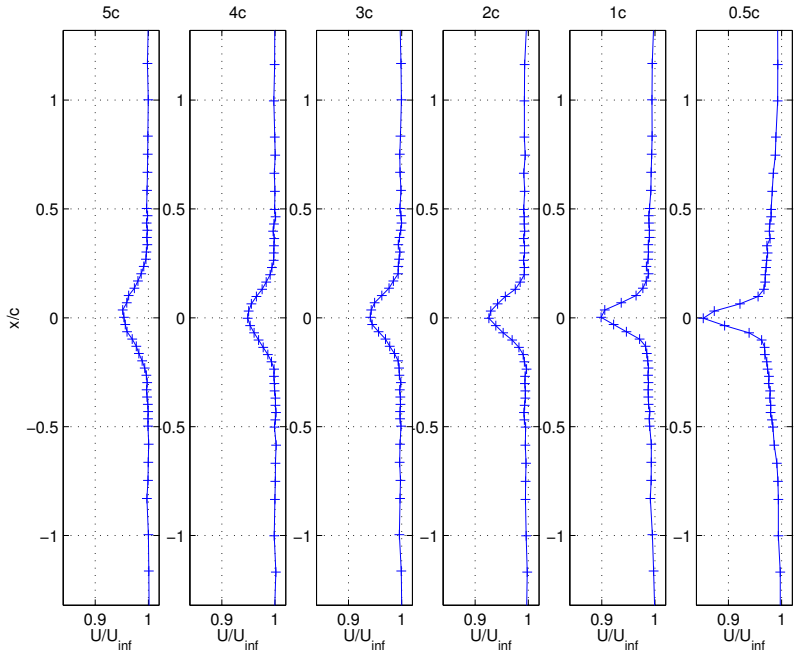

Figure 3.3. Wake profile behind a single NACA_0018 airfoil, high Reynolds number case.

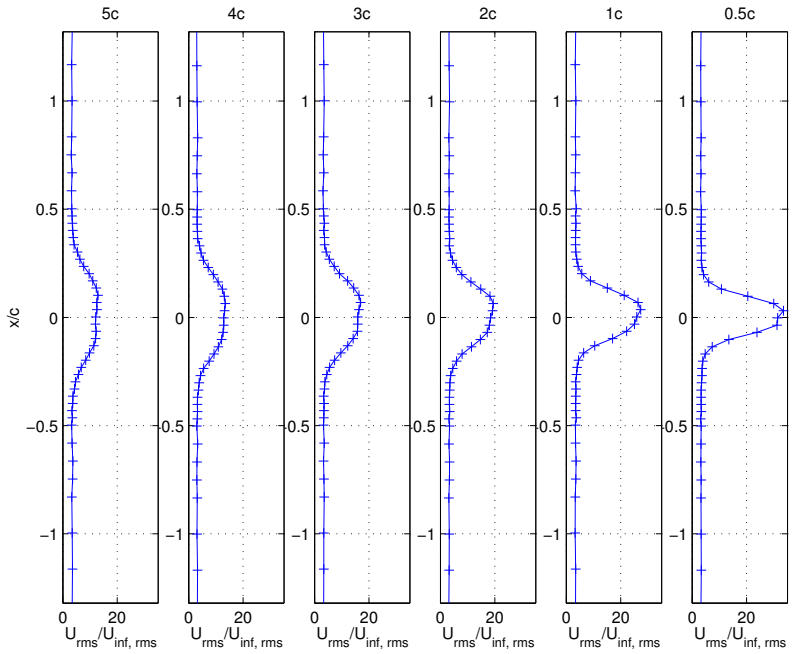

Figure 3.4. Corresponding RMS profile behind a single NACA_0018 airfoil, high Reynolds number case.

The plot is shown in Figure 3.5. Contained in this figure are the results for the two different Reynolds number cases. On the x-axis is the distance from the probe to the centerline of the airfoil nondimensionalized by the wakes half-width, b. This was taken to be half of the width of the wake at half of the velocity deficit. These values were plotted against the difference of the velocity, corresponding to probe location, and the minimum velocity for the profile. These were then nondimensionalized by the velocity deficit, taken to be the difference between the minimum velocity and the free-stream value. Also plotted in this figure was the theoretical far wake decay trend in Equation 3.1. As one would expect, there is better agreement with the far-wake theory at the further downstream chord positions and at the higher Reynolds number. In general this indicates that the wakes of the single airfoils are quite typical to others in the literature.

$$y = e^{-0.693(y/b)^2} \tag{3.1}$$

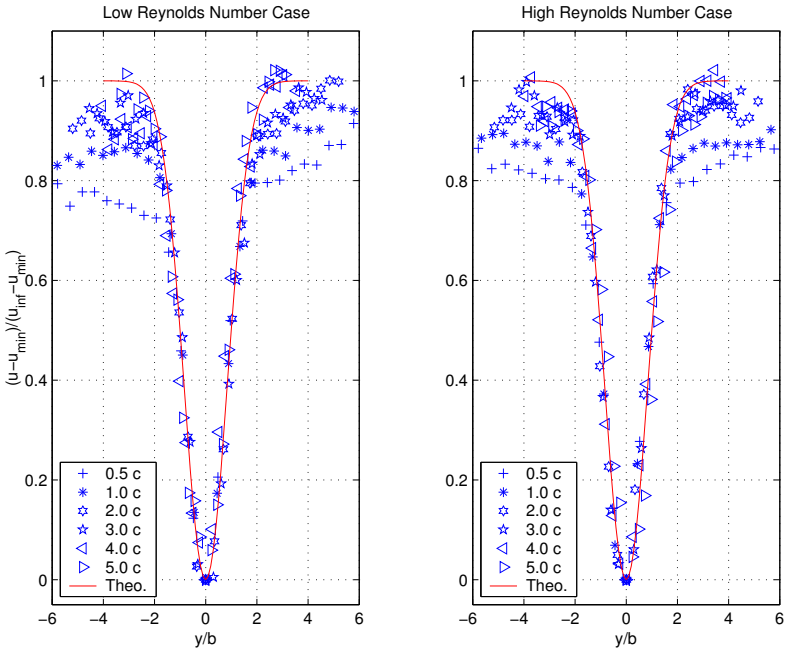

Figure 3.5. Similarity plots for single airfoil.

3.2 Twin Airfoils

After completion of the single airfoil testing, two NACA_0018 airfoils, mounted side-by-side, were tested. As with the single airfoil, the first tests performed were hot-wire measurements behind the two unactuated airfoils, to again define baseline cases. These experiments were performed for the same two free-stream velocities as the single airfoil case. The second set of investigations used flow visualization techniques and are presented in Section 3.4.

3.2.1 Wake Profiles

Initially there was no knowledge of how close the two airfoils could be positioned before their two wakes would start to interact with one another. To investigate this

question, experiments were conducted where the space between the airfoils was varied. The spacings tested included $1/3^{rd}$, $2/3^{rd}$, and 1 chord length. This was done to find the closest spacing that the airfoils could have and still act independently 3 to 4 chord lengths downstream of the trailing edge of the airfoil. The reason for the choice of the 3 chord lengths is based mostly on its physical distance. Three chord lengths, with a 3.1 in. (7.87 cm) chord, translates to 9.3 inches (23.6 cm). This is close to the nominal minimum distance, which is 10 in. (25.4 cm), that the moving-wake generator could be placed upstream of the turbine blade cascade in its first intended application.

The first results of these investigations are shown in Figure 3.6. These correspond to an airfoil spacing of $1/3^{rd}$ chord length. It is immediately apparent from the figure that the velocity in the wakes and between the two airfoils never returns to the free-stream value. It is also clear from this figure that by two chord lengths downstream, the two wakes have blended to the point where they appear as the wake behind a large single airfoil. In terms of the RMS of the velocity fluctuations, the wakes have combined enough that by even a 1/2 chord length downstream, the two wakes are indistinguishable. This can be seen in figure 3.7. From these figures, it is obvious that this spacing is too close for the intended purpose.

The airfoils were moved farther apart to a distance of $2/3^{rd}$ chord for the next set of measurements. These results are shown in Figure 3.8. The mean velocity profiles are substantially better than those presented in Figure 3.6 in that at the 1/2 and 1 chord positions there is a definite flatting of the mean velocities in between the airfoils in the center of the test section. Note however that due to the channeling of the flow between the airfoils, though uniform, the mean value is still less than that of the free-stream. It is not until two chord lengths downstream that the mean centerline velocity returns to the free-stream value. After this position, the centerline velocity

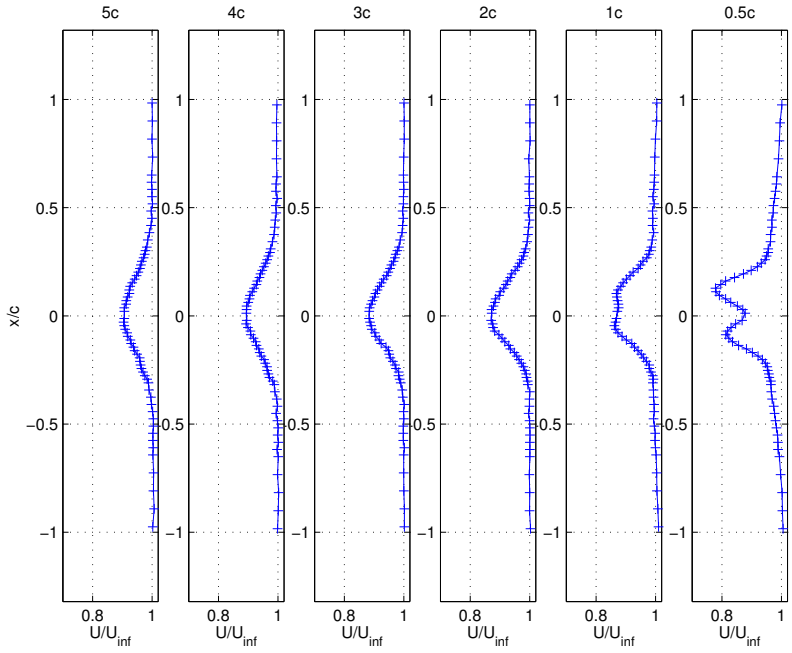

Figure 3.6. Wake profiles behind two NACA_0018 airfoils at $1/3^{rd}$ chord spacing, low Reynolds number case.

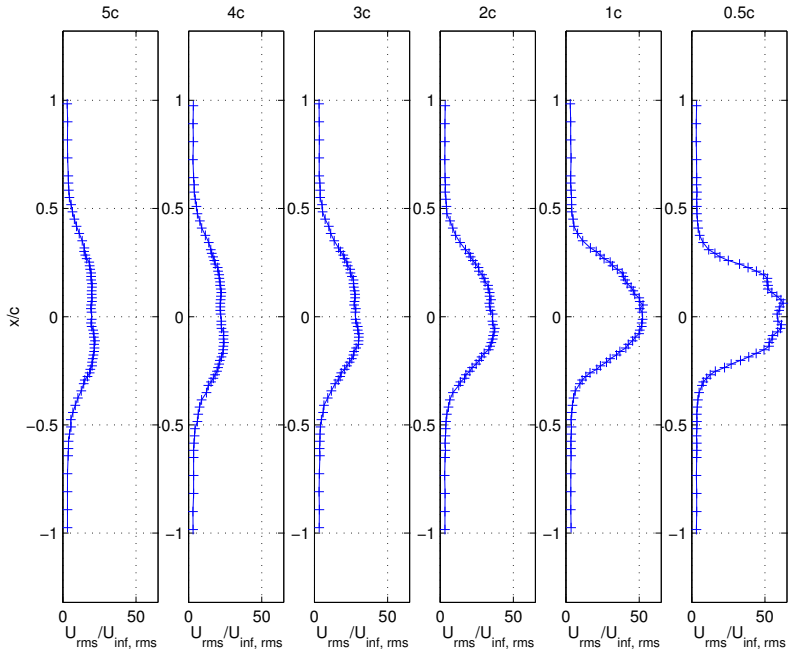

Figure 3.7. Corresponding RMS profiles behind two NACA_0018 airfoils at $1/3^{rd}$ chord spacing, low Reynolds number case.

value slowly starts to diverge from that of the free-stream velocity value due to the wakes mixing. This outcome is similarly shown in Figure 3.9, but the trend starts to appear farther upstream at the 1 chord length downstream position. These results show that although the mean velocity results are very close to the desired outcome, the RMS results indicate that there is still some interaction between the wakes and that the airfoils needed to be spaced further apart to obtain the desired effect.

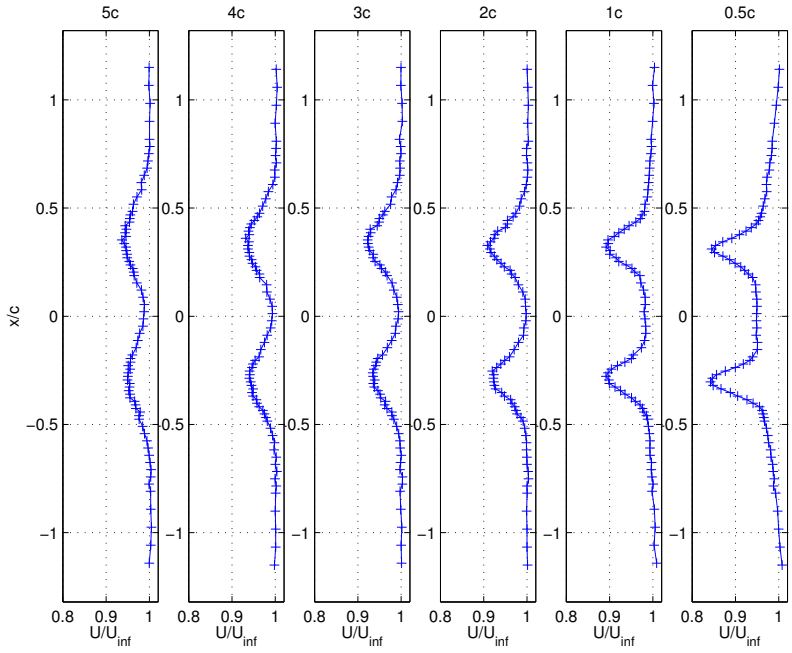

Figure 3.8. Wake profiles behind two NACA_0018 airfoils at $2/3^{rd}$ chord spacing, low Reynolds number case.

The next wider spacing that still kept the airfoils symmetrically placed in the test section was 1 chord length. The mean velocity profiles of this case are shown in Figure 3.10 and the corresponding RMS velocities profiles can be seen in Figure 3.11. As expected by the improvement seen in the $2/3^{rd}$ chord case, there was an improvement with this larger spacing, but possibly more than what was necessary. It is clear from Figure 3.10 that there is no significant influence of the airfoils on each other down to a streamwise distance of 5 chord lengths. The RMS velocity profiles seen in Figure 3.11

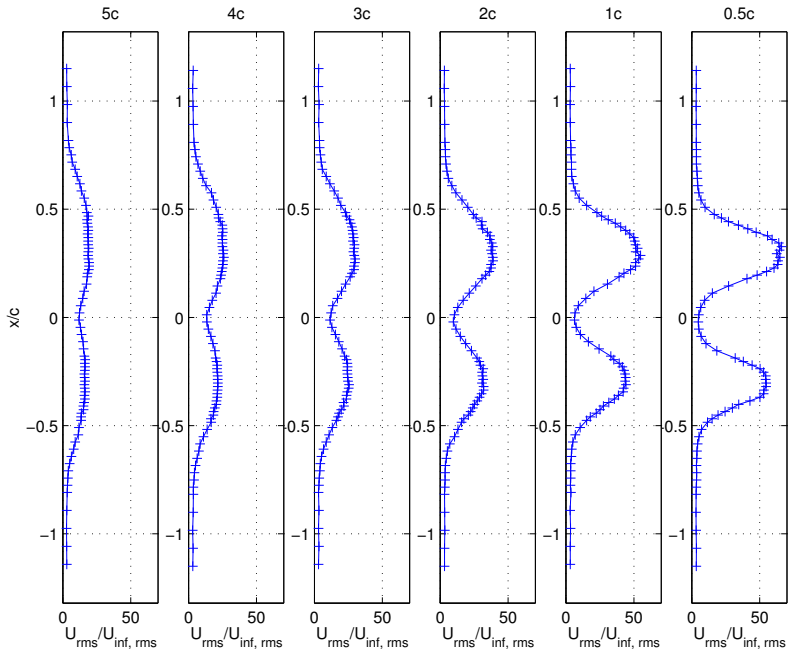

Figure 3.9. Corresponding RMS profiles behind two NACA_0018 airfoils at $2/3^{rd}$ chord spacing, low Reynolds number case.

show that the wakes are are not very close together. This is apparent from having a region of constant RMS velocity in the center span between the airfoils.

It was decided, based on the results obtained for the $2/3^{rd}$ chord spacing case while expecting the initial wake width would slightly decrease when the wind tunnel velocity was increased, that these results were sufficient to try the higher velocity cases. The slight wake narrowing would delay the downstream location where the two wakes would start to mix and therefore should make the $2/3^{rd}$ chord spacing the ideal spacing, depending of course on exactly how the use of the plasma actuator(s) affects the wakes.

The experiments for the higher velocity tests followed the same order of airfoil spacing as the lower velocity tests. The results for the first experiment, the $1/3^{rd}$ chord case, can be seen in Figure 3.12. The asymmetry of the two wakes at the 1/2 chord position is more pronounced in this case than the lower velocity case of the

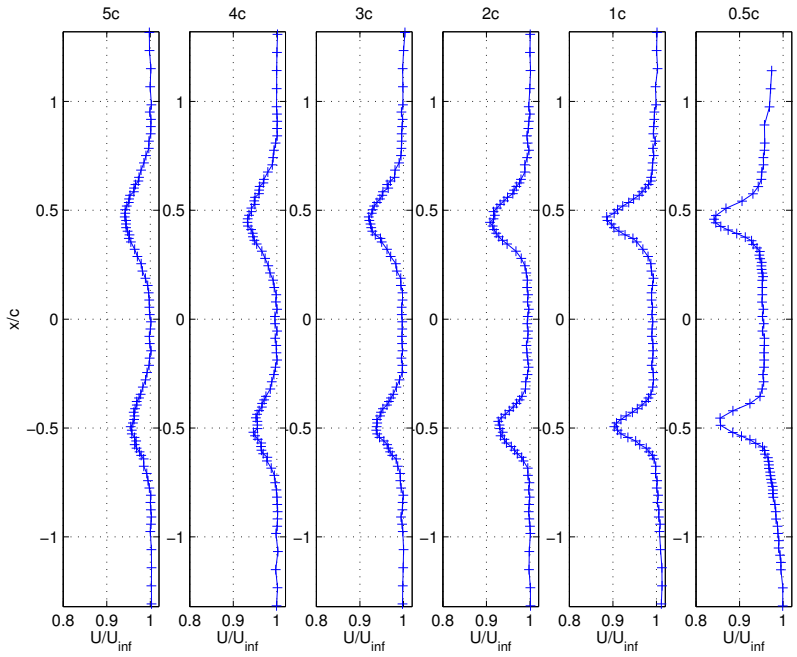

Figure 3.10. Wake profiles behind two NACA_0018 airfoils at 1 chord spacing, low Reynolds number case.

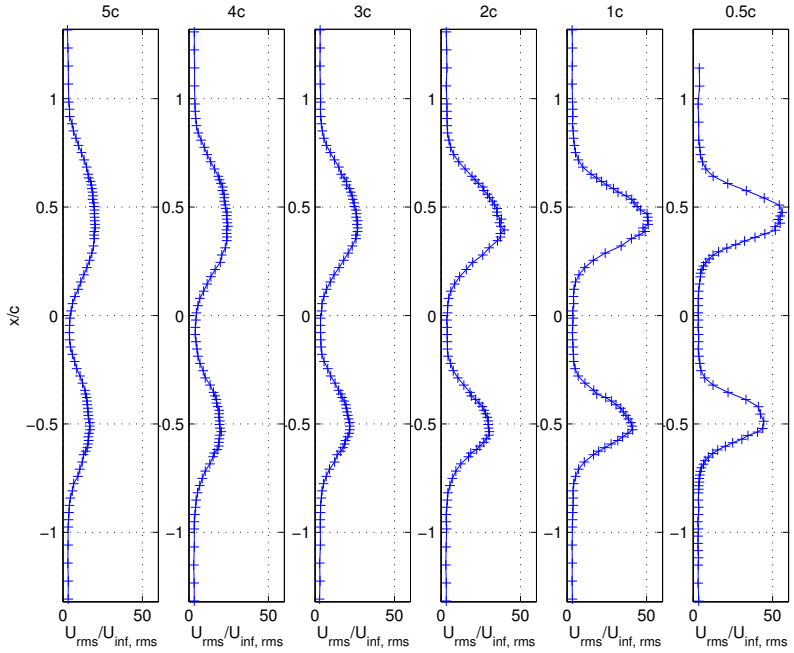

Figure 3.11. Corresponding RMS profiles behind two NACA_0018 airfoils at 1 chord spacing, low Reynolds number case.

same spacing and the airfoil has a larger wake deficit. This asymmetry is thought to be caused by the wakes interacting with each other. In general though, this result is similar to the low velocity case of the same spacing in that at all of the chord positions shown, the wakes are interacting with each other. The RMS velocity profiles show the same trend as the lower velocity case and can be seen in Figure 3.13

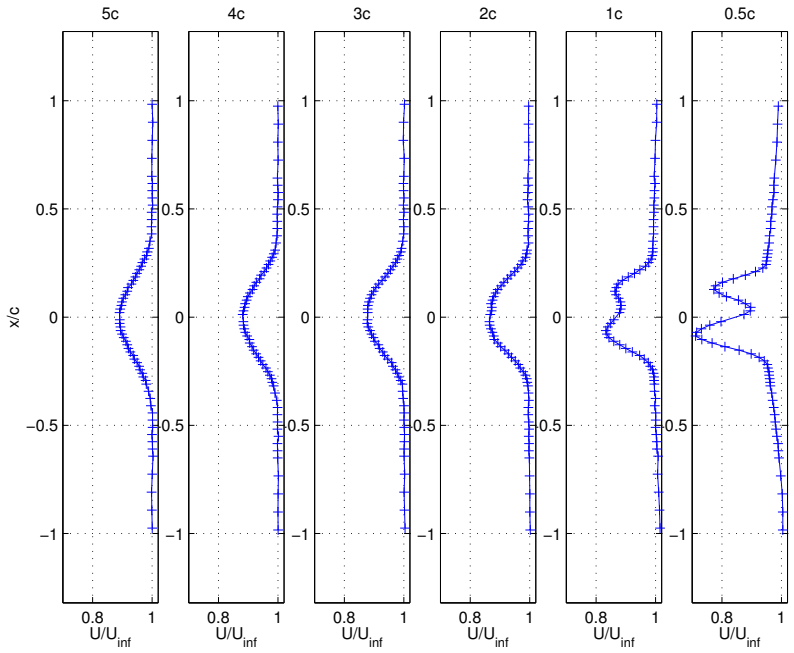

Figure 3.12. Wake profiles behind two NACA_0018 airfoils at $1/3^{rd}$ chord spacing, high Reynolds number case.

With the airfoil spacing set at $2/3^{rd}$ chord, the results again resembled those at the same spacing that were obtained at the lower velocity. As expected, the wake interactions were delayed slightly downstream. This can be seen in Figure 3.14. This figure shows no significant wake interaction until 4 chord lengths downstream. This improvement is also reflected in the corresponding RMS velocity profiles seen in Figure 3.15. They show the wakes interacting closer to the 2^{nd} chord location, as opposed to the 1^{st} chord location shown in Figure 3.9 for the lower velocity case. From these results it is clear that, at least for the two velocities tested, the $2/3^{rd}$ chord spacing

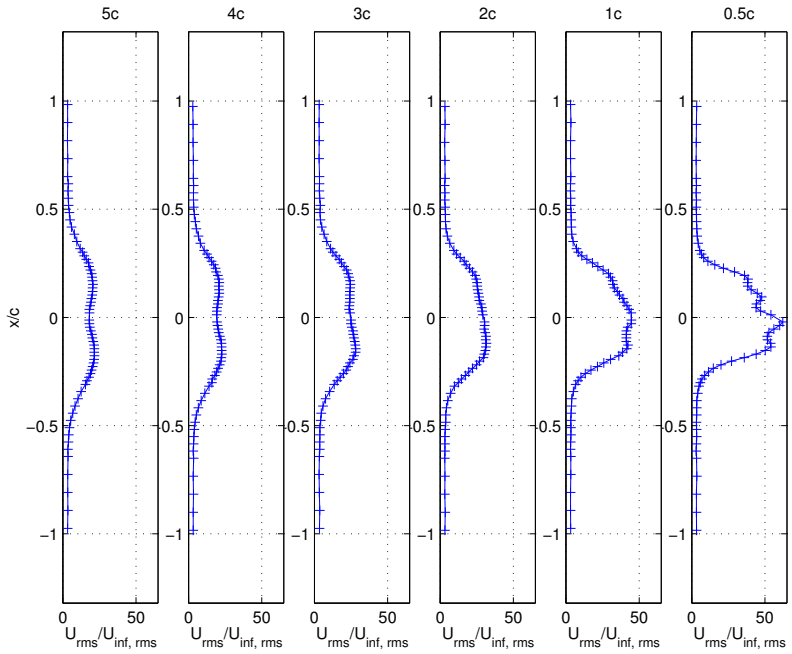

Figure 3.13. Corresponding RMS profiles behind two NACA_0018 airfoils at $1/3^{rd}$ chord spacing, high Reynolds number case.

is the best choice for testing the plasma actuator.

Finally, for completeness, and because the effect of adding the plasma actuator was still unknown, the largest spacing of 1 chord width was tested. These results are shown in Figure 3.16. As expected from the lower velocity tests, we observe that the wakes act independently at all of the chord positions. In Figure 3.17, a larger region of constant RMS velocity is observed between the wakes than in the lower velocity case for the same spacing. This indicates that the wakes are thinner at the higher velocity.

To better illustrate and summarize the interaction of the two wakes, Figure 3.18 was included. This figure shows the normalized mean centerline velocity plotted against downstream location for the different spacings. It is apparent from this that, with the exception of the 1/3 chord spacing case, the 1 chord case, as expected, had the least interaction and returns to close to the free-stream velocity after the 2^{nd}

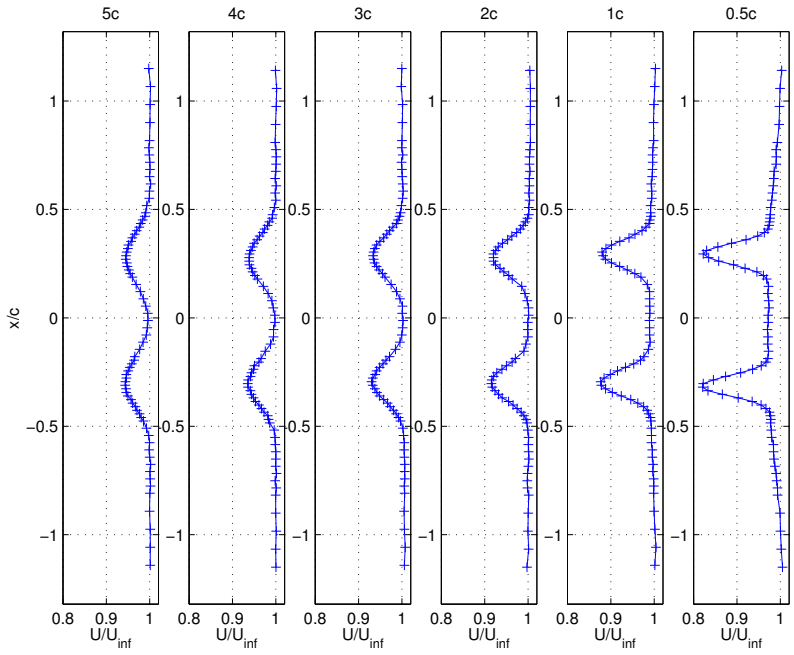

Figure 3.14. Wake profiles behind two NACA_0018 airfoils at $2/3^{rd}$ chord spacing, high Reynolds number case.

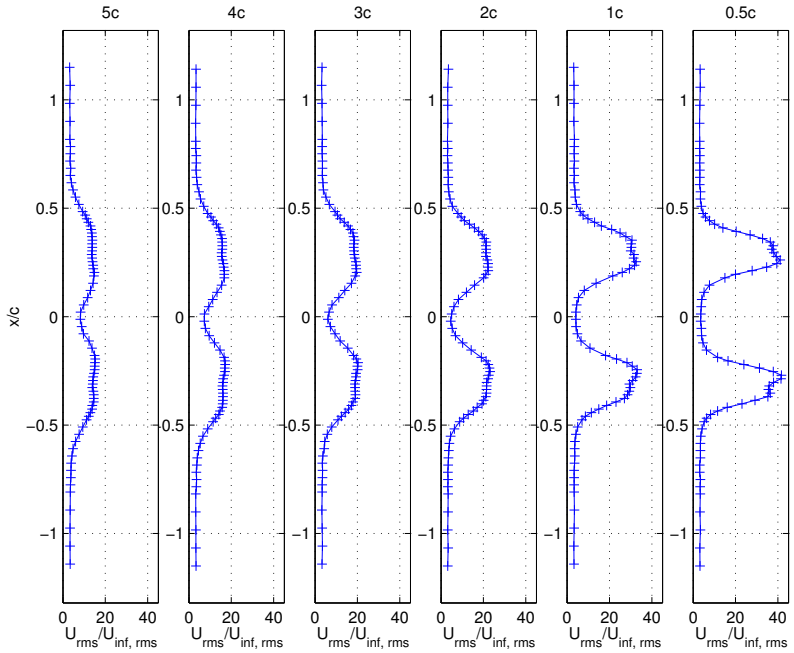

Figure 3.15. Corresponding RMS profiles behind two NACA_0018 airfoils at $2/3^{rd}$ chord spacing, high Reynolds number case.

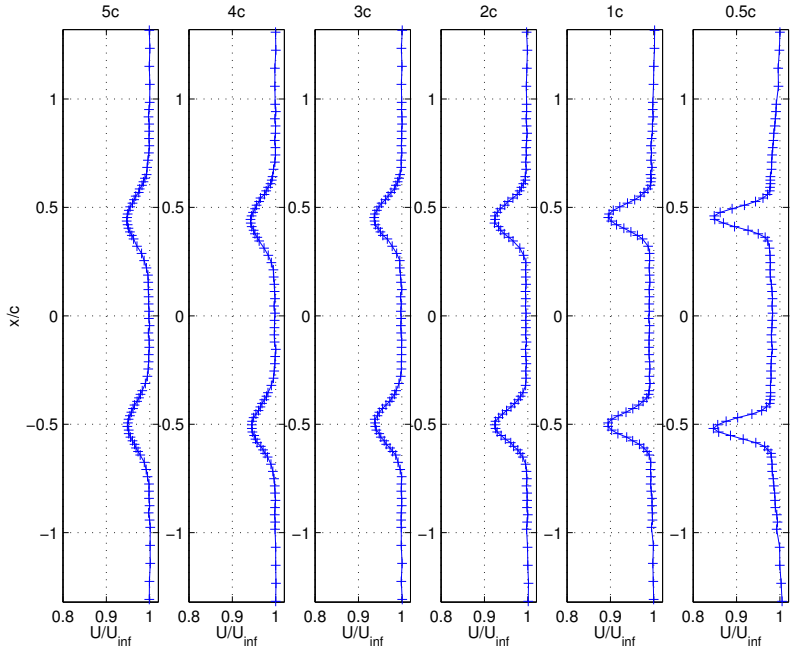

Figure 3.16. Wake profiles behind two NACA_0018 airfoils at 1 chord spacing, high Reynolds number case.

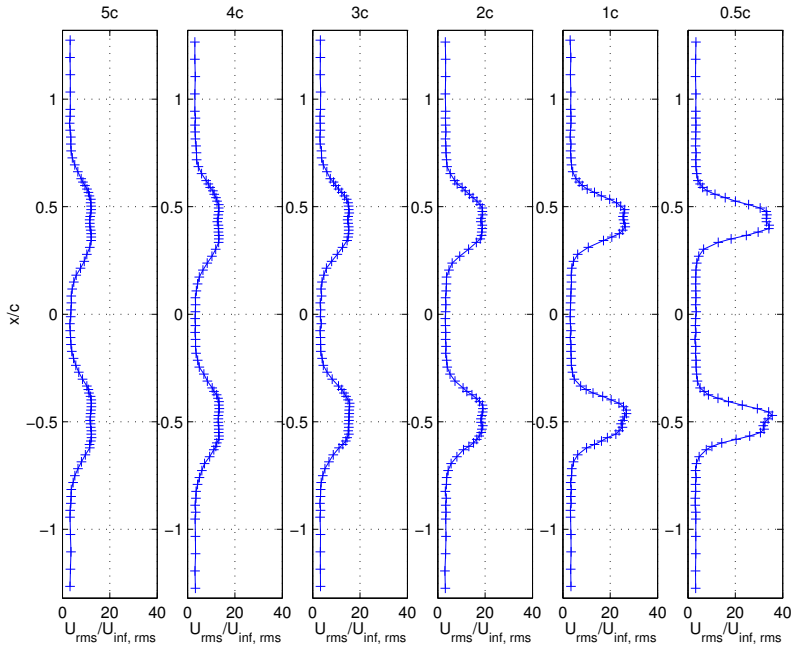

Figure 3.17. Corresponding RMS profiles behind two NACA_0018 airfoils at 1 chord spacing, high Reynolds number case.

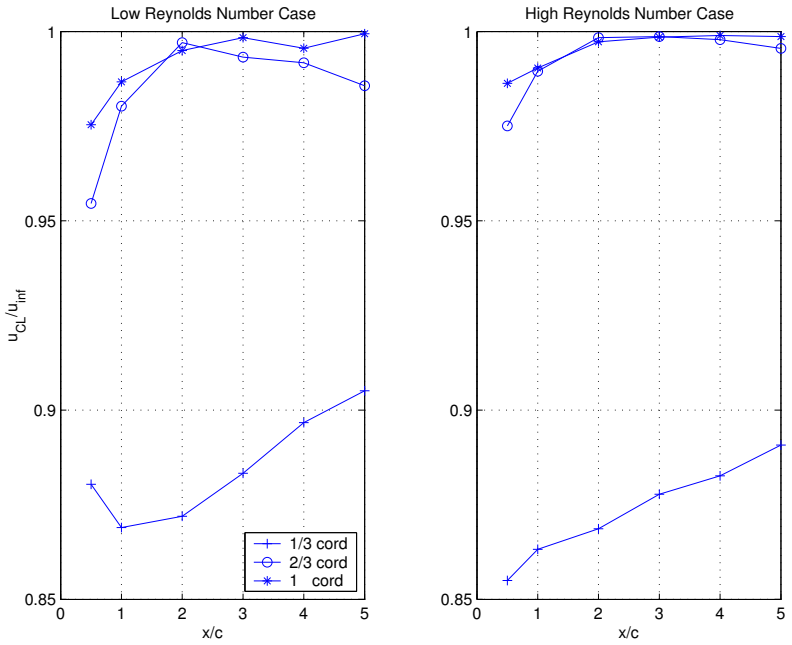

Figure 3.18. Centerline velocity decay for different spacings.

downstream chord location.

3.2.2 Similarity Plots

The following section re-illustrates the stream profile results presented in Section 3.2.1. These similarity plots were constructed in the same manner as the single airfoil similarity plot shown in Figure 3.5. Because there are now two airfoils, in addition to the subplots for the two different free-stream conditions, there is also a subplot corresponding to the wakes of the upper and lower airfoil. This was done to keep the results separate for easier comparison once the plasma actuator was added.

The first similarity plot, shown in Figure 3.19, is for the 1/3 chord spacing case. For this case, because the wakes merged, after the 1^{st} downstream chord location the wakes were treated as a single wake. As such, the same values of the combined single wake were used for the upper and lower peaks after the 1^{st} downstream chord location. These plots again have the theoretical trend depicted by Equation 3.1.

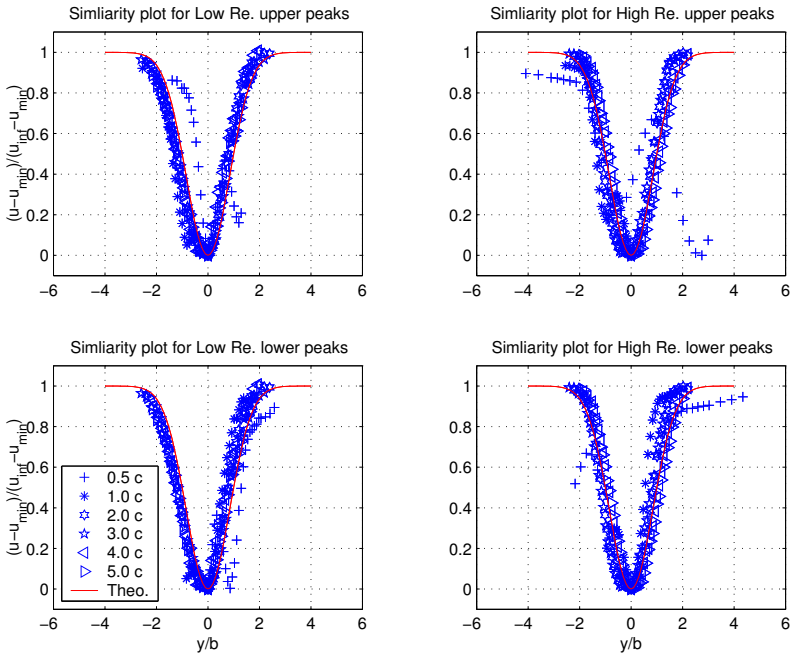

Figure 3.19. Similarity Plots at 1/3 chord Spacing.

This next similarity plot is for the 2/3 chord spacing case. As seen with previous cases, the results plotted in Figure 3.20 show better agreement with theory at the further downstream chord locations. Overall, the plot shows good agreement with theory.

The last spacing case is shown in Figure 3.21. This again shows good agreement with theory.

3.3 Comparison: Single Airfoil to Twin Airfoils

The following section presents some comparisons of the hot-wire data of the single airfoil case to the twin airfoil cases. This was done to better illustrate the effects of the wake interactions.

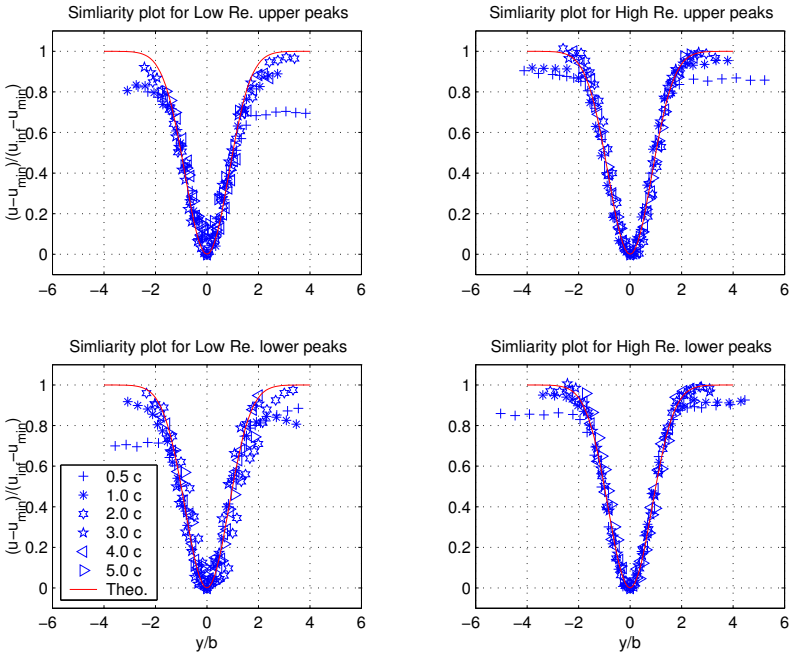

Figure 3.20. Similarity Plots at 2/3 chord Spacing.

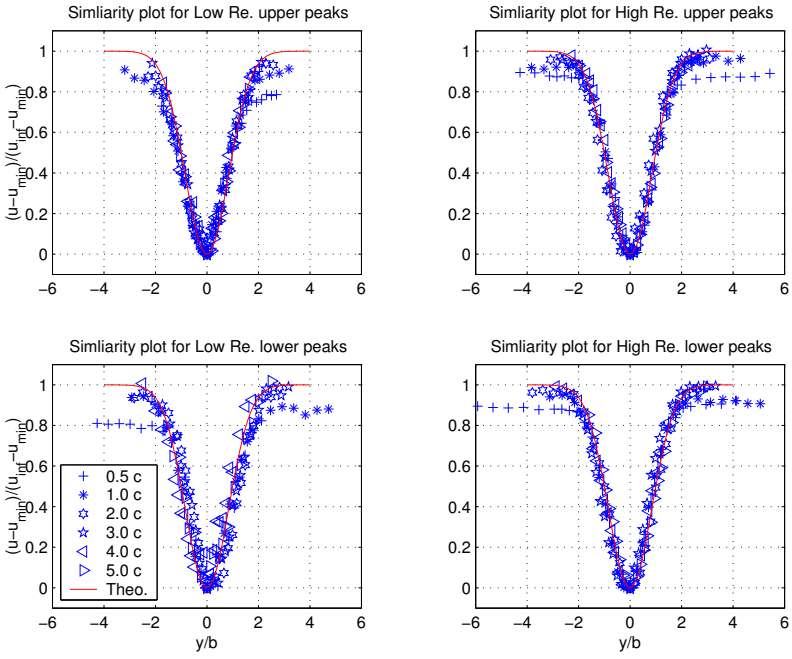

Figure 3.21. Similarity Plots at 1 chord Spacing.

The first comparison was done by looking at the velocity deficits of the wakes. As was done before, the two Reynolds number cases and the airfoil's wakes were plotted individually. The results of this are shown in Figure 3.22. The deficits are expressed as fractions of the free-stream velocity. Mostly for illustrative purposes, a theoretical trend line, of the form of Equation 3.2, is included.

$$y = A\sqrt{\frac{x}{c}} + B \tag{3.2}$$

As depicted in the Figure 3.22, the same 'A' and 'B' constants were used in all of the subplots. This was done to keep from cluttering the figure with numerous equations with slightly different constants. The results plotted in the figure show good agreement with theory for the single airfoil case and, in terms of the decay trend, reasonable agreement for the twin airfoil cases. The main difference is the starting point of the deficit.

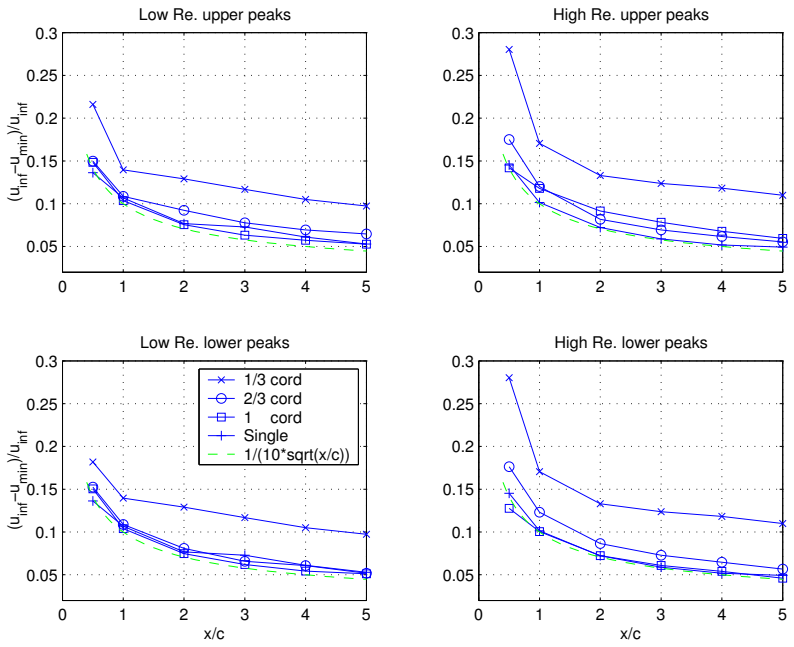

Figure 3.22. Velocity decay for different spacings and single airfoil.

Similarly, Figure 3.23 shows the decay of the peak turbulence intensity behind the

airfoil(s). For this plot two different theoretical trends were included, one for each the low and high Reynolds number cases. The theoretical trends of the form of Equation 3.2 were not matched perfectly or to the same cases. However, the results do show basic agreement of the decay trends with the theory. Again, the main difference between the cases is the initial starting point or magnitude of the turbulence at the 1/2 chord location.

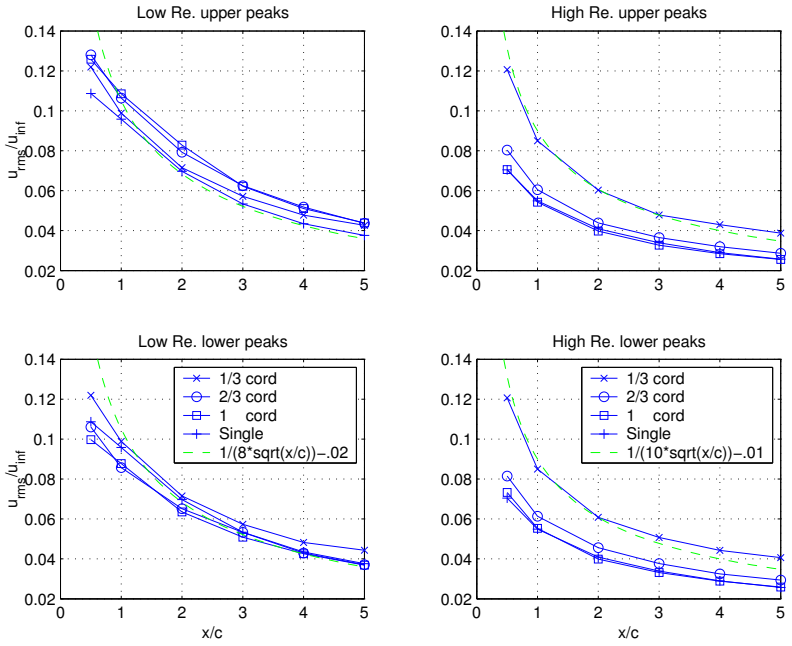

Figure 3.23. RMS decay for different spacings and single airfoil.

This last figure, Figure 3.24, shows the decay of the half width with the distance downstream. For these cases, the theoretical form of the decay trend follows Equation 3.3.

$$y = A\sqrt{x} + B \tag{3.3}$$

Again, only one representative trend was used for illustrative purposes to keep from cluttering the figure. From this figure, it is apparent that 1/3 chord spacing, low Reynolds number case, does not follow the theoretical trend. For the two low Reynolds

number subplots, the two wakes were considered merged for all of the chord locations. The 1/3 chord spacing, high Reynolds number, case however does seem to follow the trend, after the 1/2 chord location where the wakes had merged and the half-width was treated as a single wake. Inspection of the figure shows that the single airfoil and wider twin airfoil spacings follow the same basic theoretical trend, although the constants will be slightly different for each case. The different constants reflect the differences in the locations where the wakes merged. The reason for different choice of where the wakes were considered merged was based on the ability to extract information. The wakes were considered separate for long as possible for each case. However, some cases simply would be separate longer than others, as was the case for the high Reynolds number case.

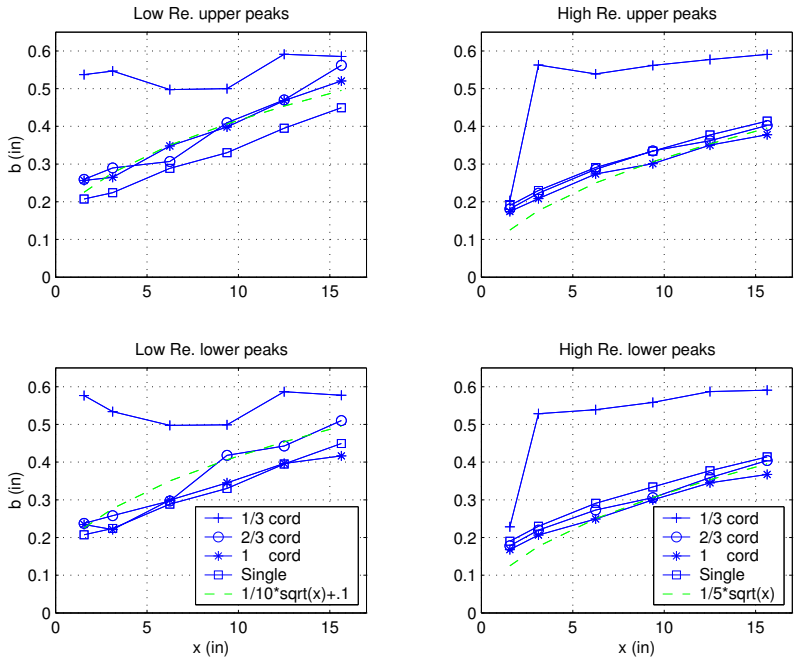

Figure 3.24. Wake half-width decay for different spacings and single airfoil.

At this point, it was decided that the results seen thus far were sufficient to proceed with the investigations using the plasma actuator. In order to obtain a global view of

the effect of the actuator on the wake, flow visualization experiments were conducted.

3.4 Flow Visualization

The following section presents the results of the flow visualization experiments, pertaining to the airfoil tests, which followed the hot-wire measurements. Flow visualization techniques using a horizontal smoke-wire were used to give immediate qualitative feedback from the testing on the various spacings with the plasma actuators. The test arrangements investigated were the same as those for the previously discussed hot-wire measurements for the various spacings. Again, this was done in order to establish the wake interactions prior to adding the actuator, thus providing a visual base line case for comparison for when the plasma actuator was added.

As mentioned in Section 2.6, due to the limitations of the smoke-wire flow visualization technique and in order to obtain good flow visualization results, the free-stream velocity had to be decreased to 15.4 ft/s (4.69 m/s). This is half of the lower velocity case discussed earlier in this chapter. The new velocity corresponds to an axial chord Reynolds number of 50K for the previously mentioned Pratt & Whitney Pack-B blade experiments.

Figure 3.25 shows the $1/3^{rd}$ chord spacing case which appears to reflect the hot-wire measurements for the same spacing. These are consistent with the hot-wire measurements in which they indicate that the wakes are interacting everywhere by appearing as the single wake of a large bluff body with in phase vortex shedding. Glancing at the dates in these images is a reminder that the images had to be inverted due to the effect caused by the mirror/camera setup as discussed in Section 2.6. Now, after the inversion, the images correctly correspond to the previously shown hot-wire data, meaning the upper airfoil wakes in the plots are the same as the upper airfoil wakes in these images.

Figure 3.25. Flow visualization for non-actuated $1/3^{rd}$ chord spacing case at 15.4 ft/s (4.69 m/s).

Similarly for the $2/3^{rd}$ chord spacing case, Figure 3.26 shows a region of little or no influence in between the airfoils on the right side of the figure, but as one moves downstream to the left, the wakes begin to interact with each other and appear as a single larger wake.

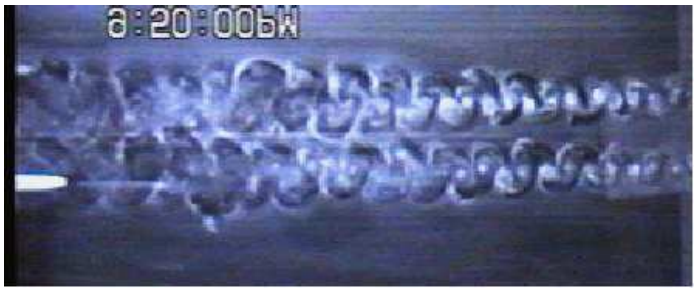

Figure 3.26. Flow visualization for non-actuated $2/3^{rd}$ chord spacing case at 15.4 ft/s (4.69 m/s).

The last image, Figure 3.27, is again a reflection of the hot-wire measurements in that at no point does there appear to be any interaction between the wakes.

Now that the base line cases were completed, plasma actuators could be added to the airfoils and additional experiments conducted. Based on the previous data, the 1 chord spacing case was chosen as the first test spacing. Even though the $2/3^{rd}$ chord case seemed like the better choice in terms of the application, it was thought that the 1 chord case would better show the effect of the actuator. Then, once the effect was

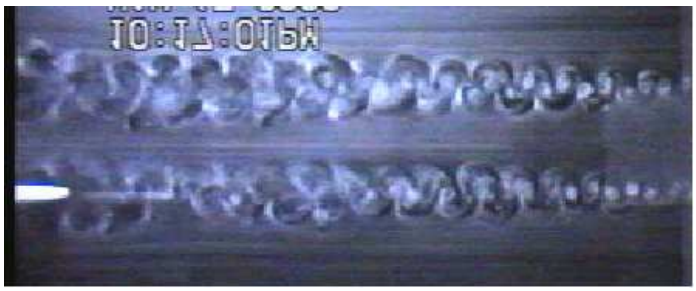

Figure 3.27. Flow visualization for non-actuated 1 chord spacing case at 15.4 ft/s (4.69 m/s).

understood, the blades could be moved closer together, if necessary.

To start, a Kapton type of actuator was placed on the upper airfoil. For these tests, the placement of the actuator and the power supplied were the main parameters varied. Four different locations were tested at three different voltage levels. The locations of the plasma actuator were at the leading edge, 25, 27, and 30 percent chord. The voltage levels used were off(zero), lower electrode at 12.5 KVpp, and then a combination that had both the lower electrode and upper electrode supplied a voltage potential at 12.5 KVpp but with signal on the lower electrode inverted. This effectively doubles the voltage potential between the two electrodes, making the maximum voltage potential across the actuator 12.5 KV. The 27 percent chord location corresponds to the point of maximum thickness of the airfoil. The actuator was placed on the lower airfoil such that when the airfoil was placed back in the test section, the induced flow caused by the actuator was in the channel between the airfoils and directed upstream. The idea here was to help force the flow to separate and thus create a larger wake.

Shown first in Figure 3.28 are the wakes of the two airfoils. The upper airfoil in the figure has a plasma actuator attached to it such that the edge of the actuator is aligned at the 25 percent chord position. This is just forward of the point of maximum

thickness. To help illustrate the effect of the actuator, Figure 3.28-A shows the wakes with the actuator 'off', and Figure 3.28-B shows the wakes when the actuator is turned 'on' at the 6.3 KV voltage potential. That is, one electrode is being supplied power and the other is grounded. It is apparent that there is no real distinguishable effect by the actuator on the flow.

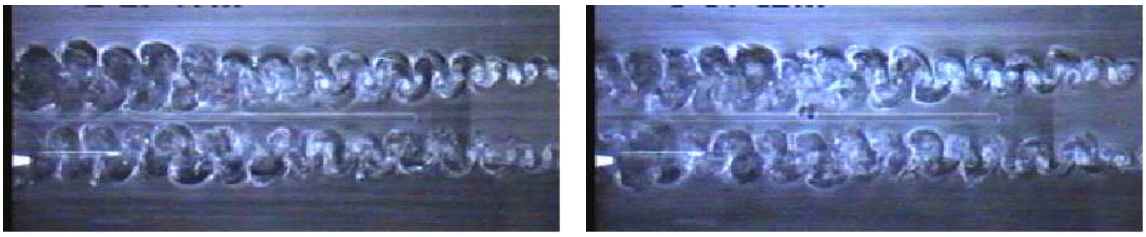

A: Actuator 'off' B: Actuator 'on' (upper airfoil)

Figure 3.28. Comparison with actuator at 25 percent chord, forward of the point of maximum thickness of airfoil, at 6.3 KV potential.

The power was then increased and these results are shown in 3.29. Again with sub-figure A being the 'off' case and sub-figure B being the 'on' case. In Figure 3.29-B there appears to be some effect by the actuator. It can be seen by close observation of the edges of the upper wake, in approximately the middle of the image, that the vortical structure of the wake has been broken up some. This is in contrast to the 'off' case were the half moon shapes are still very distinguishable along the wake edges.

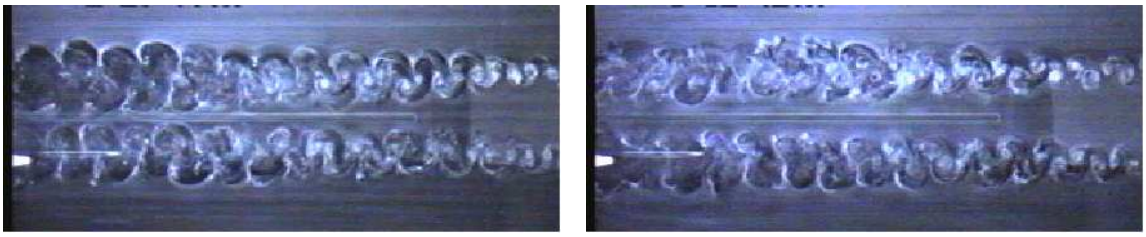

A: Actuator 'off' B: Actuator 'on' (upper airfoil)

Figure 3.29. Comparison with actuator at 25 percent chord, forward of the point of maximum thickness of airfoil, at 12.5 KV potential.

Because the actuator affect was thought not to be sufficient for the intended purpose, a second location was tested. The actuator position was changed to the point of maximum thickness. These results are shown in Figure 3.30. Again sub-figure A shows the case where the actuator is 'off' and sub-figure B shows the case with the actuator 'on' at a 6.3 KV voltage potential. The effect of the actuator is much more apparent here than at the 25 percent chord position. The wake is much more turbulent throughout the whole image.

A: Actuator 'off' B: Actuator 'on' (upper airfoil)

Figure 3.30. Comparison with actuator at 27 percent chord, point of maximum thickness of airfoil, at 6.3 KV potential.

Checking the effects of increasing the power gave the results shown in Figure 3.31. Surprisingly though, Figure 3.31-B shows that increasing the power actually seemed to decrease the affect of the actuator. Careful observation of the downstream side of the image suggests that the width of the upper wake has increased slightly. But clearly in this case, there are distinct vortical structures still present in the upper wake, which were not as apparent in the 6.3 KV potential case.

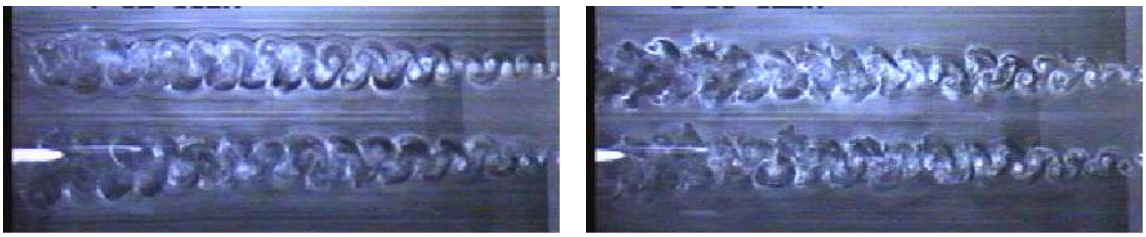

A: Actuator 'off' B: Actuator 'on' (upper airfoil)

Figure 3.31. Comparison with actuator at 27 percent chord, point of maximum thickness of airfoil, 12.5 KV potential.

Because of the improvement seen when the actuator was placed at the point of maximum thickness, it was decided to try and move the actuator slightly further downstream. Keeping with approximately the same step size, the actuator was moved to the 30 percent chord position. These results for both the 6.3 KV and 12.5 KV potential cases are shown in Figure 3.32 and Figure 3.33, respectively. The actuator had little to no effect in either the 6.3 KV or 12.5 KV voltage potential cases. The reason for this could be that by this point on the airfoil the flow has already separated, thus the actuator can not work to separate the flow.

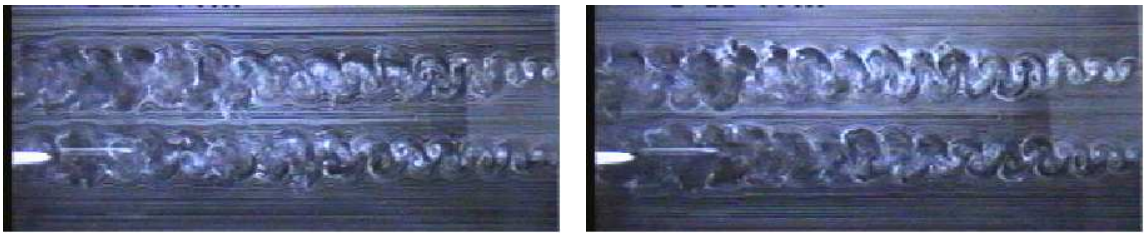

A: Actuator 'off' B: Actuator 'on' (upper airfoil)

Figure 3.32. Comparison with actuator at 30 percent chord, behind the point of maximum thickness of airfoil, 6.3 KV potential.

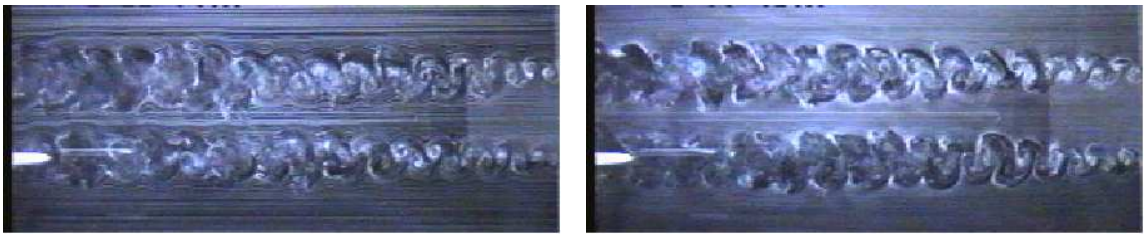

A: Actuator 'off' B: Actuator 'on' (upper airfoil)

Figure 3.33. Comparison with actuator at 30 percent chord, behind the point of maximum thickness of airfoil, 12.5 KV potential.

The results thus far seemed to indicate that this plasma actuator and airfoil setup would not produce a large enough affect to be useful for the moving-wake generator. It was decided then that a different setup should be investigated. Flat plates were chosen as the new setup and are presented in Chapter 4.

CHAPTER 4

RESULTS: FLAT PLATES

Results thus far showed that the plasma actuator can affect the flow, but for the moving-wake generator, the current results needed to be improved. It was decided to simplify the idea and try flat plates whose flow could be more easily manipulated. Many different actuator sub-setups were tried in addition to the many plate configurations and subsets. The actuator variations included changing the dielectric material, the thickness of the dielectric material, the size of the electrode, the number of electrodes, the position of the electrode, plate thickness and the leading edge contour. This chapter will present the some of the results of experiments using Configurations 2, 3, and 4. The main sections of this chapter correspond to the different configurations. For these and Configurations 5 and 6 presented in Chapter 5, the only free-stream velocity tested was 15.4 ft/s (4.69 m/s). This was the same velocity used for the flow visualization for configuration 1 and again corresponds to the 50K Reynolds number case for the Pack-B turbine blades.

4.1 Configuration 2

Like the airfoils, Kapton and copper tape was used as the dielectric material and electrodes respectively to make the actuators. The Kapton setup made it easy to change the actuator design. Due to this ease of variation, many different actuator designs could be tested. Refer to Section 2.5.2 for more information on the experimental

setup. The only investigations performed on Configuration 2 used flow visualization. This was due to problems encountered with the longevity of the Kapton actuators. Quantitative measurements using a hot-wire could not be completed before the actuator failed. The flat plates were first tried at a zero degree angle of attack and then at other various angles. A summary of the flow visualization results are presented in the following subsections.

4.1.1 Zero Angle of Attack

For the application of the moving-wake generator, it was thought to try and minimize the turbulence caused by the apparatus itself. In other words, the amount of blockage and effect on the flow without the plasma actuators running should be minimized as much as possible. To do this, the two plates were set side-by-side, at a zero degree angle of attack, thus creating a channel between the two plates.

The first experiments had an actuator setup that used a single actuator whose upper electrode was positioned 0.125 in. (3.18 mm) from the leading edge of the plate. In terms of the chord, this was at the $1/16^{th}$ chord location. Also, the electrodes themselves were both 0.125 in. (3.18 mm) wide. The orientation was chosen such that the flow induced by the actuator was in the channel of the plates and directed upstream. This was chosen to try to separate the flow and cause a blockage in the channel between the plates that would impede the flow entering the channel. This would in turn cause a large velocity deficit in the wake profiles downstream of the channel, basically making the two plates and channel act like a single bluff body. In these tests, the lower electrode was supplied a 5.0 KHz triangular waveform of up to 3.8 KVpp and the upper electrode was grounded, thus making the highest voltage potential across the actuator 1.9 KV. This setup did not have any noticeable effect on the flow. Another attempt was made having the actuator at the mid-

chord location but again without positive results. All these tests were done at 1/2 chord and 1/4 chord plate spacings. Based on the the immediate feedback from the flow visualizations, most of these tests were not documented because there was no noticeable change in the flow.

After the previous tries, some attempts were made at using a four actuator array, with the same intention of blocking the flow from entering the channel. The actuators were arranged so that there was an electrode positioned at the $1/16^{th}$, 1/4, 1/2, and 3/4 chord locations, again using the 0.125 in. (3.18 mm) width electrodes. This case also had the lower electrodes grounded and the upper electrodes supplied the 3.8 KVpp, 5.0 KHz triangle wave. The 1/4 chord plate spacing case is shown in Figure 4.1. In the figure, the upper plate is the plate with the plasma actuators. It is apparent from this that the actuators had little to no effect. This setup was tried at 1/4 chord and 3/8 chord plate spacings with similar results. Following these tests, a different set of transformers were used that had more windings, thus a voltage higher gain, which would yield a higher voltage potential across the plasma actuators' electrodes. Doing this gave some improvement but still not enough, so another set of four actuators were added to the neighboring plate.

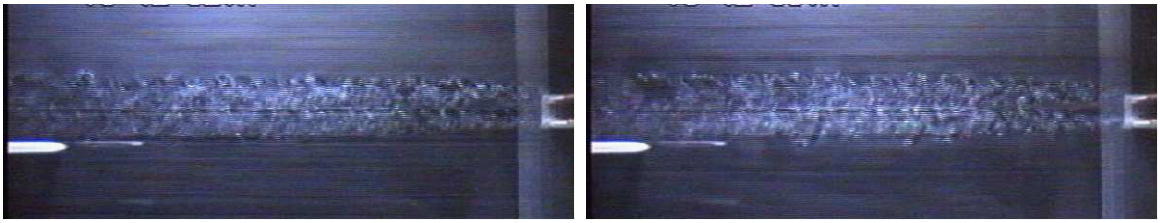

A: Actuator off B: Actuator on (lower plate)

Figure 4.1. Four actuators with 1/2 chord plate spacing at a maximum voltage potential of 1.9 KV.

Keeping with the idea of trying to deter the flow from entering the channel, the same four actuator array was added to the neighboring plate such that both arrays were in the channel between the plates and inducing a flow upstream. Shown in

Figure 4.2 are the results of these tests at 1/4 chord plate spacing. Figure 4.2-A, is the case of having the actuators 'off', Figure 4.2-B is the case of having the actuators on the upper plate in the figures 'on', and lastly, Figure 4.2-C shows the result of having the actuators of both plates 'on' at the same time. Note that the wakes shown in the pictures are not turned or shifted by the plates. The reason the wakes do not appear to follow the plates is because the camera and mirror were not perfectly in line with the center of the test section. The plates edges seen in the picture are at the bottom of the test section, and the smoke is in the middle of the test section, but due to the angle of the camera, they appear to not line up. In this case, a 13.6 KVpp triangle wave was supplied to the lower electrode(s), making the maximum voltage potential across the actuator 6.8 KV. Though not very much, these images do show some effect of the actuator, but more affect was needed so a completely different approach was tried.

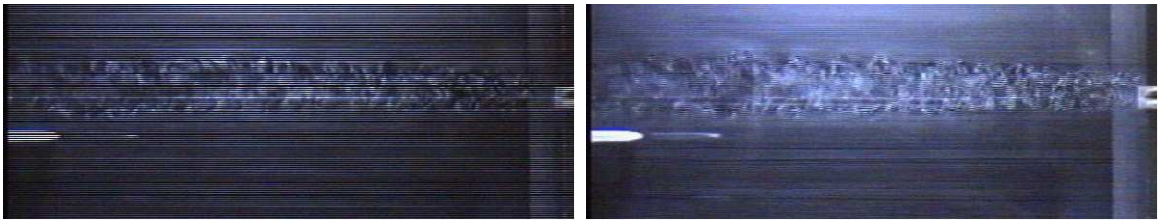

A: Actuator off

B: Actuator on (lower plate)

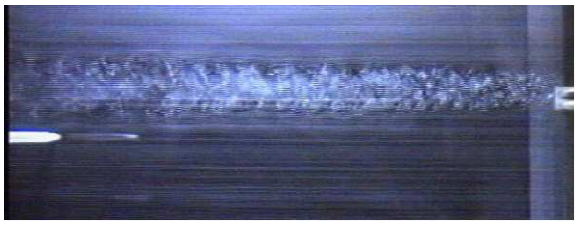

C: Actuators on (both plates)

Figure 4.2. Four actuators with 1/4 chord plate spacing at a maximum voltage potential of 6.8 KV.

4.1.2 At Angle of Attack

Work done by Post[18] showed the ability of using the plasma actuators to reattach the flow of a completely separated airfoil at high angles of attack. With this idea in mind, it was decided to start with a separated flow and work to reattach it, as opposed to the previous tests of trying to separate the flow around the body. In terms of the moving-wake generator, this would effectively invert the operating method. Instead of using it in a way such that the use of the actuator would create a larger flow disturbance by widening the wake, the reattaching method would reduce the flow disturbances by narrowing the wake. If so desired, one could work between an 'on/off' actuator case as opposed to an 'off/on' case. This would produce a downstream effect similar to what was intended by the zero angle of attack method.

To implement this new method, the plate spacing was increased to 1 chord length and the plates were set at various angles of attack. The choice of spacing was based on the results seen with the airfoil and the projected area of the plate to the flow based on highest angle of attack tested. At a 16^o angle of attack, the projected width is 0.551 in. (1.40 cm) compared to the 0.558 in. (1.42 cm) maximum thickness of the NACA_0018 airfoils tested.

The lower plate in the following figures was implemented with a single actuator positioned at the leading edge of the plate such that the actuator would work to pull the flow towards the suction side of the plate and add momentum to the boundary layer. This would work to reattach the flow to the plate. The choice of actuator position was based on results seen in the work of Post[18]. The different angles of attack tried included 0, 5, 10, 12, 14, and 16 degrees with a maximum actuator voltage potential of 11.2 KV. This was achieved by supplying an 11.2 KVpp triangle wave to both the upper and lower electrode of the actuator, in phase but with the signal on the upper electrode inverted. The following figures show some of these results. Note

that in the following figures, the lower plate is the one with the plasma actuator.

Careful observation of the wakes behind the lower plate in Figure 4.3 show that there was only a slight narrowing of the wake. As discussed in Section 2.6, the appearance that the plates in the figure are not parallel is an optical illusion caused by the camera/mirror setup. The angle of attack was then increased. As the angle was increased, the actuator effect became more noticeable.

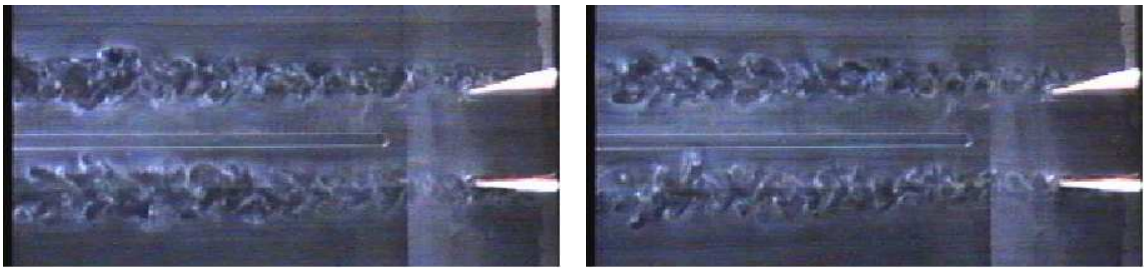

A: Actuator off B: Actuator on (lower plate)

Figure 4.3. One actuator at leading edge of plate at zero degrees, 11.2 KV voltage potential, and 1 chord plate spacing.

In the 5^o angle of attack case shown in Figure 4.4, the effect of the actuator is much more noticeable. The wake behind the lower plate is more narrow than the upper wake and looks more uniform. This effect is even more noticeable in the 10^o case.

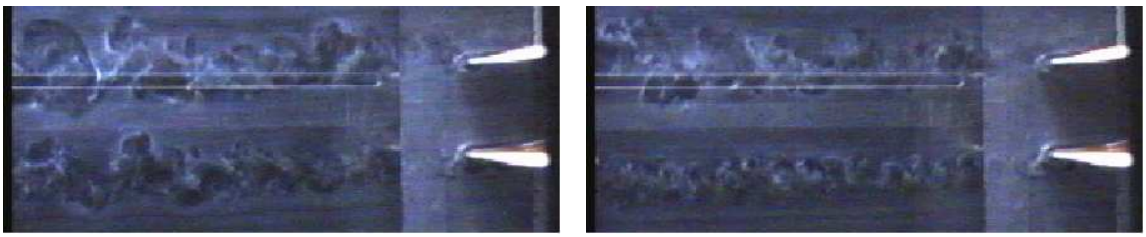

A: Actuator off B: Actuator on (lower plate)

Figure 4.4. One actuator at leading edge of plate at 5^o, 11.2 KV voltage potential, and 1 chord plate spacing.

Again, these images need to be viewed with some caution. In Figure 4.5 the lower plate looks like it is at close to zero angle of attack but careful comparison of

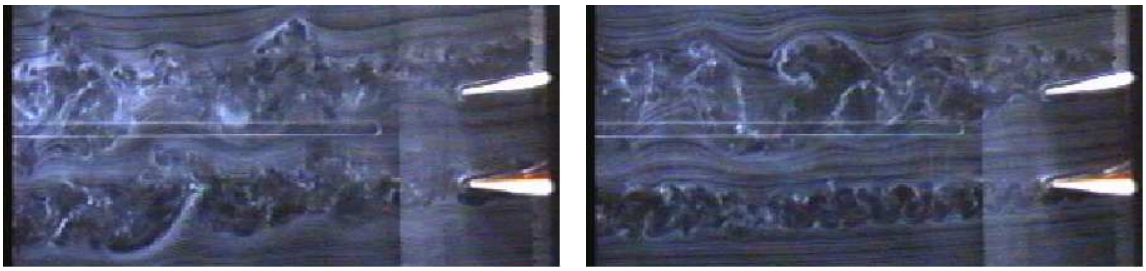

A: Actuator off B: Actuator on (lower plate)

Figure 4.5. One actuator at leading edge of plate at 10^o, 11.2 KV voltage potential, and 1 chord plate spacing.

the holders at the end of the plates shows that the angle of the two plates is the same. Sub-figure B clearly shows by the thinning of the wake that the flow is being reattached to the plate.

The last case shown is that of the greatest angle investigated. This angle was 16^o. The result is shown in Figure 4.6. Again, it is clear that the actuator helps to reattach the flow subsequently reducing the width and unsteadiness of the wake.

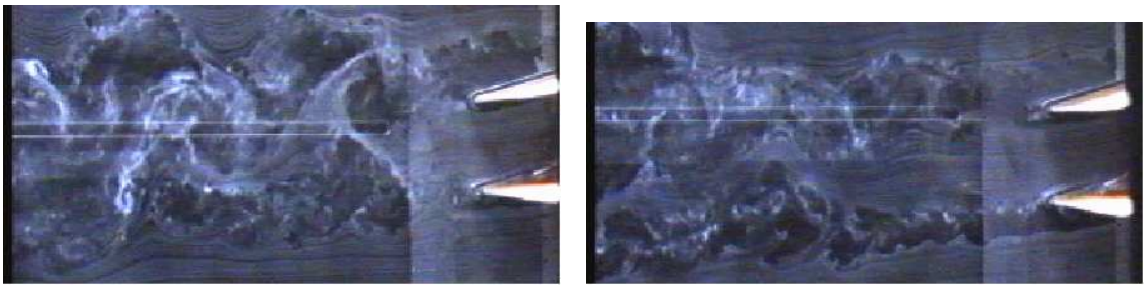

A: Actuator off B: Actuator on (lower plate)

Figure 4.6. One actuator at leading edge of plate 16^o, 11.2 KV voltage potential and 1 chord plate spacing.

As a side note, viewing the flow visualization for the 10 and 16 degree angles of attack, the thinning of the wake of the actuated blade appeared to affect the wake of the unactuated blade. More than likely, there was some degree of communication or cross-forcing of the wake structures that was reduced when the strength, or width, of the one wake was reduced by the actuator.

The previous results were very promising and sufficient to return to the hot-wire

measurements to quantitatively investigate the wakes. The stream profiles for these cases however proved to be difficult to obtain. As mentioned in Section 2.3, there were long times associated with taking the individual wake profiles. The individual profiles took close to 10 minutes, thus making the full set of stream profiles take close to two hours to perform. Half of this time the plasma actuator would be in use. The actuators lasted anywhere from around 5 to 20 minutes, so the full set of profiles could not be completed before the actuator burned out. Because each actuator was hand made, it was thought that they would be too inconsistent to replace after each individual wake profile to complete the set of stream profiles. Different thicknesses of Kapton were tried to increase durability and overcome this problem. Up to three layers of 2 mil (0.051 mm) were tried, which was used for the flow visualization images previously shown. Also a single layer of 5 mil (0.127 mm) Kapton was tried.

Though increasing the Kapton thickness in some cases helped, other problems with the pliability of the thicker Kapton were sometimes encountered. Adhesive problems with the copper tape also developed. Using a flat plate and orienting the actuator on the leading edge caused a very sharp turn of the copper tape over the edge of the plate. When used for long periods of time the adhesive would heat up and start to fail. This would allow the copper tape to start to separate from the Kapton and cause the actuator to fail. Because it was not possible to complete the measurements needed to validate the setups that, based on the flow visualization, were working the implementation of these for the moving-wake generator did not seem feasible. Thus a new approach was needed. The new approached used actuators made from factory copper clad, FR4 material printed circuit boards.

4.2 Configuration 3

Configuration 3 was the first configuration to test the copper clad, FR4 material printed circuit boards. As detailed in Section 2.5.3, the copper was machined off on a LPKF CNC machine leaving only the electrodes and leads for wire attachment. Electrodes were left on both sides of the PC-board to use the FR4 material as the dielectric material. Investigations of the configuration used both flow visualization and hot-wire measurements. The results of which are presented in the following subsections.

4.2.1 Flow Visualization

As with Configuration 2, flow visualization was chosen as the starting point for the experiments. Some representative flow visualization results will be presented. The results presented will be for 3 different angles of attack at two different voltage potentials. The voltage potential varied due to a change in the length of the actuator electrode.

Changing the actuator length changed the highest voltage potential that the system could maintain between the electrodes. Using the longer electrode, the system could only achieve a voltage potential of 8.40 KV. Whereas, with shorter electrodes, the system could achieve a potential of 11.2 KV. Again these potentials were produced by using the two channels to supply two separate triangle waves to the electrodes. This voltage limitation was a result of changing the powering system for the plasma actuator. The original desire with the new setup was to match the output voltage used with the previous setup, which was two triangle waves of 11.2 KVpp. The new setup could achieve this but drew considerably more current, between 4.5 and 5 amps depending on how long the actuator had been running.

Upon switching to the PC type actuator, and seeing the initial flow visualization results, it was decided to return to the original idea of starting with an attached flow and using the actuator to separate it. To this end, the angle of attack was reduced, as compared to the previous tests, to range from -3 to -7 degrees. Positive angles of these were also tried but were found to be less effective. The main reason for the choice of the negative angles was to have the upper plate be the one with the actuator and stay with the concept of separating the flow. Because of the non-symmetric leading edge, to have the plates at a positive angle of attack, relative to the flow, they would have to be flipped over and swapped. Recall from Section 2.5.3 that in this configuration, since the plate itself is being used as the dielectric material, plasma will form on both sides of the plate, thus inducing two flows, one upstream and one downstream. As with the airfoils and the previous flat plates, the upstream flow induced by the plasma was in the channel created by the two plates, thus again working to block the main flow from entering the channel.

Recall from Section 2.4 that the active edge of the plasma actuator of the PC design type could not be manufactured on the leading edge of the plate. Choosing electrode widths of 1 in. (2.54 cm), forced the active edge of the plasma actuator to be moved to the mid-chord location. One experiment was done to see if changing the location of the active edge of the electrode would be beneficial. To do this, what is considered the lower electrode was shortened to 0.50 in. (1.27 cm). Doing this shifted the active edge to the 1/4 chord location. The end result was not as effective as having the active edge at the mid-chord location. Part of the reason for this is the detrimental effect of shortening the width of the lower electrode[17]. So the 1.0 in. (2.54 cm) actuator width was returned to and was used for all of the following results.

As before, shown in Figure 4.7 is an 'off/on' comparison. The case shown is the negative -3^o case with an 8.0 x 1.0 in. (20.3 x 2.54 cm) lower electrode. Comparing the wakes of the upper plate in sub-figure A and B shows that there is an effect of the actuator. As opposed to the previous effects of narrowing the wake, the wake of the upper plate in this case is distinctly wider.

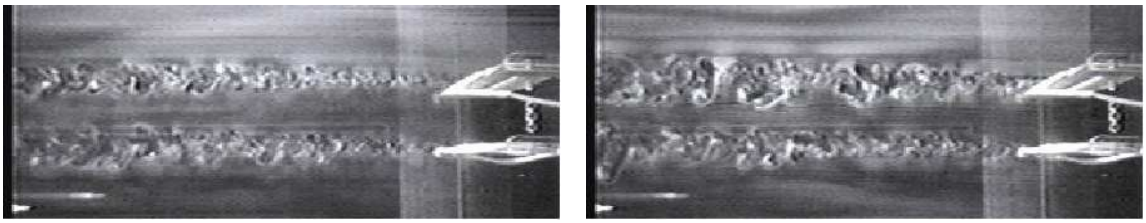

A: Actuator off B: Actuator on (upper plate)

Figure 4.7. -3^o, 1 chord plate spacing, and 8.4 KV maximum voltage potential case.

The -5^o case shown in Figure 4.8 shows some widening of the wake but also some large unsteady regions. These regions seem to distort the wake. On average, these distortions could show up as an even wider wake in a mean hot-wire profile.

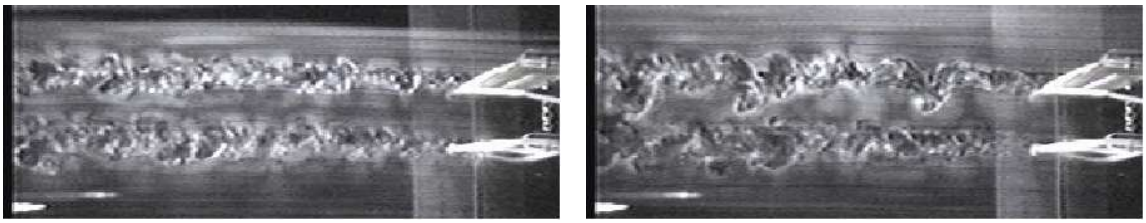

A: Actuator off B: Actuator on (upper plate)

Figure 4.8. -5^o, 1 chord plate spacing, and 8.4 KV maximum voltage potential case.

This last case shows some even more unsteadiness in the upper wake. In Figure 4.9 it can be seen that the amount of interaction between the two wakes is increased in the 'on' case in addition to the unsteadiness of the wake.

Repeating the three previously shown angles of attack with the 4.75 in (12.07 cm) electrode gives the following results. For the -3^o case, Figure 4.10 showed an even greater effect than the previously seen -3^o case with the lower voltage potential

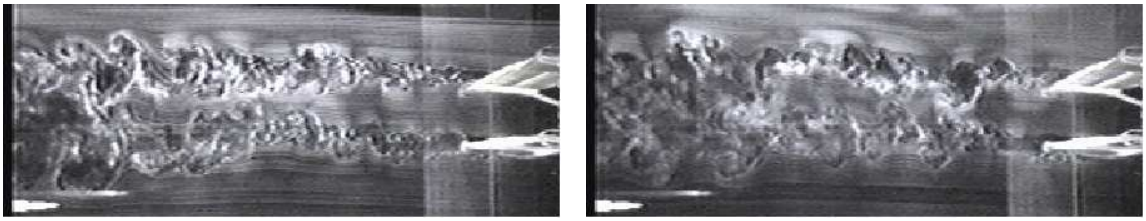

A: Actuator off B: Actuator on (upper plate)

Figure 4.9. -7^o, 1 chord plate spacing, and 8.4 KV maximum voltage potential case.

shown in Figure 4.7. The upper wake here is much wider and appears very unsteady. So much so that the wakes of the two plates begin to interact, whereas previously there was a significant calm region between the wakes. Note again that the plasma actuator was still on the upper plate in the figures.

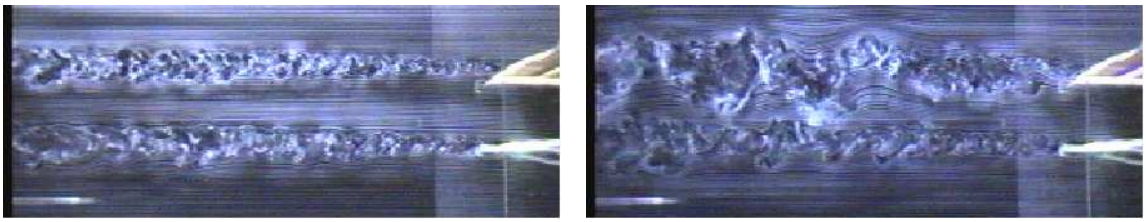

A: Actuator off B: Actuator on (upper plate)

Figure 4.10. -3^o, 1 chord plate spacing, and 11.2 KV maximum voltage potential case.

As with the last case, the actuator effect is very apparent and much more pronounced than in the previous -5^o case. The upper wake in Figure 4.11 is again wide and very unsteady. Although, when compared to the higher voltage potential -3^o case, there really is not much of an improvement, thus making the relative difference between the 'off' and 'on' case less.

This last figure, Figure 4.12, again shows an improvement over the lower voltage case. The wake width and unsteadiness, by eye, does appear to be the greatest in this case but again, the relative improvement when compared to the higher voltage -3^o case seems to be less.

As before, all of these flow visualization results were very promising and a more

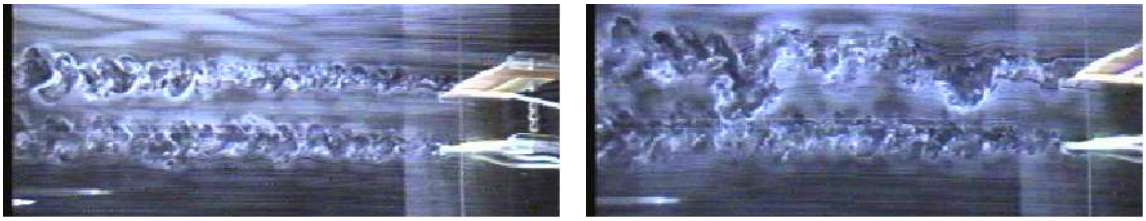

A: Actuator off B: Actuator on (upper plate)

Figure 4.11. -5^o, 1 chord plate spacing, and 11.2KV maximum voltage potential case.

A: Actuator off B: Actuator on (upper plate)

Figure 4.12. -7^o, 1 chord plate spacing, and 11.2 KV maximum voltage potential case.

quantitative investigation would now be conducted using a hot-wire probe. This would give better spanwise mean and RMS quantities at the different downstream chord locations, as opposed to the instantaneous results shown in the previously discussed flow visualization images.

4.2.2 Hot-Wire Measurements

Presented here are the results from the hot-wire measurements following the flow visualization experiments of Configuration 3. First to be presented are the results that reflect the flow visualization experiments for the negative -3^o angle of attack cases. These include the cases of 1 and 1/2 chord plate spacings.

Based on the greatest relative improvement seen using the flow visualization, the starting point for the quantitative investigations using the hot-wire was chosen to be the 11.2 KV voltage potential, -3^o angle of attack, and 1 chord plate spacing case shown in Figure 4.10. This was decided on to minimize the size of the nominal disturbance caused by the passive plate and the potential problems that could be

caused by turning the flow more with the higher angles of attack. Also there were concerns with the discreetness of the disturbance propagation across the test section for the application of the moving-wake generator. The lower angle could allow more plates to be used which would reduce the discreetness.

The first set of stream profiles shown in Figure 4.13 clearly shows the effect of the actuator. The individual wake profiles shown were normalized by an average of 10 points, 5 points on either end of the wake profiles shown in the figure. The probe position was normalized by the plate chord length. It is apparent from Figure 4.13 that there is a still a fairly large area of undisturbed flow in between the two plates. These results show that the actual range of disturbed region caused by the actuator was not as great as suggested by the flow visualization results shown earlier. That statement is based on the hot-wire data at the 3^{rd} and 4^{th} downstream chord locations. At these locations there is no indication of the large turbulent region stretching to the neighboring wake that appeared in Figure 4.10, the earlier corresponding flow visualization result.

However, in terms of the application of the moving-wake generator, the idea seemed to be working in that at 5 chord lengths downstream when the actuator was turned 'on', the region of undisturbed flow between the blades decreased to almost zero. The desire though was to have more wake interaction in the case of having the actuator 'on'. According to Figure 4.13, the 1/2 chord spacing should be enough to keep the wakes from interacting in the case of having the actuator 'off', but have them significantly interact when the actuator was turned 'on'. Therefore, as a second attempt, the space between the plates was reduced to 1/2 chord and the stream profiles redone.

The new spacing was enough to keep the wakes from interacting in the unactuated case as expected, but the structure change in how the wakes decayed and the effect

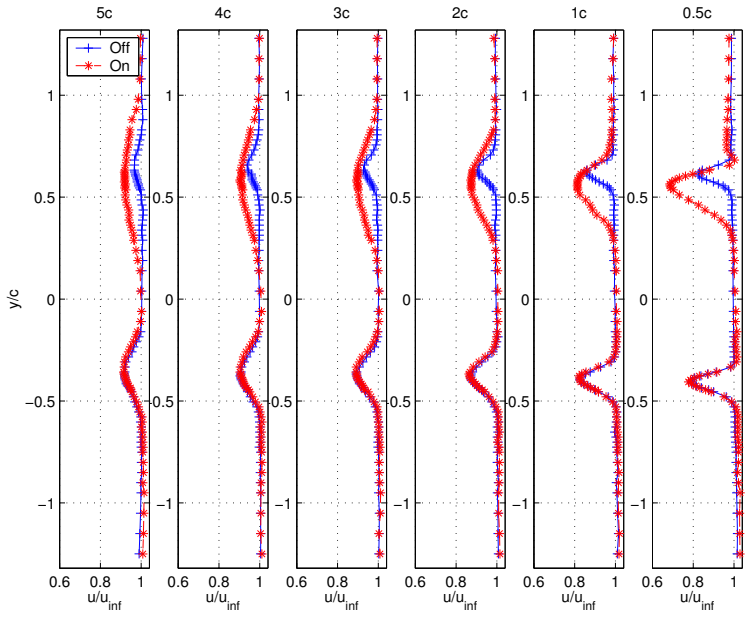

Figure 4.13. Stream profiles behind two flat plates at an angle of attack of -3^o with a plate spacing of 1 chord.

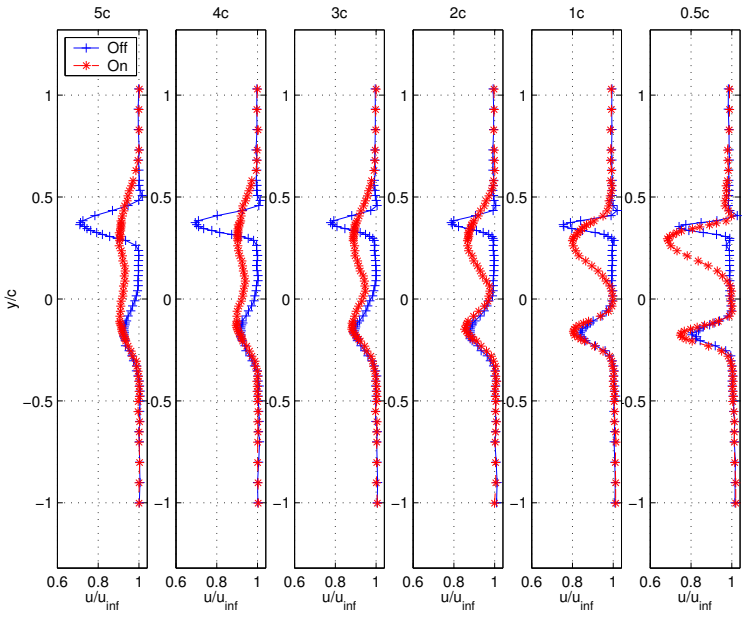

Figure 4.14. Stream profile behind two flat plates at an angle of attack of -3^o with a plate spacing of 1/2 chord.

of having the actuator 'on' was not anticipated. Notice in Figure 4.14 that the top wakes in the unactuated case decay very slowly with down stream location, whereas the lower wakes, simply by eye, appear to decay as the earlier results did. Contrarily, when the actuator is turned 'on' the rate of decay seems to increase.

To better illustrate the decay of the wakes, it was desired to plot the fraction of the free-stream velocity of the minimum velocities behind the plates against the downstream location. Before doing this it was necessary to check if the wakes were self-similar. As was done with the airfoils, a set of similarity plots were constructed for the -3^o angle of attack, 1 chord plate spacing case of Configuration 3 shown in Figure 4.13. The plots for the actuator 'off' case are shown in Figure 4.15 and the plots for the actuator 'on' case are shown in Figure 4.16. These plots show that the wakes are self-similar. The disagreement of the data points for the 'Upper Peaks', meaning the upper wakes, near the free-stream is believed to be caused by a cascade affect. Recall

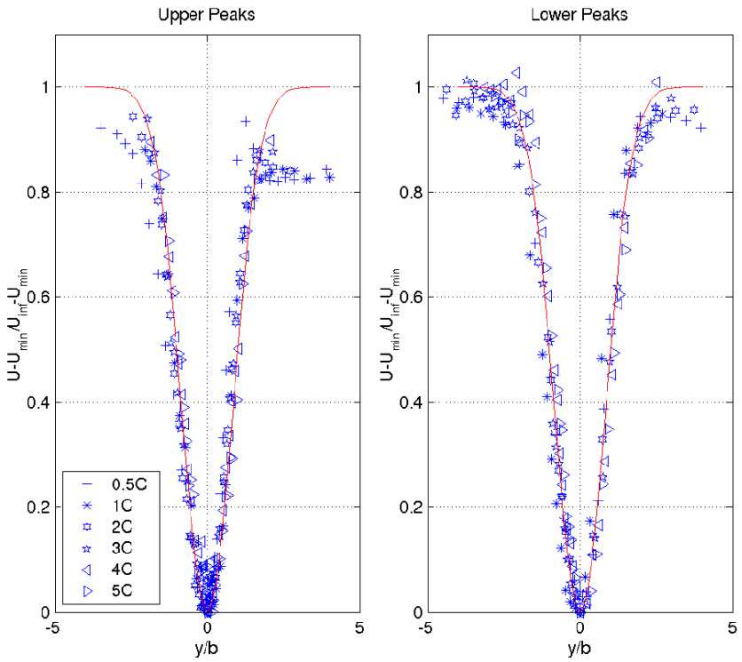

Figure 4.15. Similarity plot for two flat plates at an angle of attack of -3^o with a plate spacing of 1 chord and the actuator 'off'.

that the flow is being turned towards the upper plate because of the negative angle of attack of the two plates. These plots again have the Gaussian distribution depicted by Equation 3.1 added for comparison.

The similarity plots showed that the wakes are self-similar so the fractional velocity deficits for the two different cases were plotted together. Figure 4.17 shows this result at the different downstream chord locations. Each velocity deficit was normalized by it's respective free-stream average value. Plotted with these are some theoretical trends of the form of Equation 3.2, which is reasonable based on the self-similarity of the wakes. The upper subplot in Figure 4.17, corresponding to the upper plate with the plasma actuator, shows that the wakes of most of the cases shown decay as expected.

The effect of the actuator in these cases is to simply change the starting point of the decay. The trend still follows the form of Equation 3.2. The A coefficient in

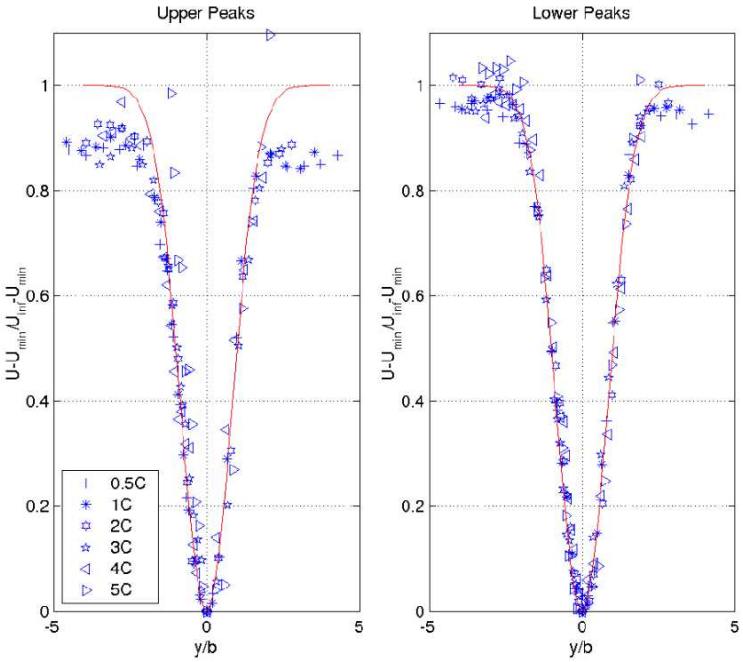

Figure 4.16. Similarity plot for two flat plates at an angle of attack of -3^o with a plate spacing of 1 chord and the actuator 'on'.

Equation 3.2 is less for the cases with the actuator 'on'.

The lower subplot in Figure 4.17, corresponds to the unactuated plate. This shows that the actuator had little effect on the wakes behind the lower plate in all of the cases.

The only case that does not follow the trend is the 1/2 chord plate spacing with the actuator 'off'. This seems to imply a cascade effect, caused by the turning of the flow because only the upper wake is being effected. Recall that the flow is being directed towards the upper plate because of the angle of attack of the plates. The use of the actuator seems to eliminate this cascade effect because the decay trend closely matches the 1 chord plate spacing case with the actuator 'on'.

The pressure transducer happened to use a carrier frequency of 5.0 KHz, the same frequency being used for the plasma actuator. The pressure transducer readings, while the actuator was in use, were affected. It was decided to try a slightly higher frequency

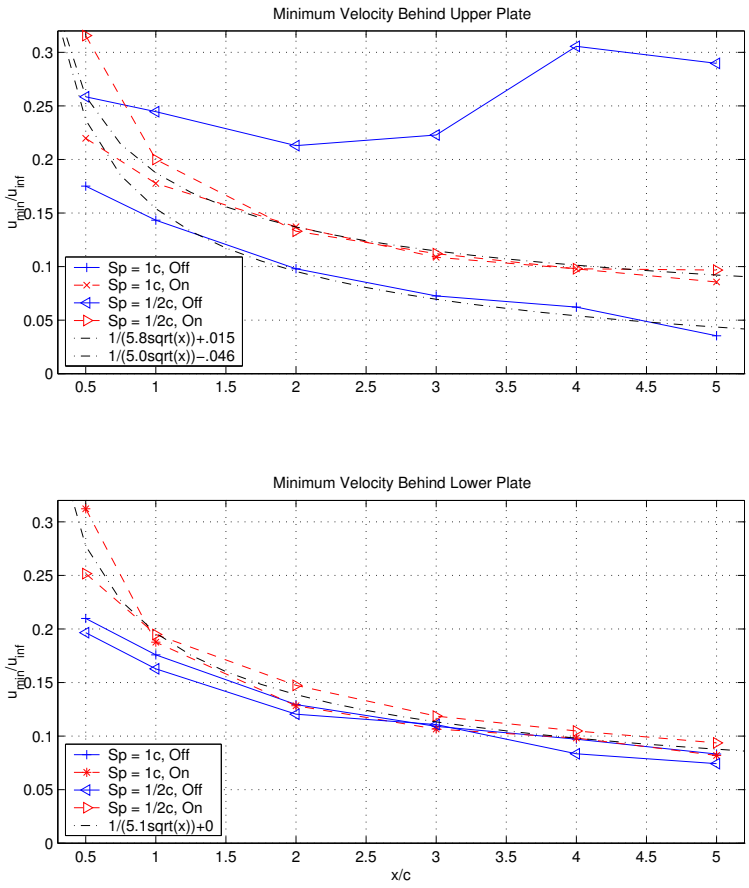

Figure 4.17. Comparison of wake decay for the -3^o angle of attack with 1 and 1/2 chord plate spacings at 5.0 KHz frequency.

of 5.5 KHz for the plasma actuator to avoid the problem. Prior to this test, a 5.5 KHz sinusoidal wave form was accidentally used instead of the triangular wave. The velocity deficits for the two 5.5 KHz frequency cases are plotted against the 5.0 KHz case 1/2 chord spacing case just shown. This result is shown in Figure 4.18. This figure was presented, even though the test frequencies were not exactly the same, to help establish the confidence in the repeatability of this configuration. Figure 4.18 shows that the small change of frequency and the wave form had little effect on the result.

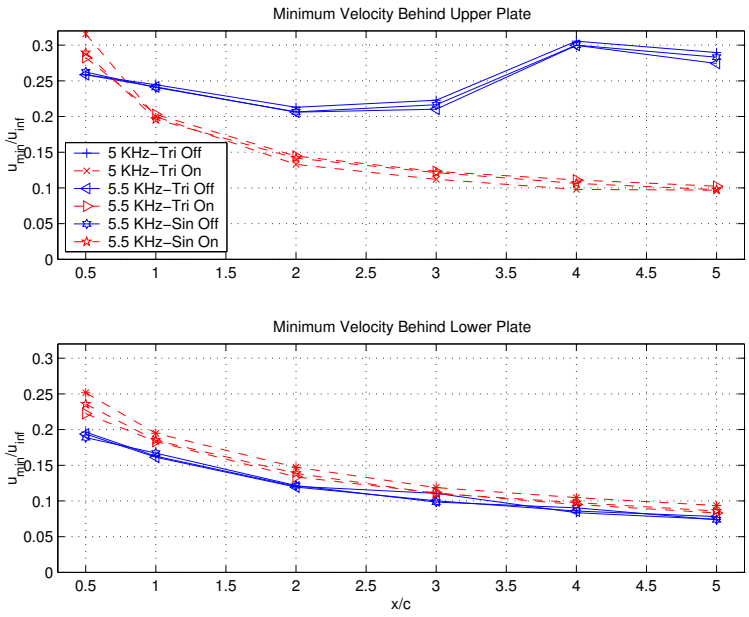

Figure 4.18. Comparison of wake decay for the -3^o angle of attack with 1/2 chord plate spacing at 5.0 KHz and 5.5 KHz frequencies.

Changing the frequency did not help the problem of affecting the pressure transducer. The main function of the pressure transducer and Pitot probe was the calibration of the hot-wire. Since the calibration took place with the actuator 'off', the pressure data from the Pitot tube taken during the wake profiles, while the plasma actuator was 'on', was just not used in any of the data reduction processes.

The change made in the setup that had the largest effect was that of the blade spacing, as shown in Figure 4.17. This suggests that, at least to a point, as the spacing between the blades decreased, the flow around the plates becomes more sensitive. The new result promoted the question of what the wakes look like if a third blade was added. Namely, is what was seen really a spacing or cascade effect and would the third wake resemble more the current upper wake, the lower wake or neither? To answer these questions a third blade was added. The addition of the third plate is what was is referred to as Configuration 4. Upon adding this plate, a new style of measurements were also performed.

4.3 Configuration 4

With Configuration 4, a new style of tests were started and the flow visualization experiments ended. The new tests were still wake profiles using the hot-wire and were what was referred to earlier as power profiles. This is because, instead of varying the downstream location, as in the case of the stream profiles, the actuator voltage potential was varied. This new style of testing helped to save time and broaden the investigation to finding results requiring less power and thus more feasible real world applications. In addition to time, this method was done in order to reduce actuator wear due to usage but still obtain workable results. The 5^{th} chord location was chosen for these experiments because of the actual distance that the 5^{th} chord location corresponds to, 10.0 in. (25.4 cm). Recall that this distance was the minimal nominal distance for the first intended application. Only the one chord location was thought to be necessary for these experiments because the wake structure at the 5^{th} chord location is a result of the upstream conditions, which are affected by the actuator.

After observing the affect of bringing the plates closer together, it was thought

that the same actuator effect on the wake could be achieved with less power. This again is also why the the power profiles started.

To this end, the maximum applied voltage was reduced. Shown in 4.19 are the results for the first set of power profiles on Configuration 4 with the reduced voltages. These were done at a 1/2 chord plate spacing and an angle of attack of -3^o. What is actually shown in the figure is the magnitude of the velocity deficit, expressed as a fraction of its local free-stream velocity, behind each plate, plotted against the applied voltage in KV. As indicated in the figure, the voltage potential was varied from zero to 6.2 KV. To illustrate the advantage of plotting only the minimum, the corresponding wake profiles are shown in figure 4.20. The later figure has the advantage in that it more clearly shows the widening of the wake dues to the effect of the actuator but in general, the figure is difficult to view. As such, the results of the power profiles will only have the minimum plotted as initially shown in Figure 4.19.

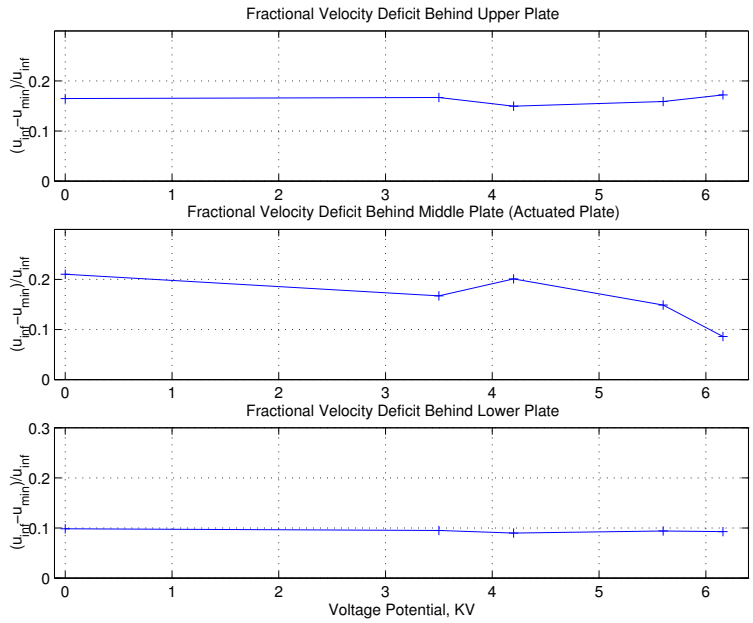

Figure 4.19. Power profile for 3 flat plates at an angle of attack of -3^o and 1/2 chord plate spacing.

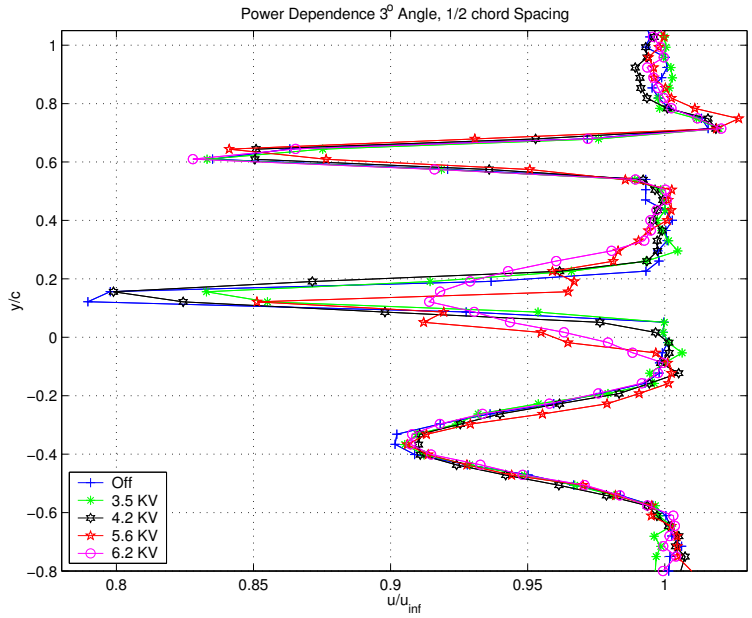

Figure 4.20. Corresponding wake profiles from power study for 3 flat plates at an angle of attack of -3^o and 1/2 chord plate spacing.

Based on the results seen thus far, it was decided to try another power profile at a 1/4 chord spacing. These results are plotted against the 1/2 chord spacing case shown in Figure 4.19 and can be seen in Figure 4.21. The 1/4 chord spacing case clearly shows a trend that was noticed in some of the new spacing cases. The noticed trend was that the sensitivity of the flow to the actuator power was decreased such that at the higher voltage potentials only marginal improvements were seen. This is beneficial in that a large effect could be achieved using less power and thus reducing the wear on the actuator, which would increase its longevity. The relative effect of the actuator between the actuator 'off' case and the maximum applied voltage case was less in this case as compared to the 1/2 chord spacing case. Also, this close spacing had a lot more undesired wake interactions. Based on these results, the 1/2 chord case was better but still worth trying to improve. As such, it was decided to reattempt the zero angle of attack orientation of the plates. The hope was that this

new close spacing effect would still be present and be able to be capitalized on.

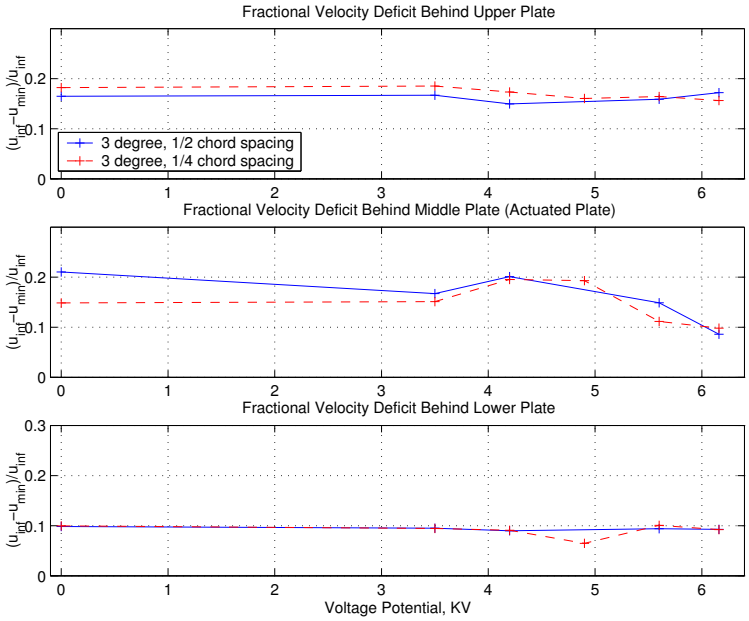

Figure 4.21. Power profile for 3 flat plates at an angle of attack of -3^o and various plate spacings.

4.3.1 0 Degree Angle of Attack

Keeping the with 3 plate configuration and closer spacing, the zero angle of attack cases were retried. With the plates at zero angle of attack, the wakes should be slightly narrower. With this in mind, it was decided to start the tests with a 1/4 chord spacing case, in addition to trying a 3/8 and 1/2 chord spacing case.

The results, in terms of the velocity deficits, are as follows. The first case of 1/4 chord can be seen in Figure 4.22. This shows a similar effect to what was seen with the 1/4 chord plate spacing -3^o angle of attack case in that the velocity deficit only slightly decreases, then momentarily increases, and then rapidly decreases.

The results for the 3/8 and 1/2 chord plate spacing cases are plotted against the 1/4 chord case for comparison and are shown in Figure 4.23. The results from the 3/8

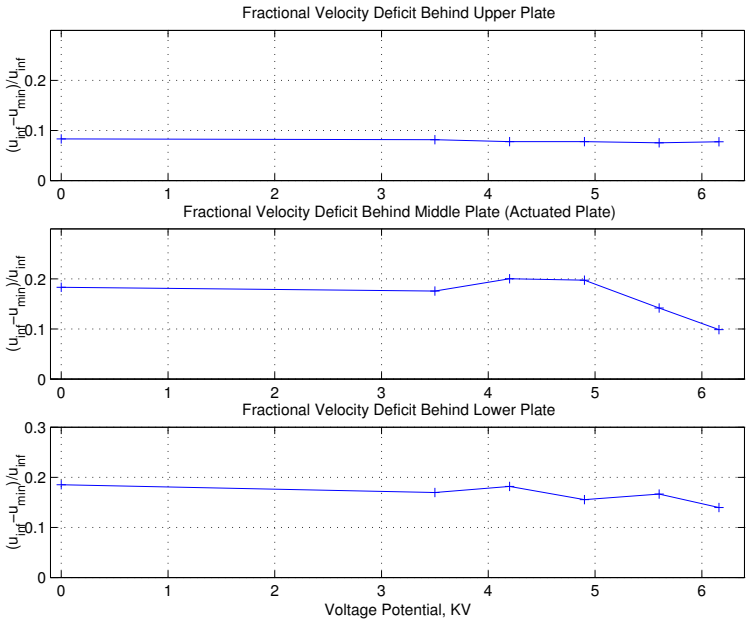

Figure 4.22. Power profile for 3 flat plates at an angle of attack of 0^o and 1/4 chord spacing.

chord spacing case do not look promising due to how sporadic they are but they do show promise in the relative difference for the 4.2 KV and 6.2 KV data points. The 1/2 chord result follows the trend of the 1/4 chord spacing case, at least for the center blade, in that at the lower voltage potential points, an increase in the wake deficit is first seen and then at the higher voltage potentials a rapid decrease of the wake deficit is seen. One explanation for the disagreement of the lower plate values is that the plate may have been bumped to a small angle of attack. Later tests remove this possibility by use a custom plate holder, see Section 2.5.5. Due to the similar affect of the plasma actuator, in terms of magnitude, seen on the different plate spacings, the wake widths were looked at to aid in choosing the optimum spacing.

Because the choice of plate spacing also depends on the downstream wake interactions, Figure 4.24 was constructed as a summary of the different spacings reflecting the wake interactions at the 5^{th} chord location. Shown in this figure are some selected

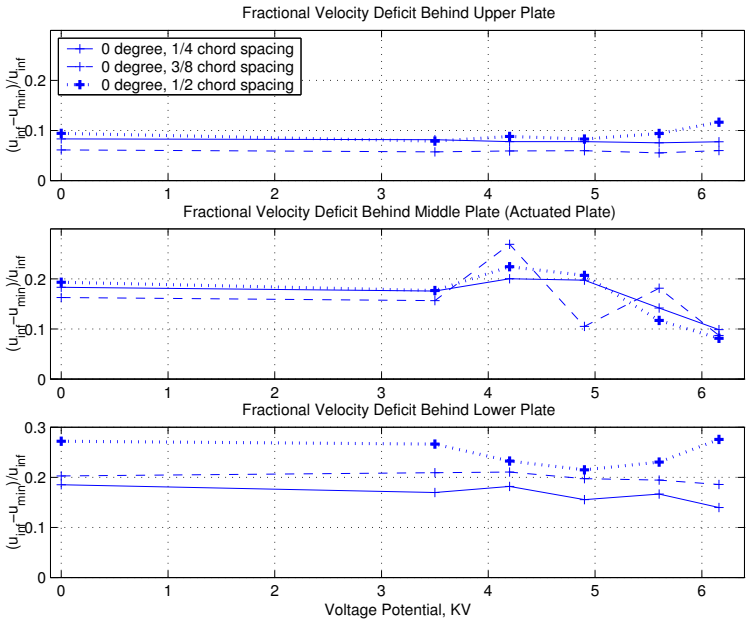

Figure 4.23. Power profile for 3 flat plates at an angle of attack of 0^o and various plate spacings.

cases of the different voltages for the three different spacings, recall that these were done at the 5^{th} chord location. The cases chosen were those with the actuator turned 'off', 4.2 KV potential, and the maximum voltage potential case of 6.2 KV. The reason for including the 4.2 KV case was that this case had the maximum but opposite effect of the maximum voltage case. One of the ideas considered here was instead of working between an 'off/on' case, the arrangement would operate between two different 'on' cases. Thus capitalizing on the maximum relative effect of the actuator and not relying only on the relative effect compared to the 'off' case.

From this data, the 3/8 chord case was chosen to be the case of study. This was based on the relative difference seen between the minimum and maximum value shown in Figure 4.23 for the middle plate and the wake interaction shown in Figure 4.24. There was no noticeable wake interaction for the 'off' case, and a small amount in the case with the maximum applied voltage. In terms of the discreetness of the

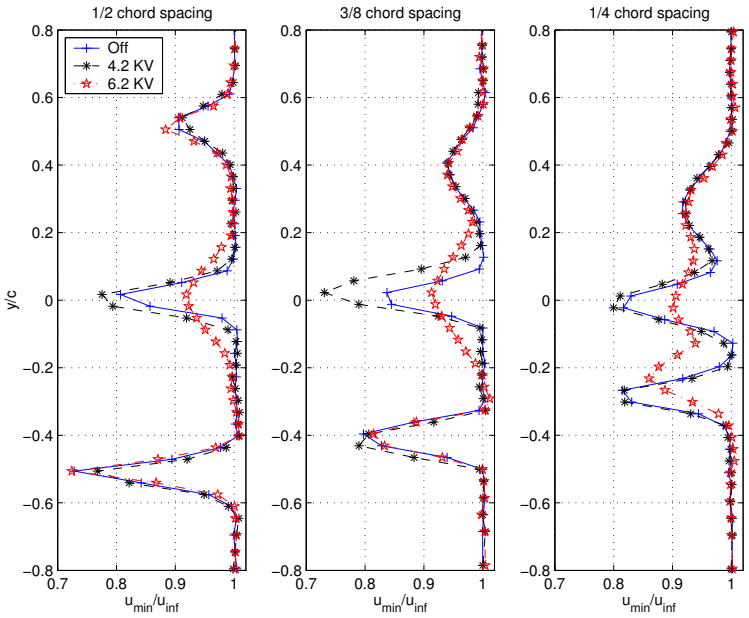

Figure 4.24. Summery of spacing effects at different applied voltage potentials.

moving-wake generator, this was thought to be the best choice. The results were not completely favorable for the 3/8 chord case in that the data points shown in Figure 4.23 looked scattered, but it showed potential.

To complete the test of the 3 plates at 3/8 chord spacing, zero degree angle of attack and 6.2 KV voltage potential, a set of stream profiles was done. These are shown in Figure 4.25. This reflects the positive results seen in the power profiles but also clearly shows that the three wakes are different in both the case when the actuator is 'off' and when it is 'on'. The discrepancies were thought to be due to the non-symmetrical leading edges of the top two plates and having a third plate that was slightly wider with a rounded leading edge. To try and eliminate the non-uniformity seen, a new set of symmetric plates were made and will be discussed in Chapter 5.

As before, a check of the wake structure of the stream profiles shown in Figure 4.25 was done by constructing a similarity plot. The reason for this was to help investigate

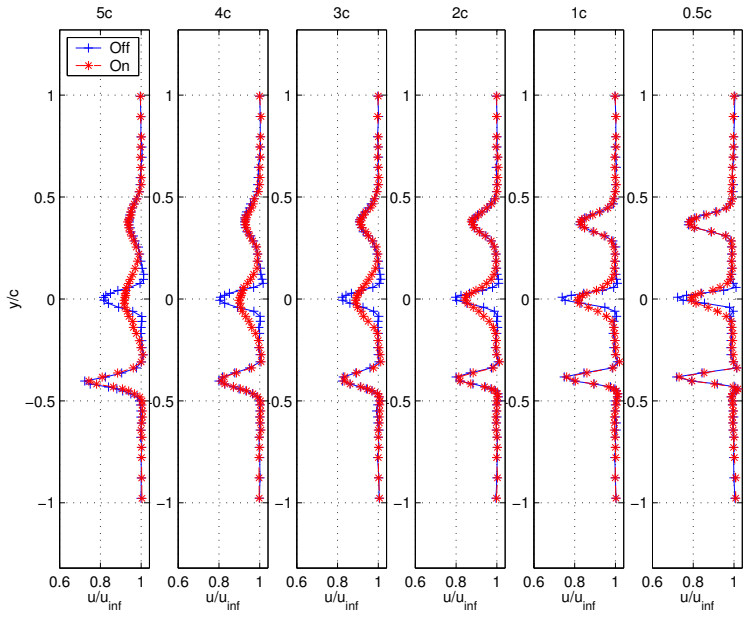

Figure 4.25. Stream profiles behind 3 plates zero angle of attack.

the differences seen in the three wakes and to verify that the wakes were self-similar so that other comparisons could be made. The results for the actuator 'off' case are shown in Figure 4.26 and the plots for the actuator 'on' case are shown as Figure 4.27. These plots show consistent agreement with theory, which implies that the wakes are self-similar even-though the stream profiles are different. These plots again have the Gaussian distribution depicted by Equation 3.1 added for comparison.

4.4 Comparison: Configuration 3 and 4 To Single Plate

The focus of this section is to compare Configuration 3 to Configuration 4. The reason this comparison does not include Configuration 2 is because the scope of the comparisons was confined to the hot-wire measurements, which could not be done for Configuration 2. Some comparisons within Configuration 3 have already been made showing the change in wake structure caused by changing the plate spacing. This was discussed in Section 4.2.2. But the question still remains of how this compares to a

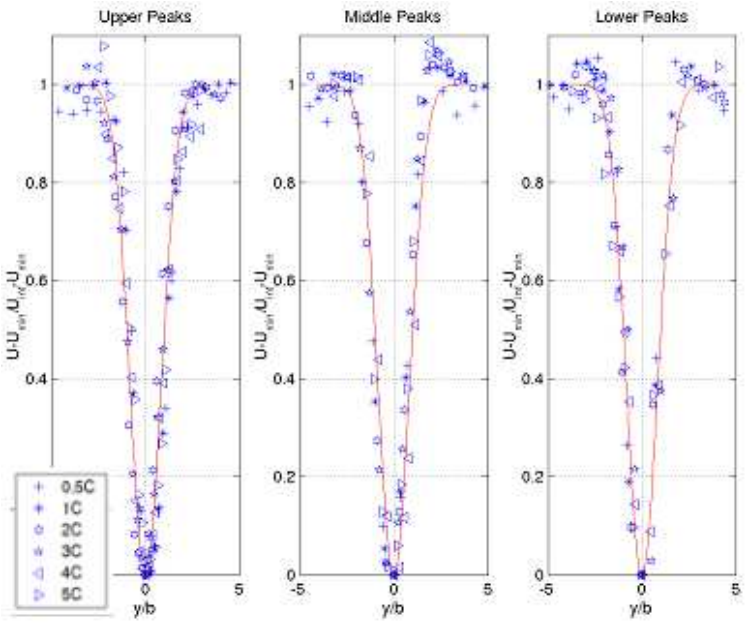

Figure 4.26. Similarity plot for three flat plates at zero angle of attack with a 3/8 chord plate spacing and the actuator 'off'.

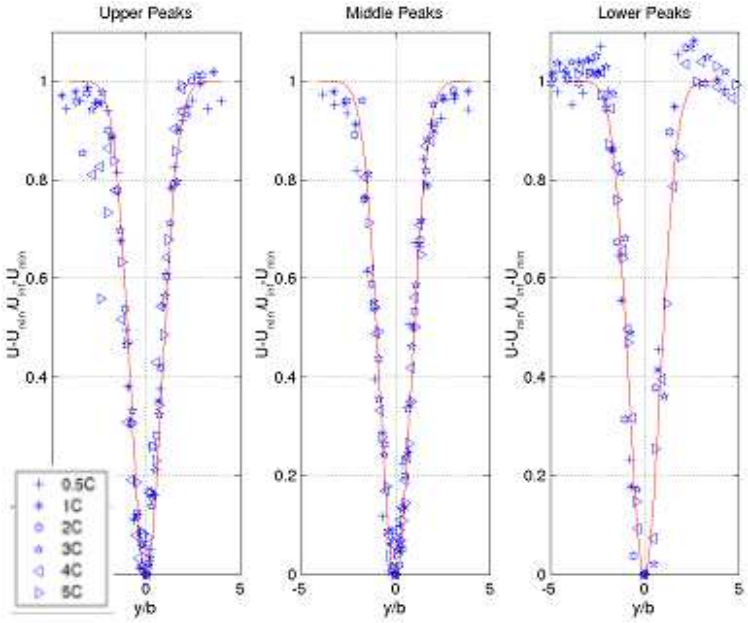

Figure 4.27. Similarity plot for three flat plates at zero angle of attack with a 3/8 chord plate spacing and the actuator 'on'.

single plate and to Configuration 4. Also, which result is the best so far in terms of the moving-wake generator.

Before comparisons could be made to a single plate, stream profiles behind a single plate had to be done. The plate chosen to be used as the single plate, was the previously used middle plate of Configuration 3, which is the same as the lower plate of Configuration 2. A drawing of this setup is shown in Figure 4.28

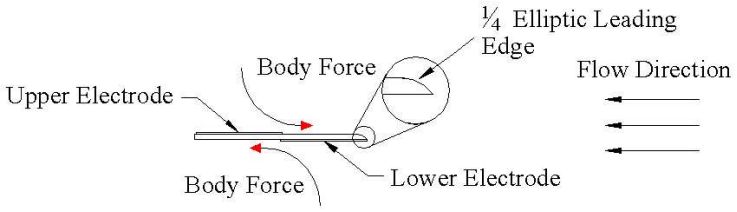

Figure 4.28. Setup for single plate with 1/4 elliptic leading edge.

Shown in Figure 4.29 are the stream profiles behind the single plate. Notice here that the actuator is widening the wake and causing a larger velocity deficit. At the 5^{th} chord location, the wake is not symmetric. This is most likely due to the fact that the actuator is inducing a flow on both sides of the plate. In this case, the upstream induced flow is on the top side of the plate, whereas the downstream induced flow is on the bottom side of the plate. This agrees with Figure 4.29 in that if the flow is forced upstream, downstream of that a larger deficit would exist, and vise-versa. The asymmetry could also be partially caused by the asymmetry of the leading edge of the plate. Recall that the plate used for this test had a leading edge in the shape of a 1/4 ellipse that curved away from the lower electrode of the plasma actuator, as discussed in Section 2.5.3. In this plate orientation, the upper and lower electrodes are on the top and bottom surfaces of the plate, respectively.

This widening of the wake and the increasing of the velocity deficit behind the plate was seen before in the -3^o angle of attack with 1 chord spacing case shown in

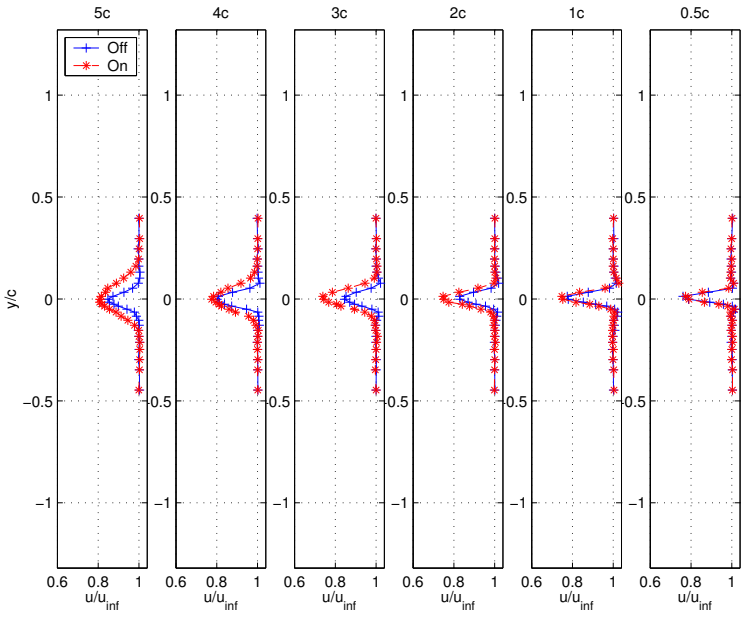

Figure 4.29. Stream profiles behind single plate with 1/4 elliptic leading edge.

Figure 4.13. This reinforces the idea that the two plates in the 1 chord spacing case were acting independently.

Once the stream profiles behind the single plate were done it was important to compare the relevant results, which would be to the zero angle of attack cases of Configuration 4. The comparison shown in Figure 4.30, which is a comparison of the fractional velocity deficits behind each of the plates of the Configuration 4, zero angle of attack, 3/8 chord plate spacing case shown in Figure 4.25, to the zero angle of attack, single plate case shown in Figure 4.29. As was done earlier with the different spacings of Configuration 3, the velocity deficits where expressed as fractions of the respective local free-stream velocities. In Figure 4.30 there are three subplots. Each subplot corresponds to one of the three plates in Configuration 4 and shows the deficits for that plate. The unactuated (top and bottom) plates are included to show any affect that the actuator may cause on the neighboring plates. The top subplot shows

that the wake acts like the wake behind a single plate, and is marginally effected by the use of the actuator. In the middle subplot, the actuator 'on' case for the single plate is included to show the contrast of the effect of the actuator, which seemed to be caused by the close spacing of the plates, as reflected in the stream profiles of Figures 4.13 and 4.14. The bottom subplot again shows that the actuator has little to no affect on the wake, but the wake does not seem to act like a single wake. One reason for this could be the difference in leading edges. Recall from Section 2.5.4 that the plate added to Configuration 3 to make Configuration 4 had a symmetrically rounded leading edge and was slightly wider than the other two plates.

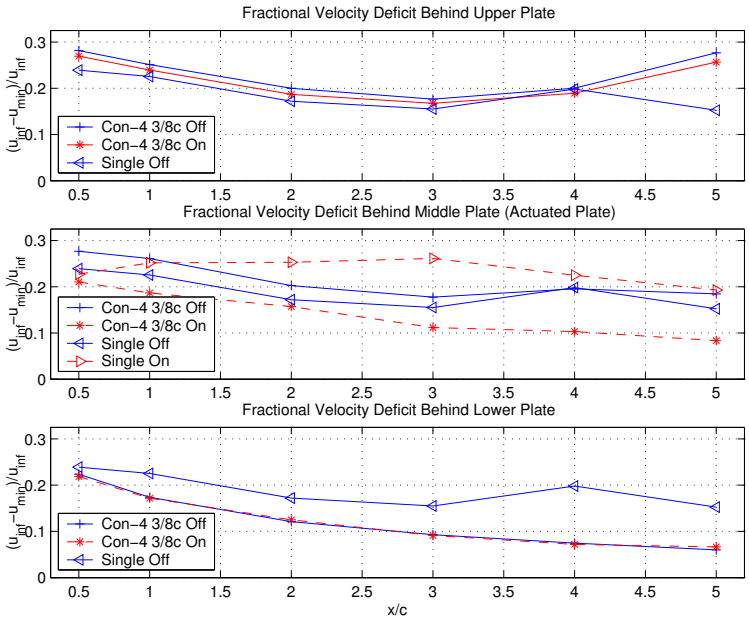

Figure 4.30. Comparison of stream profiles to single wake case with the 1/4 elliptic leading edge.

Although the wakes of the different configuration can not be compared directly without further non-dimensionalizing, due to the differences in geometry, the magnitudes of the actuator effect can be compared. The important thing to keep in mind in terms of the first intended application, is that the difference in minimum should

be the greatest at the 5^{th} chord location. This way, pulsing the actuator 'on' and 'off' would cause a large velocity fluctuation whose frequency can be controlled by the frequency of the pulsing.

To summarize the results thus far, and better illustrate the actuator effect at the 5^{th} chord location, Figure 4.31 was constructed to compare the magnitudes of the actuator effect at the 5^{th} chord location. This figure shows the value of the difference of the velocity deficit between the 'off' and 'on' cases for the wake profiles. Below the figure is a table that has a description that corresponds to the number designation in the figure. This figure contains a large amount of information in that it summarizes all of the stream profile cases and all of the power profile cases done thus far using the plasma actuator.

Many conclusions can be drawn from Figure 4.31. For instance, the -3^o angle of attack, 1/2 chord spacing, cases of Configuration 3 are clearly the best in terms of the magnitude. However, keep in mind that the voltage supplied to the actuator for these cases was 11.2 KV. This voltage potential has the drawback of reducing the life of the actuator.

Also, the addition of the third plate making Configuration 4 may have hindered effect of the actuator but the degree of this is unknown because the voltage potential and was also changed between the two configurations. This effect is seen by comparing Designations 3 and 6. In the comparison of Designations 6 and 7, the reduced spacing hurt the performance of the actuator.

Comparisons of Designations 8, 10, and 11, also show the benefit of the wider spacing. However, based on the results of designations 2 and 3, this improvement is only beneficial to a point.

Lastly, comparing the results for Designations 9 and 10 shows some inconsistency in the result in that these two experimental setups were the same; the only difference

was how the data was gathered. The values in Designation 9 were obtained from a power profile, and the values for Designation 10 were from the velocity stream profile.

Over all, the results thus far have been favorable. The -3^o angle of attack, 1/2 chord spacing, cases of Configuration 3 have the best results but require more power, limiting the actuator life span, and have the potential to be more intrusive to the flow. The zero degree angle of attack cases of Configuration 4 show the most promise in terms of the effect for the power required and the intrusiveness on the flow. Based on the wake comparisons of Configuration 4 for the different spacings, the 3/8 chord case seemed to be the best and was chosen for the next set of experiments using uniformly produced flat plates. This is discussed in Chapter 5.

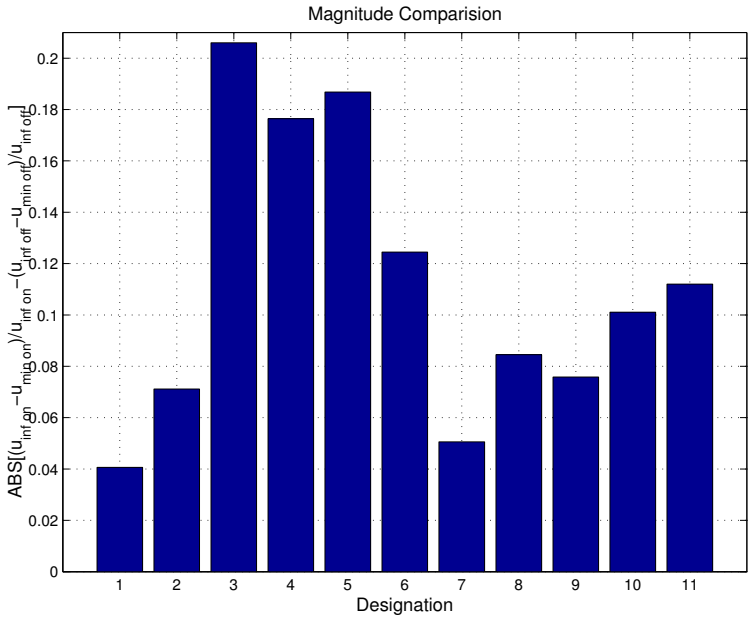

Desig.	Conf.	Angle (^{o})	Spacing (c)	Profile	V.P. (KV)	Note
1	-	0	-	Stream	6.2	S.P. 1/4 Elliptic L.E.
2	3	-3	1	Stream	11.2	
3	3	-3	1/2	Stream	11.2	
4	3	-3	1/2	Stream	11.2	5.5 KHz tri. wave
5	3	-3	1/2	Stream	11.2	5.5 KHz sine wave
6	4	-3	1/2	Power	6.2	
7	4	-3	1/4	Power	6.2	
8	4	0	1/4	Power	6.2	
9	4	0	3/8	Power	6.2	
10	4	0	3/8	Stream	6.2	
11	4	0	1/2	Power	6.2	

Figure 4.31. Summary of actuator effect at the 5^{th} chord location for all the stream and power profiles thus far.

CHAPTER 5

RESULTS: UNIFORM FLAT PLATES

After compiling the previous results and observing the sensitivity of the plates due to spacing and orientation, it was decided to repeat the experiments. This time however, using plates that were fabricated as uniform as possible. This was referred to earlier as Configuration 5. The intent with the new setup was to try to eliminate one of the variables contributing to the inconsistencies observed in the experimental results. As such, the plates were re-manufactured on a LPKF CNC milling machine designed for the manufacturing of prototype circuit boards. In addition to these plates, a new type of plate/actuator setup was made using the LPKF CNC machine and was referred to as Configuration 6 in Section 2.5.6. Configurations 5 and 6 will both be discussed in this chapter.

5.1 Configuration 5

The first investigation made using the new plates, was to check the uniformity of the wakes behind the plates. As the first experiment, each plate was assigned a letter, A,B, or C and wake profiles were done behind the plates at the 5^{th} downstream chord location. All six permutations of the letters A, B, and C, meaning the plate orders, were tested. The results of this are shown in Figure 5.1. If the setup was perfect and all of the plates were identical regardless of the plate order, the wake profiles would all be the same. It is apparent from this figure that some imperfections must still

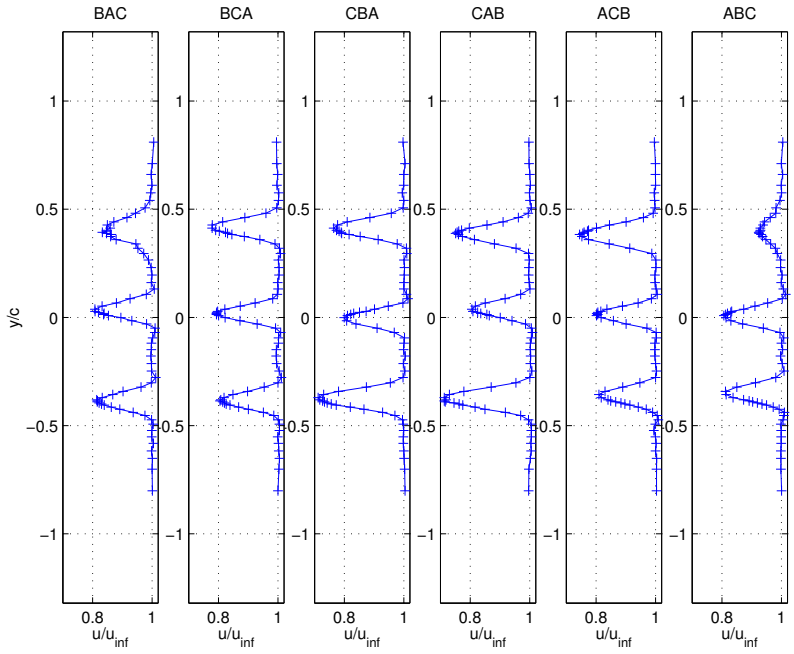

Figure 5.1. Investigation of wake dependence on plate order, uniform plates.

exist. None the less, the plate order of BCA was chosen for all of the future tests using these plates. This order case had the most uniform wakes in terms of minimum velocity and width.

Once the plate order was chosen, investigations into the actuator effect could be conducted. As before, to test the effectiveness of the actuator, power profiles were chosen as the starting point. These results are shown in Figure 5.2. The trend behind the middle plate is similar to those seen in Chapter 4, in that there was a small initial increase in the velocity deficit and then a substantial decrease. Note that the voltages used in the plot are all slightly larger than they should be and could not be corrected. The reason for this is because a 4 Ω resistor was placed in series with, but just before, the high gain transformers. This was done to improve the impedance-matching of the circuit. Because the current going to the transformers was not measured, the voltage drop across the 4 ohm resistor could not be calculated. As such, the voltages used in

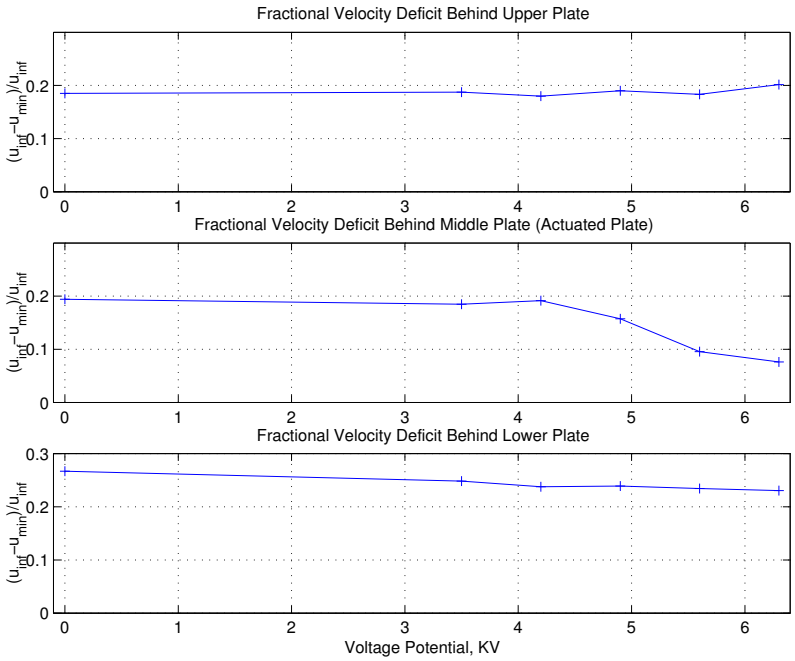

Figure 5.2. Power profiles for 3 uniform plates at zero angle of attack with 3/8 chord spacing.

the plot are the theoretical values without the resistor.

The addition of the resistor did enable the plasma system to obtain higher voltage potentials, as measured before the resistor. The degree to which this improved the system, in terms of the voltage potential at the actuator, was not determined.

After looking at some of the previous data it was decided to repeat the power profiles shown in Figure 5.2, but this time increasing the maximum voltage potential across the actuator to 7.7 KV. This was the new maximum voltage of the system with the 4 Ω resistor. This test was done to check earlier results that indicated a peak effect at a voltage potential lower than what the plasma system was capable of supplying. Also this second test was done to see if the previous chosen optimum voltage of 6.3 KV changed at all from the addition of the 4 Ω resistor. If the magnitudes of the velocity deficits shifted to a higher voltage value, meaning that actual velocity deficits decreased at the different voltage potentials, it would imply that the added 4

Ω resistor caused a noticeably lower voltage potential at the actuator, thus requiring a higher input voltage to obtain the same actuator affect. The new results are plotted against the old results for comparison and can be seen in Figure 5.3. The new results show very good agreement with the old results and confirm that the 6.3 KV potential is still the most efficient choice in terms of the affect and power requirement. The conclusion of this is that the added resistor does not noticeably reduce the voltage potential at the actuator, causing a change in the actuator effect.

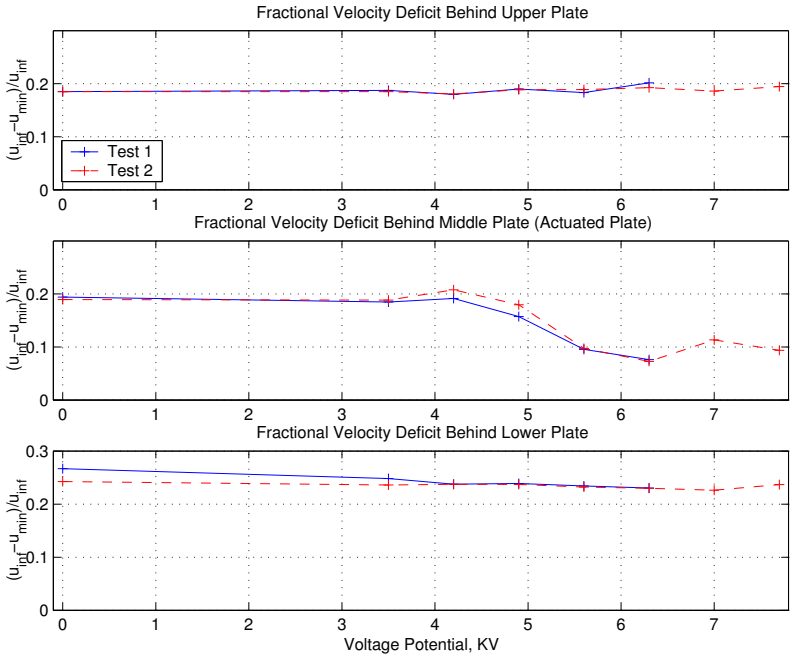

Figure 5.3. Extended power profiles for 3 uniform plates at zero angle of attack with 3/8 chord spacing.

Based on Figure 5.3, the 6.3 KV potential continued to be used for further investigations. This was because it had the greatest effect at this voltage and also based on the indication that the higher voltages seem to slightly affect the neighboring wakes, as seen in the upper and lower subplots in Figure 5.3. The next step was to do a stream profile investigation. This tests was conducted twice to check the repeatability of the results. The results for the first test are shown in Figure 5.4 and the results

for the second test are shown in Figure 5.5.

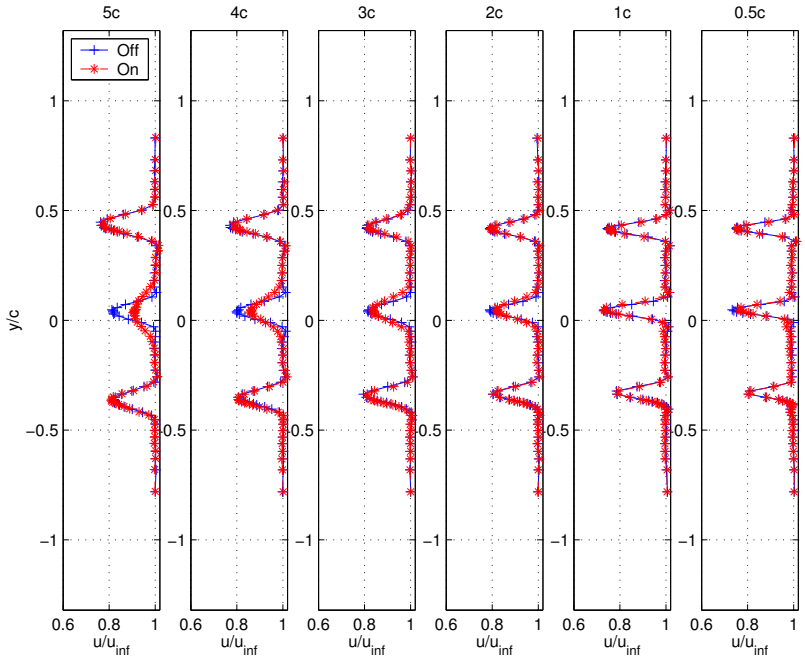

Figure 5.4. Stream profiles for first test of uniform plates.

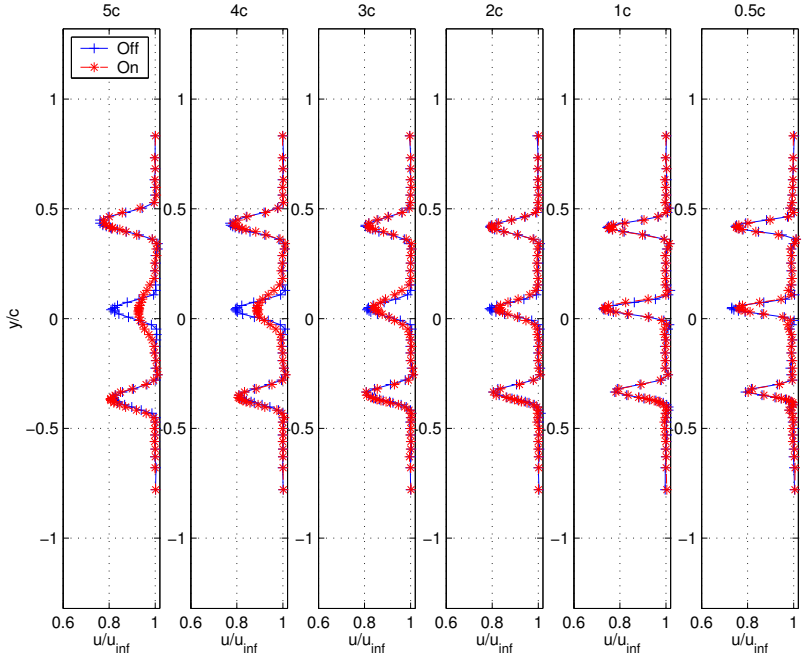

Figure 5.5. Stream profiles for second test of uniform plates.

To ease the comparison, the fractional velocity deficits of the wakes were replotted together in Figure 5.6. The results from the second experiment were slightly better than the first set in that at the 5^{th} chord location, the second test shows approximately 2 percent more of a velocity deficit. The deficits behind the other plates for both the 'off' and 'on' cases agreed well. Overall, the trends were similar to the 'off/on' cases shown previously and the results were deemed to be sufficient to try another setup, after comparing to a single plate.

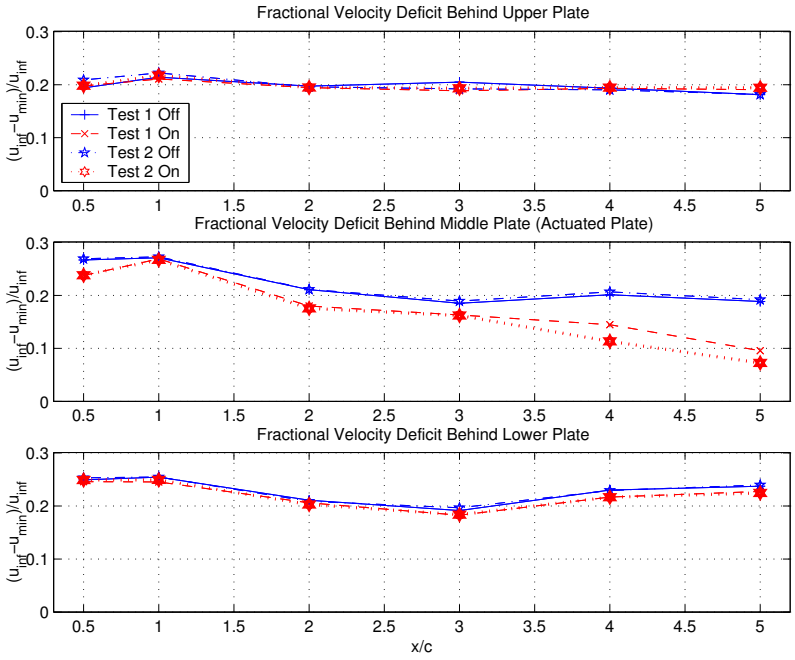

Figure 5.6. Wake decay comparison for the two sets of stream profiles.

5.1.1 Comparison: Configuration 5 To Single Plate

As with the last chapter, it was desired to compare the aforementioned results of Configuration 5 to a single plate. However, because the leading edges of the uniform plates were different than what was used in the previous experiments, the single plate tests had to be repeated, using one of the new uniform plates, before the comparison

could be made. The middle plate from Configuration 5 was chosen as the single plate because this was the plate that had been used for the plasma actuation in the experiments of Configuration 5.

Staying consistent with the tests of the last chapter, the only experiment conducted on the single plate was a set of stream profiles. The results of this can be seen in Figure 5.7. Contrary to the previous single plate results shown in Figures 4.29 and 4.30, the wakes of this new single plate resembled the wakes behind the actuated plate in the closely spaced 2 plate, 3 degree angle of attack, 1/2 chord plate spacing case of Configuration 3. This trend was also seen in the closer plate spacings of Configurations 4 and 5. The decay trend with the actuator 'on' was unexpected for the single plate because, up till now, this higher rate of wake decay for the actuated case was only seen in the close spacing test setups. Previously, this effect was thought to be solely a wake interaction effect caused by the plates' close spacings. This new result implies that the affect can also be dependent on, and caused by, the leading edge geometry.

To better illustrate how the wakes are decaying, as before, Figure 5.8 shows the fractional velocity deficits behind the 3 plates of Configuration 5, plotted against the single plate case. Contrary to the implications of the calm region between the plates shown in Figure 5.5, the trend in the velocity deficits behind the upper and lower plates imply some wake interaction or effect caused by the wakes. For the case of the upper plate the velocity deficit decays only slightly. For the lower plate, the velocity deficit initially decays but then starts to increase again as the wakes widen. These trends are much more pronounced than what the single plate case shows. The single plate, other than the change between the 1/2 and 1 chord downstream locations, show that the wakes decay more as expected, but still has the flatting with only a slight increase at the 4^{th} and 5^{th} chord location. The trends seen for the center plate

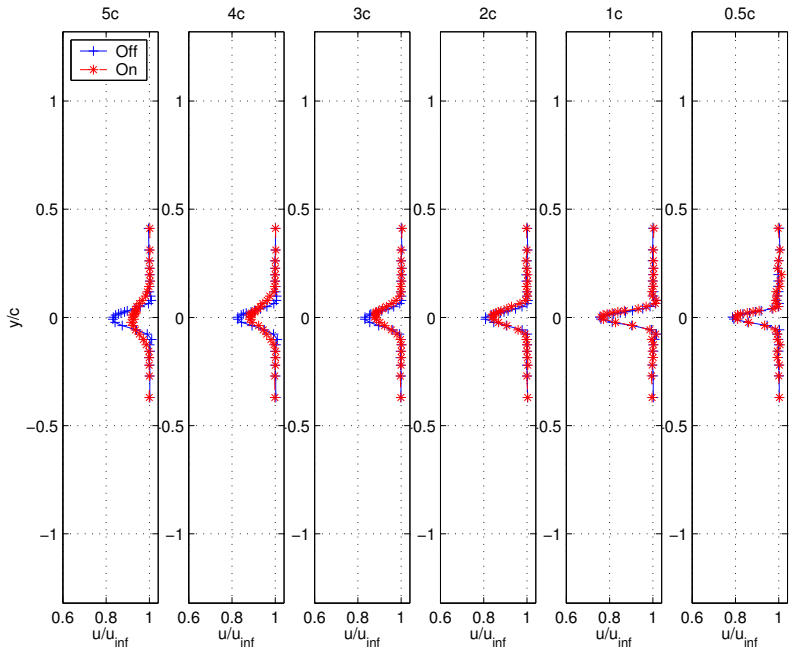

Figure 5.7. Stream profiles behind the new single plate with round leading edge.

are very similar, but the initial starting value is different. The actuator, for both the single and multiple plate case, produces a larger and more continuous decay for the actuated plate.

Summarizing the results for Configuration 5 and the single plate, Figure 5.9 shows the magnitudes of the actuator effect. Shown here are the results of the stream profiles and power profiles for the two tests of Configuration 5, along with the one single plate stream profile case. What this shows is that the results are generally repeatable. The magnitude of the velocity difference of the first stream profile test is 16.8 percent less than the average of the four similar cases, which was 0.112 with a standard deviation 0.013. Keep in mind that these values are fractions of the mean free-stream velocity at the 5^{th} downstream chord location. Compared to the average, the other points are within 6.8 percent. The single plate case was 11.0 percent less than the 0.112 average of the four data points. These results imply that the three plate setup is slightly

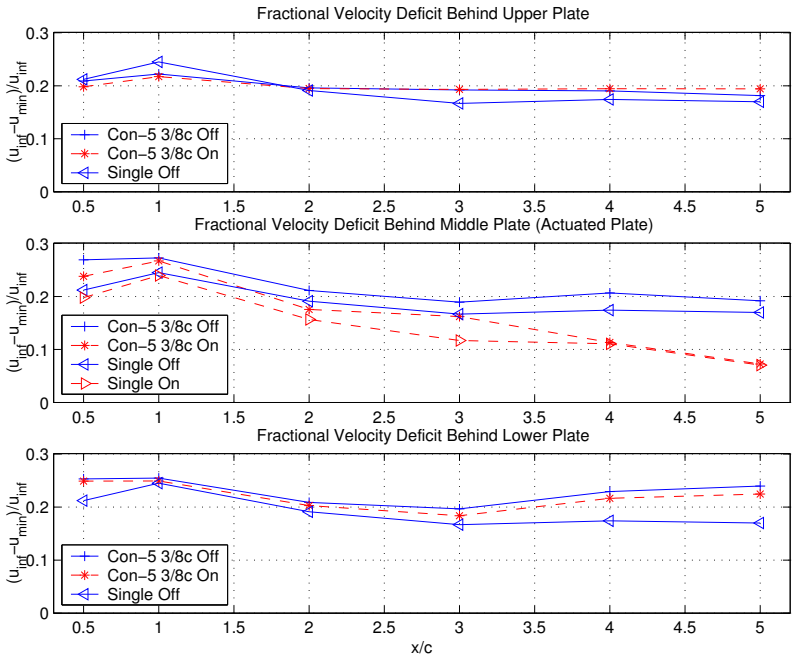

Figure 5.8. Wake decay comparison of Configuration 5 to a single plate with round leading edge.

better than the single plate, but with only one data point for the single plate it is impossible be completely confident with this implication.

5.1.2 Actuator Phasing

Based on the positive results seen in research by Corke and He[4], it was decided to investigate the effect of pulsing the actuator to reattach the flow. The benefits of this would be the reduced power required, over a given period of time to effect the same change in the flow, and increased actuator longevity. The life span of the actuator is greatly increased with this method because the actuator is not always 'on' and because it would increase the life of the dielectric material, which degrades over time.

Two power profiles were done as the first tests of the pulsing. The voltage potentials across the actuator were varied from 0 KV up to 6.3 KV. A 10 percent duty

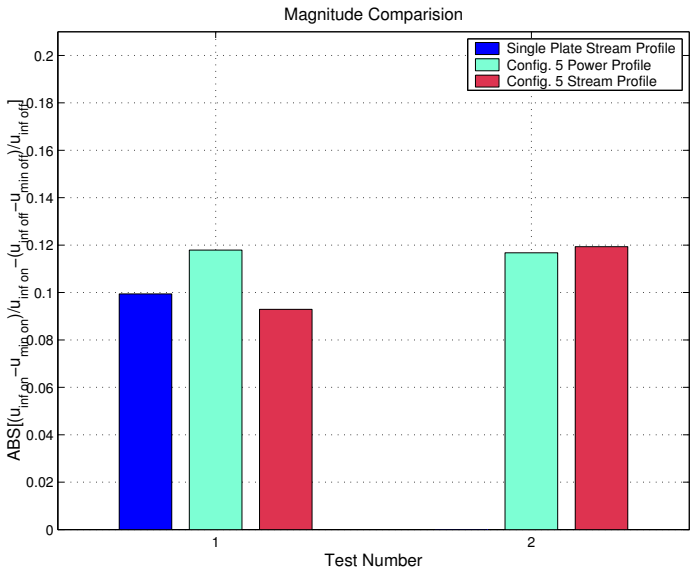

Figure 5.9. Magnitudes of actuator effect at the 5^{th} downstream chord location and at 6.3 KV.

cycle was chosen for these tests, meaning the actuator would be on 10 percent of the time of the cycle. The frequency chosen for the phasing cycle was 89.0 Hz. This was based on a Strouhal number of 1 and the free-stream velocity of 14.8 ft/s (4.51 m/s) in Equation 5.1, where c is the chord length of the plate, 2.0 in. (5.08 cm).

$$St = \frac{fc}{u_{inf}} \tag{5.1}$$

The power profiles were plotted together in Figure 5.10. The reason for the two tests was that the actuator effect seen in the first test was much lower than what was expected, so the test was repeated. It is apparent from this figure that the result was repeatable and that the pulsing of the actuator did not give nearly the effect seen in the previous experiments that continuously ran the actuator.

Following the pulsed power profiles, it was thought that maybe the frequency of the pulsing was not optimum so, as another test, the frequency was varied. With the voltage potential of the actuator fixed at 6.3 KV, the same setting as the experiments before the pulsing, the pulsing frequency was adjusted from 60 Hz to 120 Hz in 10

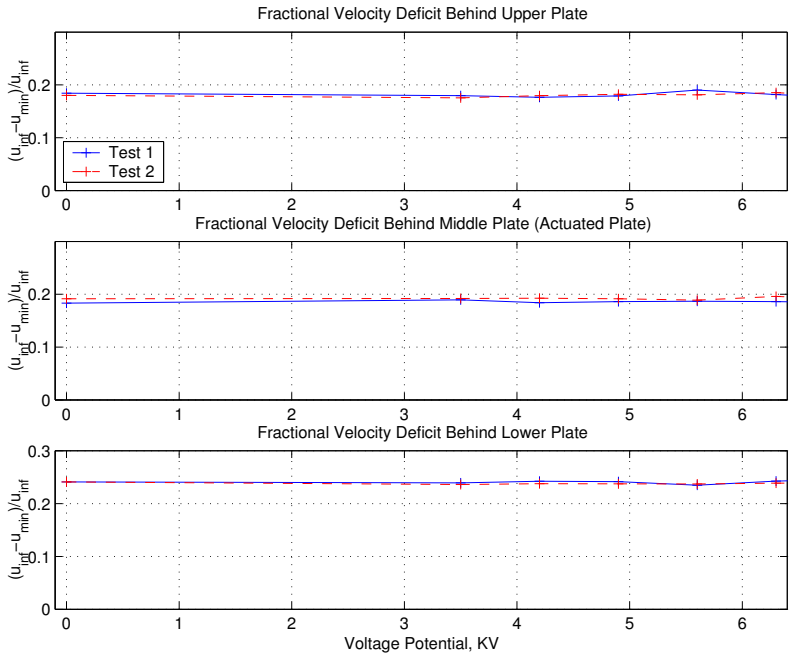

Figure 5.10. Effect of pulsing the plasma actuator at 89.0 Hz with a 10 percent duty cycle. Plates are at zero angle of attack with 3/8 chord spacing.

Hz increments. Note that the zero frequency case in the plot was a base profile done with the actuator 'off'. These tests were again done twice and the results of this can be seen in Figure 5.11. In this plot, the Strouhal number was calculated based on the average free-stream value for each run. From this, it was apparent that the pulsing had little effect. Arguably, the 10 Hz step size was too large to pinpoint the best frequency but from the results, it was thought that even at the "best" frequency the actuator effect for this setup was not going to be as good as previously seen. Therefore, this area of testing was discontinued and tests on Configuration 6 were started. Due to how little affect the actuator had, the results of the phasing will not compared to other data.

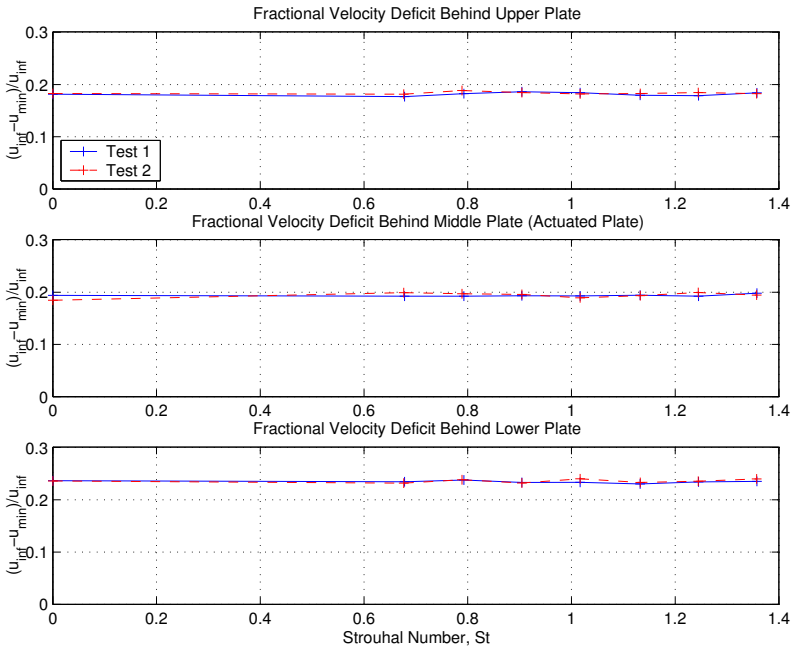

Figure 5.11. Effect of pulsing the plasma actuator over frequency range from 60 Hz to 120 Hz, at a 6.3 KV voltage potential.

5.2 Configuration 6

Though many of the results thus far were good, it was still thought improvements could be made. To this end, one more configuration was tested, Configuration 6, which was the sandwiched electrode configuration. The basic concept here was that two actuators should be better than one. Recall that this setup has an upper electrode on either side of the plate such that the flow induced by the actuators is forcing the free-stream flow in the same direction on both sides of the plate. Up till now, the actuator forced the flow upstream on one side of the plate and downstream on the other side. Both plate orientations of Configuration 6 were tried, That is, forcing the flow upstream and forcing the flow downstream. The results will be presented in the following two sections.

5.2.1 Forcing Upstream

Based on the results seen for the previous configurations, it was decided to first orient the plates such that the flow induced by the actuator was directed upstream. Prior to testing the actuator, an investigation into the plate order dependence was conducted.

As before, the plates were lettered, A, B, and C, and wake profiles were done for the 6 permutations of the letters. The results of this are shown in Figure 5.12. In terms of wake uniformity, the ABC and ACB orders were the best results. The variations in the wake profiles are most likely a reflection of the sensitivity of this close spacing and possible non-uniformities still present in the plates. Again, the reason that this test was preformed was to find the configuration that had the most uniform wake profiles.

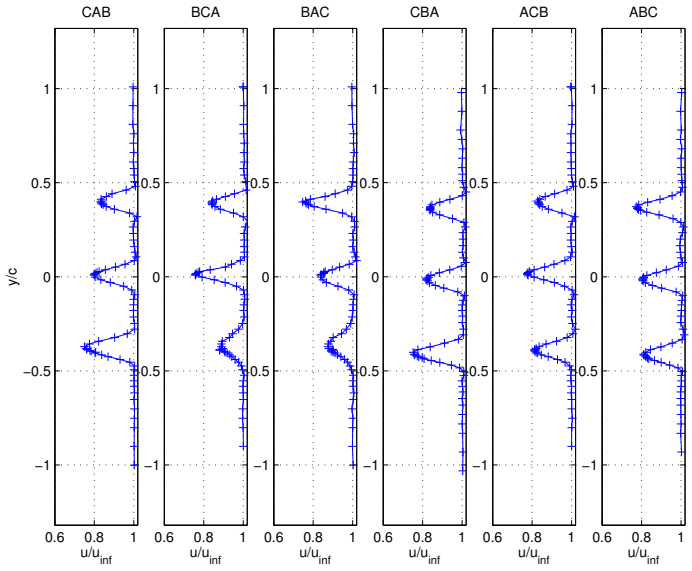

Figure 5.12. Investigation of wake dependence on plate order, sandwiched plates.

To verify the repeatability of the plate order dependence, after changing the plate order and then changing it back, the plate order tests were repeated. A comparison

of the tests on the two different days is shown in Figure 5.13. To ease the comparison between the two sets of data, it was decided to plot the data without symbols. From this data, the plate order of ABC was the most uniform and was chosen for future experiments.

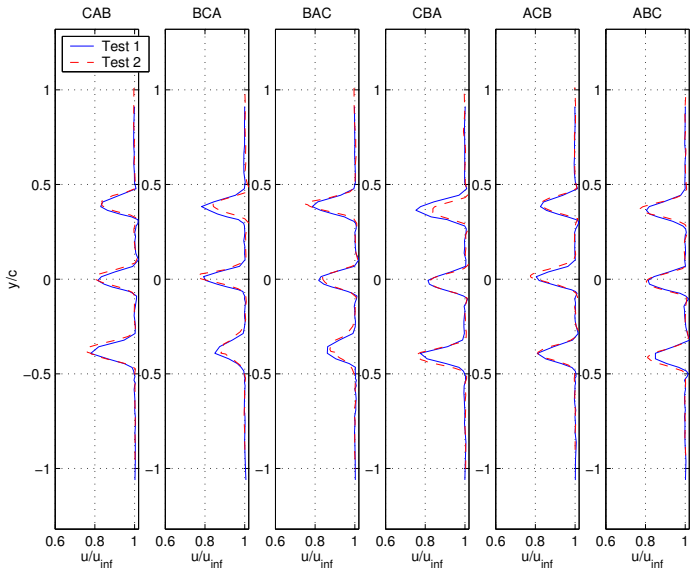

Figure 5.13. Comparison of wake dependence on plate order, sandwiched plates.

Once the choice of plate order was made, as was done with the previous configurations, an investigation into the sensitivity of the flow to the intensity of the plasma actuator was conducted. The set of power profiles resulting from this investigation are shown in Figure 5.14.

The data point at the 4.9 KV potential in Figure 5.14 looked erroneous and so the data set was repeated the following day. This result is shown, along with the previous result, in Figure 5.15. Both sets of data are plotted because after further investigation of the raw data of Test 1, no evidence of computer or experimental error, such as a voltage spike or zero-shift, was found. The trend of the second set was more consistent with expectations. It followed the trends of previous results, and was taken

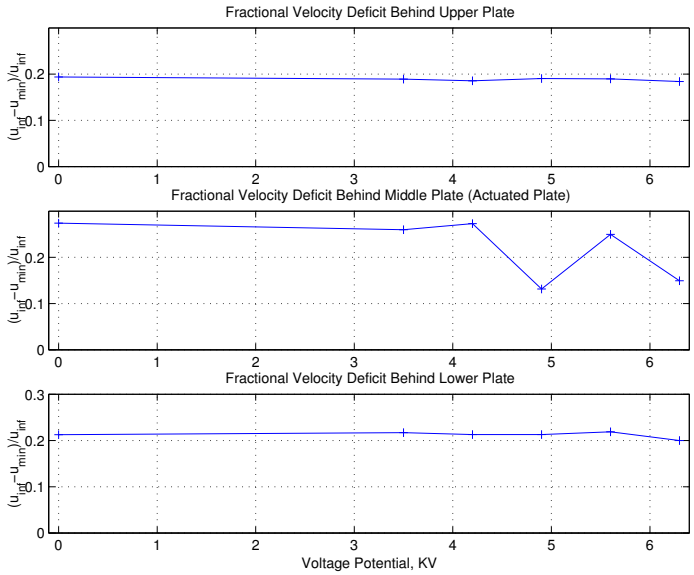

Figure 5.14. Power profile for Configuration 6 forcing upstream.

to be acceptable enough to continue on with other experiments.

The results in Figure 5.15 show that the actuator had the largest effect at the 6.3 KV potential. The next step was to obtain a complete set of stream profiles. These results are shown in Figure 5.16. The actuator effect appears to be similar to previous results in that the actuator seemed to work to increase the rate of decay of the velocity deficit. Notice though that at the 3^{rd} chord position the opposite effect occurred. Comparisons will be made in Chapter 6 to see if this setup is better or worse than Configuration 5 at the 5^{th} chord location.

As done with the previous results, Figure 5.17 shows the velocity decay of the wakes. From this figure it can be seen that after around the 3^{rd} chord position, with the exception of the middle plate's wake with the actuator on, the wake deficits start to grow after the initial decay. The middle subplot, showing the case with the actuator on, shows a jump in the velocity towards the free-stream value. The wakes are expected to uniformly decay with downstream location. The opposite effect is seen after the 3^{rd} chord position and again is most likely due to the wake interactions,

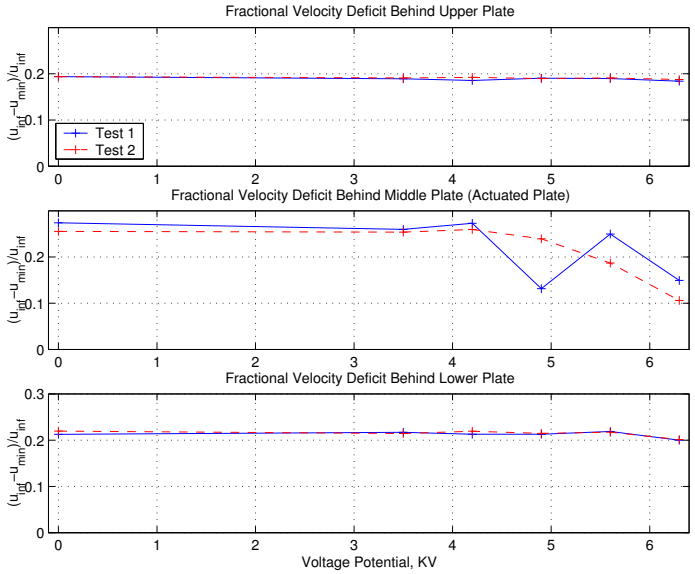

Figure 5.15. Power profile comparison for Configuration 6 forcing upstream.

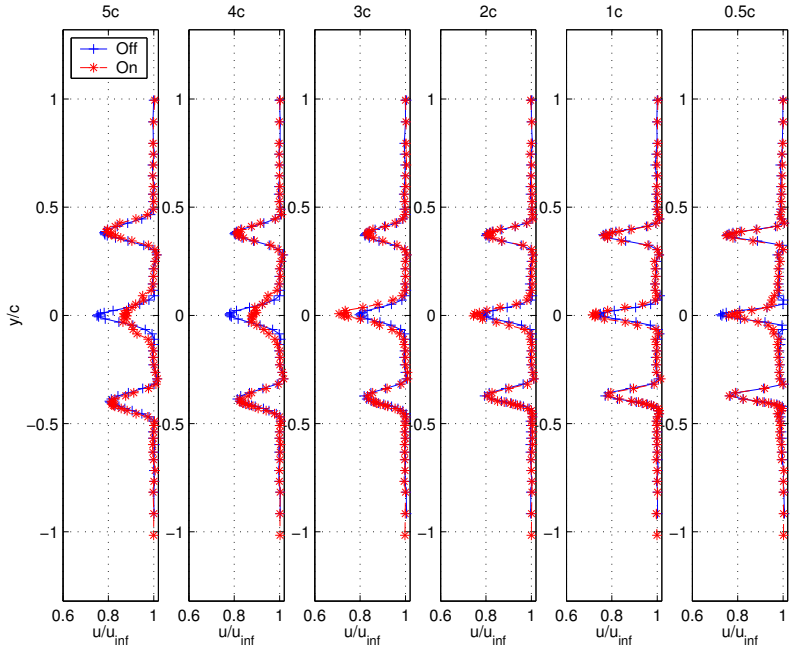

Figure 5.16. Stream profiles for Configuration 6, forcing upstream.

which can occur more downstream as the wakes widen. This plot also shows that the actuator has little effect on the wakes of the neighboring plates. In addition to the minimum velocities, some theoretical trend lines were included to help illustrate how the decay rates start to deviate from theory further downstream. The theoretical trends again follow Equation 3.2.

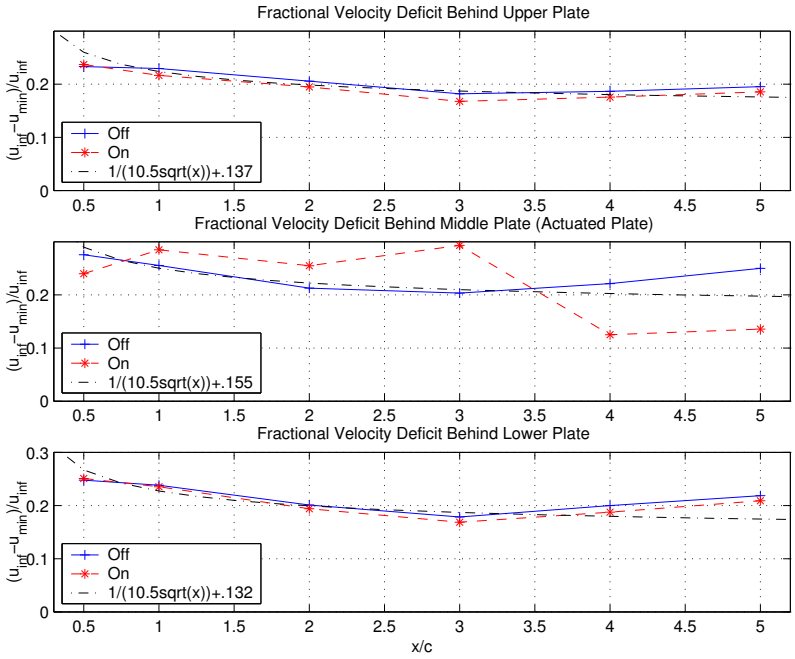

Figure 5.17. Wake decay for Configuration 6, forcing upstream.

Because of the jump seen in the data points of the actuated plate in Figure 5.17, the tests were repeated. The second test results were plotted against the first and are shown in Figure 5.18. Up to the 3^{rd} chord position, the new results show good agreement with previous tests, but after the 3^{rd} chord position the actuator seems to have little effect. It is apparent that the base case, that is with the actuator off, does not agree after the 3^{rd} chord position. The reason(s) for this disagreement is unclear at this point. Even though the cases with the actuator 'off' do not agree for the two tests, the actuator effect for the two tests does not agree in a manner consistent with the disagreement of the base cases. In other words, the actuator effect for the second

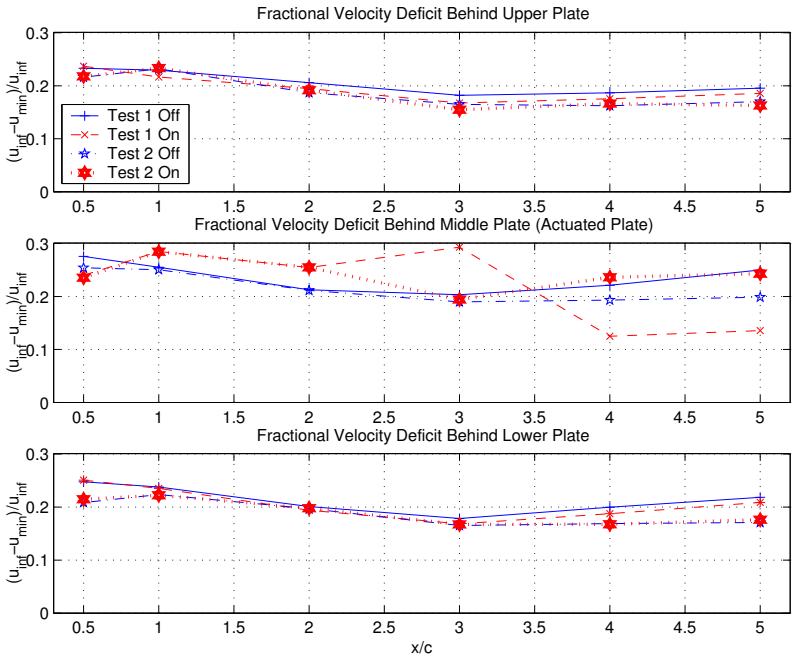

Figure 5.18. Comparison of two wake decay tests using for Configuration 6, forcing upstream.

test did not shift consistently with the shifted points of the base case, which could have implied an instrumentation drift. The actuated case was completely different.

The conclusion drawn after second the set of stream profiles was that this configuration was too sensitive. Any slight variation could cause a change in the result, thus making the results difficult to repeat. It was decided then to move on and try reversing the plates.

5.2.2 Forcing Downstream

The following investigation used the same sandwiched plates but this time turned around such that the actuator forced the flow in the downstream direction. The first probe into the effect of the actuator with this reversed orientation is shown in Figure 5.19. This was a power profile. Again, the power dependence was first looked at to decide whether or not it was worth taking a full set of stream profiles. The results

from figure 5.19 looked good in that they showed an effect, but not as dramatic as the previous tests. From this result though, it was decided to preform the full set of stream profiles.

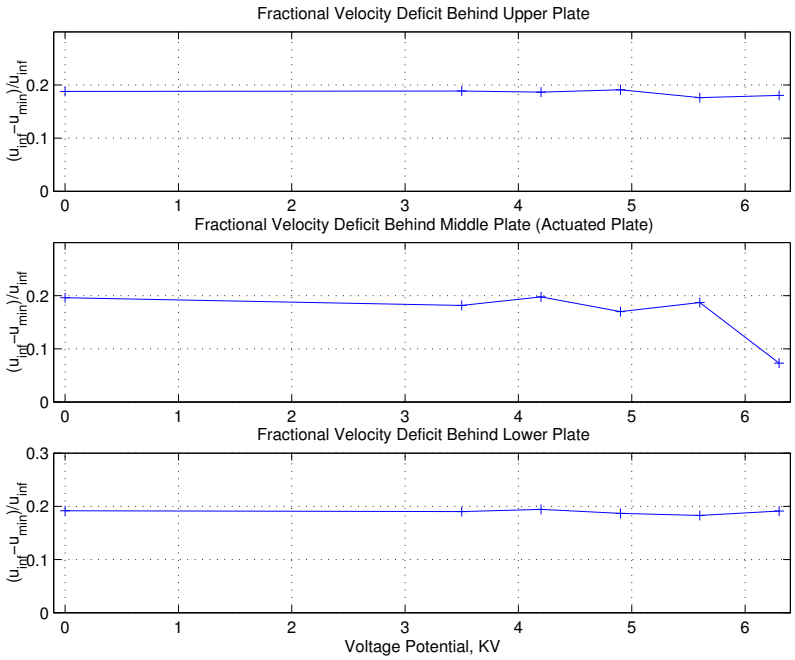

Figure 5.19. Power profiles for Configuration 6, forcing downstream.

The results of the stream profiles for the reversed plate orientation are shown in Figure 5.20. This result however does not seem to reflect the results of the power profiles shown in Figure 5.19. The most distinctly noticeable effect was at the 3^{rd} chord position.

Plotting just the fractional velocity deficits, Figure 5.21 shows some effect of the actuator and better illustrates the jump at the 3^{rd} chord position. This jump is similar to the one seen in Figure 5.17, but not as drastic. In Figure 5.21, approximately a 2 percent change in the minimum velocity is shown at the 5^{th} chord position for the actuated(middle) plate. However, according to Figure 5.19, there should be close to a 12 percent reduction in in the velocity deficit at the 5^{th} chord position, even if only at that location. After looking at this and expecting a more uniform trend, or at

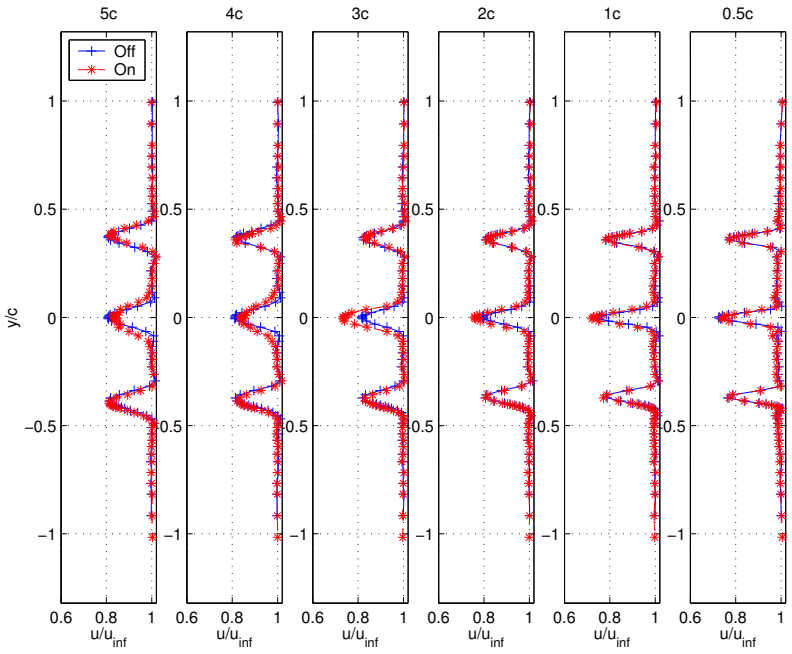

Figure 5.20. Stream profiles for Configuration 6, forcing downstream.

least again lacking the jump at the 3^{rd} chord location, it was decided to repeat this set of stream profiles.

The repeated stream profiles are shown in Figure 5.22. This case was noticeably different in that the jump seen at the 3^{rd} chord position was not there and, for the actuated cases, the peaks decayed less rapidly than the unactuated cases. Also present in these profiles, in particular at the 3^{rd} and 5^{th} chord positions, the middle peaks show some flattening and erratic behavior. The fact that the peaks for the actuated case decayed less rapidly in this experiment is not completely unexpected. It stands to reason that reversing the direction of the forcing could reverse the effect.

As was done with the upstream forcing case, the repeated results were plotted against the initial results. These are shown in Figure 5.23. As opposed to the upstream forcing setup, the base cases shown here are almost indistinguishable in the figure. But again, the effect of the actuator was not consistent for the two tests after the 3^{rd} chord position. The actuator effect for the second test seemed more consis-

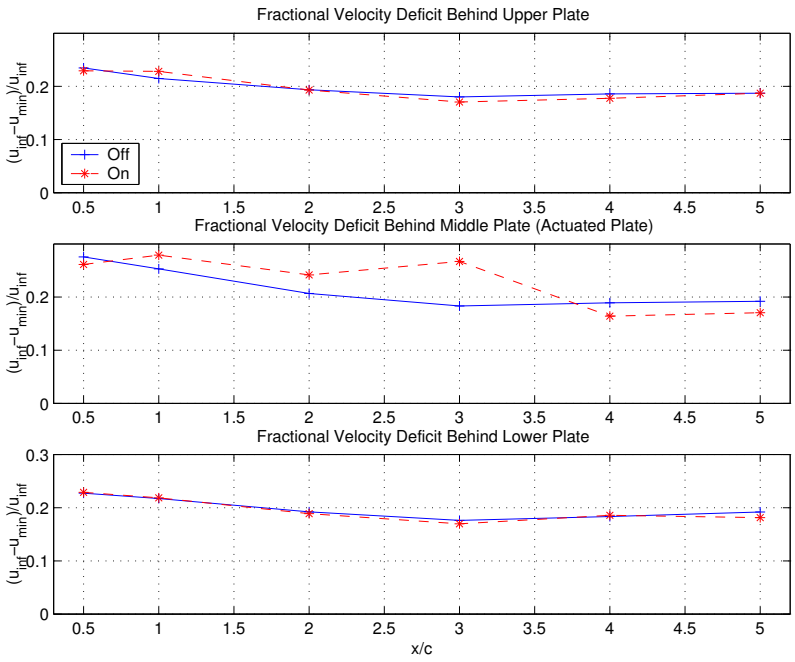

Figure 5.21. Velocities deficits for stream profiles for Configuration 6, forcing downstream.

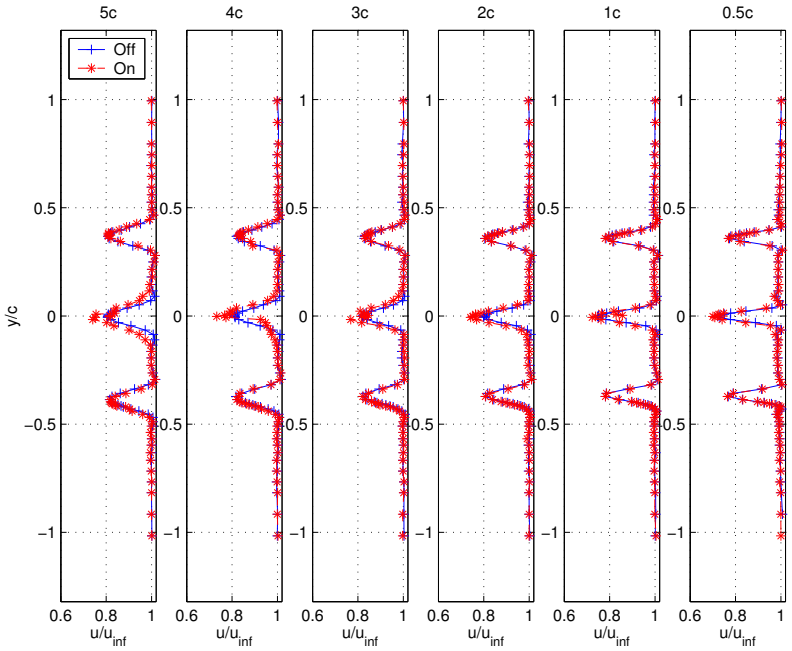

Figure 5.22. Repeated stream profiles for Configuration 6, forcing downstream.

tent in terms of the decay trend, but the result was still not consistent with the first power profile. The first power profile suggested a 12 percent decrease in the minimum velocity at this point, not a 6 percent increase.

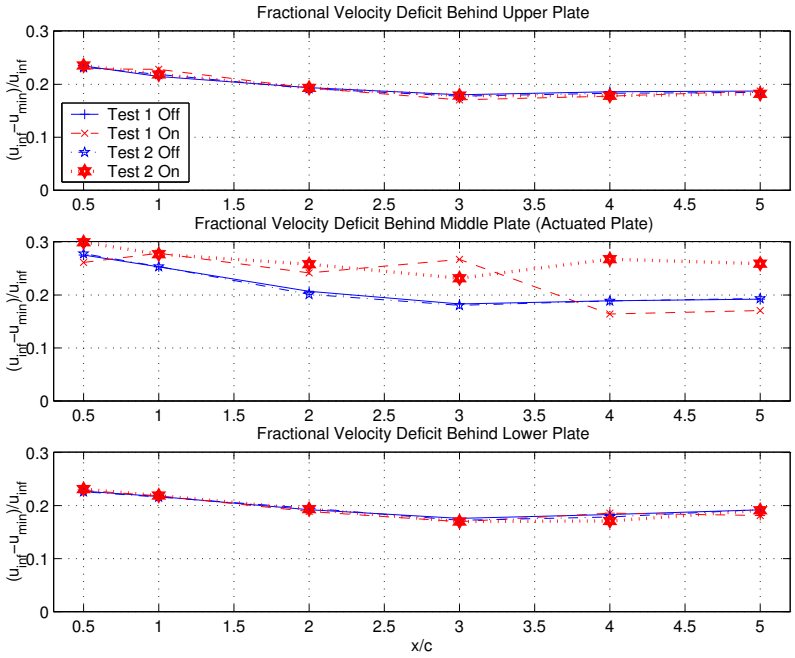

Figure 5.23. Comparison of two wake decay tests using for Configuration 6, forcing downstream.

Due to these inconsistencies, the first set of power profiles for this setup were repeated. The repeated power profiles were plotted along with the first set and are shown in Figure 5.24. From this it is apparent that the first set of results do not seem to be repeatable, with the second set of results being more consistent with the results seen in the stream profiles. As with the forcing upstream experiments, based on the inconsistencies found in these results, it was decided that this plate orientation was also to sensitive to work with and was abandoned. This was the last configuration tried.

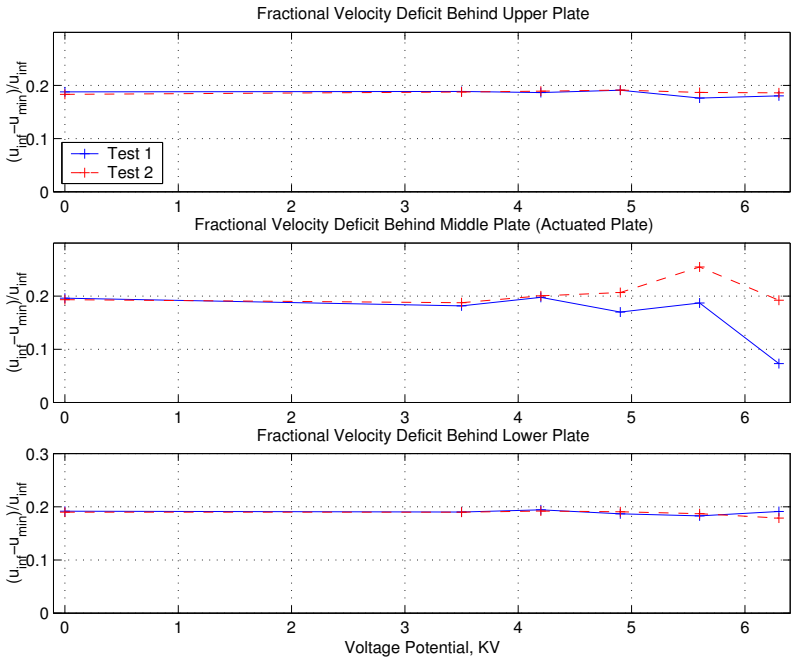

Figure 5.24. Power profile comparison for Configuration 6, forcing downstream.

5.2.3 Comparison: Upstream to Downstream Forcing

Before moving on, a quick comparison and summary of the results was done. The first of this was a combination of the middle sub-plots of Figures 5.18 and 5.23. This combination produced Figure 5.25. What this shows is that three of the four stream profiles agree, in terms of the actuator 'off' velocity deficits. For currently unknown reasons the first set of stream profiles, with the actuators forcing upstream does not agree with the others. Note that Figure 5.25 only shows the wake deficits behind the middle plate.

As a final comparison and summary of Configuration 6, as was done with the earlier tests, the magnitudes of the differences of the actuator 'off' and 'on' cases at the 5^{th} chord location and 6.3 KV voltage potential were compared. This summary is shown in Figure 5.26. The values are grouped by the first test and second test. Based on the experimental setup, for the upstream forcing cases, the results from the

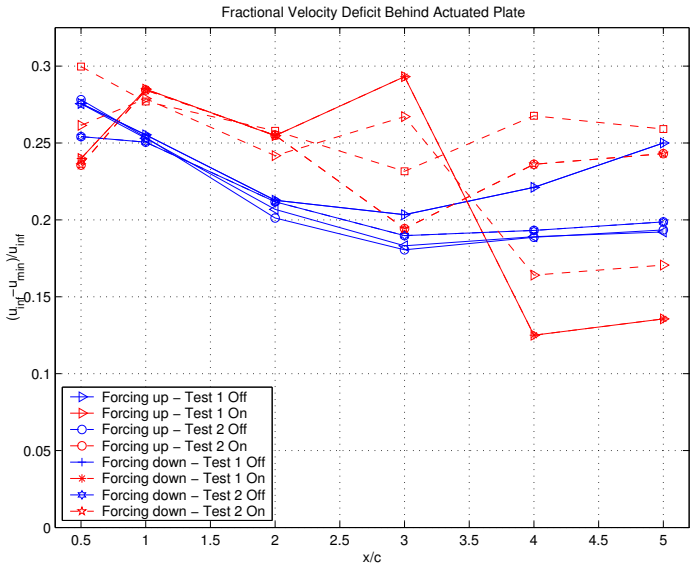

Figure 5.25. Velocity deficits behind actuated (middle) plate for the two upstream and two downstream forcing cases.

power and stream profiles should match. The same goes for the downstream forcing case. Obviously from this figure they do not agree. Averaging the four results for the upstream case give a mean of 0.108 with a standard deviation of 0.045. This standard deviation is approximately 3.5 times greater than what was seen with Configuration 5, which had a comparably sized mean. The calculations of the downstream case gives a mean of 0.053 with a standard deviation of 0.054. Having a standard deviation greater than the mean is a good indication of how erratic the experimental values were. The main thing to take from this is that these results were very inconsistent. This brings up the issue of repeatability. If the apparatus can not perform consistently, it is not useful as an experimental device. So, as mentioned before, these setups were abandoned.

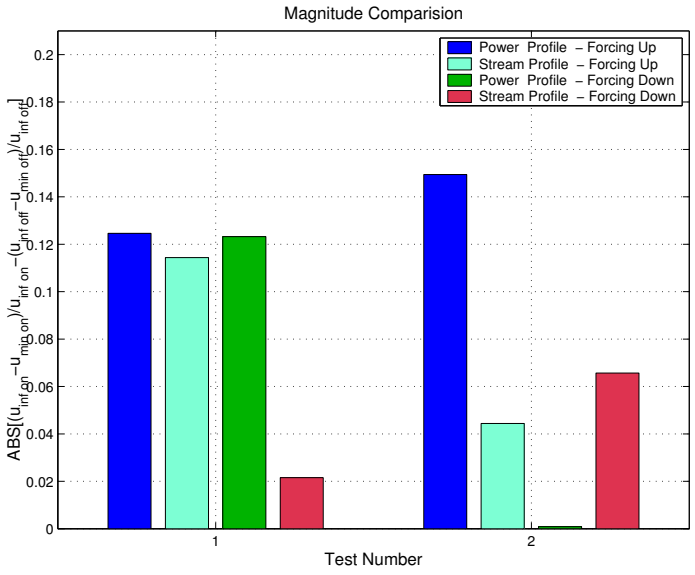

Figure 5.26. Magnitudes of actuator effect at the 5^{th} chord location and at 6.3 KV voltage potential.

CHAPTER 6

RESULTS: DISCUSSION

In this chapter, comparisons of some of the different hot-wire measurements, for the different configurations, will be presented. This is done to better illustrate some of the findings and to point out which configurations worked and in what way they worked.

6.1 Leading Edge Dependence

First to be presented are some results that discuss the leading edge dependence. This is done mostly to draw attention to the variations found in the experimental data that resulted from changing the leading edge. To illustrate the differences, the single plate cases that were compared with Configurations 4 and 5 will be compared to each other. Then, comparisons of both the single plate case to Configuration 4, which had two plates with the 1/4 elliptic leading edge and one plate with the round leading edge, and to Configuration 5, which had three plates with round leading edges.

A direct comparison of the effect of the leading edges can be made by plotting the results for the two single plates. This comparison is shown in Figure 6.1. With the exception of the 1/2 and 4^{th} chord positions, the decay trends of the cases with the plasma actuator off are very similar. However, there is a stark contrast between the plasma on cases for the two airfoils. The 1/4 elliptic leading edge, in conjunction with the plasma actuator, seems to work to hinder the turbulent mixing in the wake,

thus increasing the time, which in turn increases the downstream distance for the fractional velocity deficit to approach the free-stream value. Contrarily, the rounded leading edge, in conjunction with the plasma actuator, seems to increase the wake mixing, thus helping the velocity deficit to decrease.

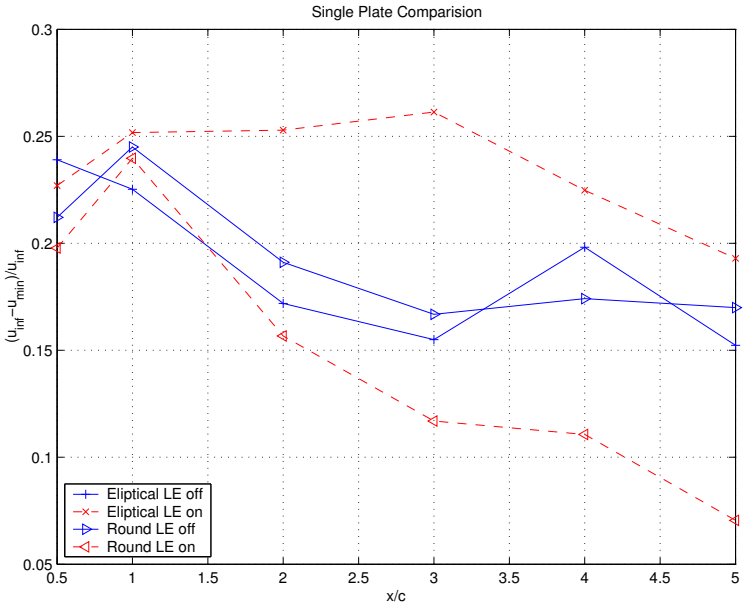

Figure 6.1. Direct comparison of single plate with 1/4 elliptic leading edge to a single plate with a round leading edge.

The results shown in the middle subplot of Figure 4.30 in Section 4.4, were replotted in the the top subplot of Figure 6.2. This shows a comparison of a single plate, with an 1/4 elliptic leading edge, to Configuration 4. Recall that Configuration 4 had two plates with 1/4 elliptic leading edges and one plate, on the end, with a round leading edge. Also, that the plate with the plasma actuator was the same plate used for the single plate test, and the Configuration 4 test, compared in the figure, thus both had 1/4 elliptic leading edges. Because the results for the plates with the plasma actuators were the primary interest, only those will be compared. The bottom subplot of Figure 6.2, shows the comparison of the same single plate case to the actuated plate of Configuration 5. Recall that the plates in Configuration 5

all had round leading edges. Notice that the single plate case, with the 1/4 elliptic leading edge, with the actuator 'on', does not match any of the other actuated cases. This is not the case in the next comparison.

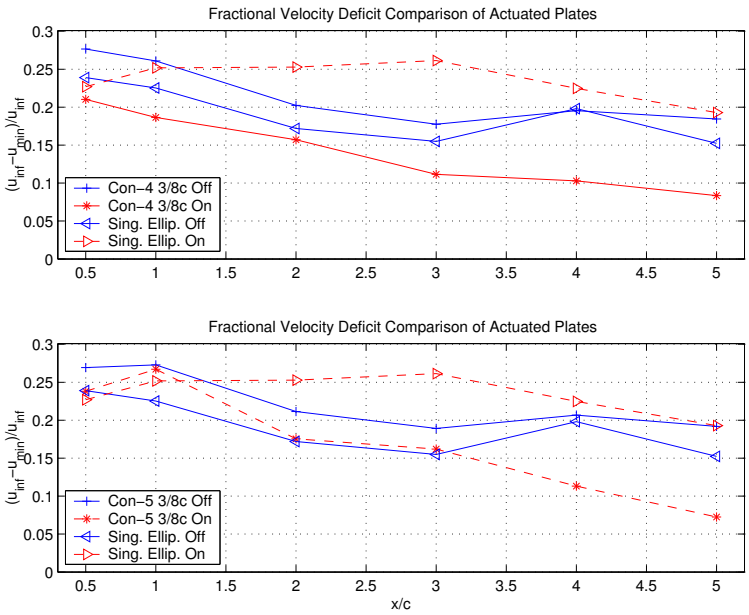

Figure 6.2. Comparison of single plate with 1/4 elliptic leading edge to multiple plate configurations with different leading edges.

The last figure of this section, Figure 6.3, compares the single plate with the rounded leading edge case, to the three plate cases of Configurations 4 and 5. As before, the top subplot in this figure is just re-plotting the results for the actuated plates shown in Figure 5.8. The bottom subplots are the comparison of the single plate with the rounded leading edge to Configuration 4. Unlike before, these results agree very well. The single plate with the rounded leading edge has the same trend as the close spacing, uniform, three plate case of Configuration 5 and, for the cases with the actuators 'on', the magnitudes of the deficits closely match. The single plate comparison to the close spacing case with the 1/4 elliptic leading edged plates, for the actuator 'on' case, are almost indistinguishable for some of the downstream locations.

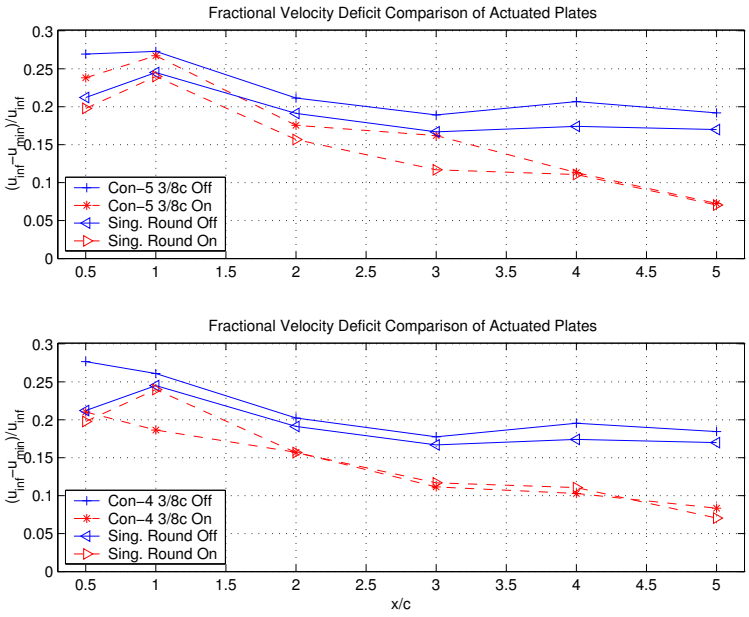

Figure 6.3. Comparison of single plate with round leading edge to multiple plate configurations with different leading edges.

What these results show is that the leading edge and plate spacing can, in conjunction with the use of the plasma actuator, effect how the wakes decay. Depending on the desired result or setup conditions, varying the leading edge geometry could be more beneficial than the varying the plate spacing, or vise-versa.

6.2 Actuator Effect: At 5 Chord Lengths Downstream

Many results have been presented in this thesis. The point of this section is to summarize the results, discuss some of the more positive ones and to some extent compare then to other moving-wake generator designs.

To start, the magnitudes of all the velocity deficits of all the hot-wire experiments conducted at the 5^{th} chord position and optimum voltage potential across the actuator presented in this thesis were collected and are represented in a master summary in Figure 6.4. This includes all of the 5^{th} chord position stream profile cases for

Configurations 3 through 6 and the two single plate cases. Also, this figure includes all of the power profiles done at the optimum voltage for Configurations 4 through 6. Below the figure is a table that contains a summary of the experimental setup corresponding to the number designation shown in the figure. The summary table contains the designation number, configuration number, angle of attack of the plate, the chord spacing of the plates, the profile type, voltage potential of the test and notes where needed.

A final comparison of results at the 5^{th} chord location are shown in Figure 6.5. This shows the mean and standard deviation, where possible, of similar test cases that were presented in the master summary. Only select setups of interest are presented. In the table under the figure, there is a column labeled 'Master Desig.'. This is a list of the data points used that correspond to the Master Designation list from Figure 6.4 in the calculation of the mean and standard deviation. The results discussed in Section 4.2.2 illustrate why Master Designations 3,4, and 5 could be averaged, though the setups where not exactly the same. With the other averages, the only things different between the points was the day the test was done and whether it was a stream or power profile. All other test conditions such as the configuration, orientation, spacing, and power supplied were all the same. This figure, along with the table, collectively shows what worked at the 5^{th} chord location. Some of advantages and disadvantages of the different setups will be discussed next.

Clearly from Figure 6.5 Designation 1 was the most effective and most repeatable setup. However, caution has to brought to the voltage potential needed to each this affect. Also attention should made to having the plates turned, the location of the minimum velocities for the 'off' and 'on' cases will not be the same, nor will they be in line with the plate, whereas for the zero angle of attack cases, the peaks are in line with each other and the plate. Recall that the 11.2 KV potential was chosen

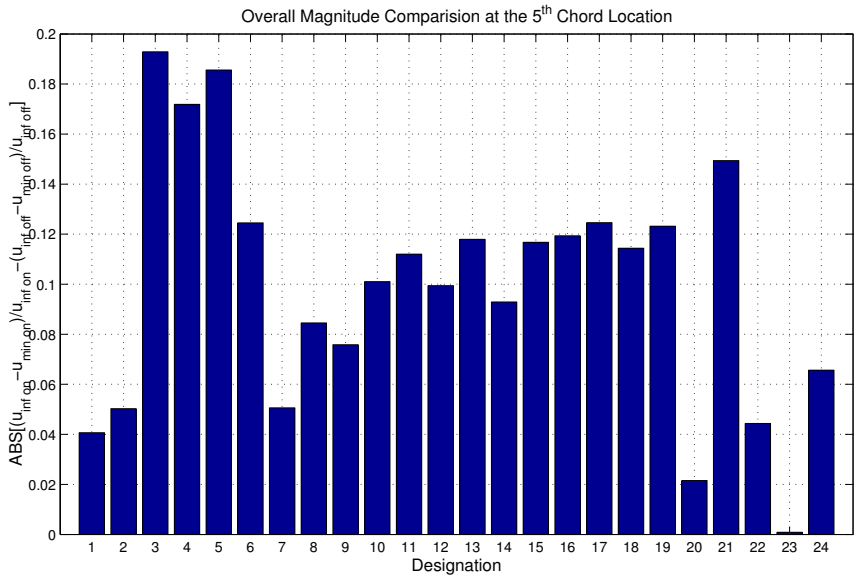

Desig.	Conf.	Angle (^{o})	Spacing (c)	Profile	V.P. (KV)	Note
1	-	0	-	Stream	6.2	S.P. 1/4 elliptic L.E.
2	3	−3	1	Stream	11.2	
3	3	−3	1/2	Stream	11.2	
4	3	−3	1/2	Stream	11.2	5.5 KHz tri. wave
5	3	−3	1/2	Stream	11.2	5.5 KHz sine wave
6	4	−3	1/2	Power	6.2	
7	4	−3	1/4	Power	6.2	
8	4	0	1/4	Power	6.2	
9	4	0	3/8	Power	6.2	
10	4	0	3/8	Stream	6.2	
11	4	0	1/2	Power	6.2	
12	-	0	-	Stream	6.3	S.P. Round L.E.
13	5	0	3/8	Power	6.3	Test 1
14	5	0	3/8	Stream	6.3	Test 1
15	5	0	3/8	Power	6.3	Test 2
16	5	0	3/8	Stream	6.3	Test 2
17	6	0	3/8	Power	6.3	Forcing Up Test 1
18	6	0	3/8	Stream	6.3	Forcing Up Test 1
19	6	0	3/8	Power	6.3	Forcing Down Test 1
20	6	0	3/8	Stream	6.3	Forcing Down Test 1
21	6	0	3/8	Power	6.3	Forcing Up Test 2
22	6	0	3/8	Stream	6.3	Forcing Up Test 2
23	6	0	3/8	Power	6.3	Forcing Down Test 2
24	6	0	3/8	Stream	6.3	Forcing Down Test 2

Figure 6.4. Master summary of actuator effect at the 5^{th} chord location for all the stream and power profiles presented.

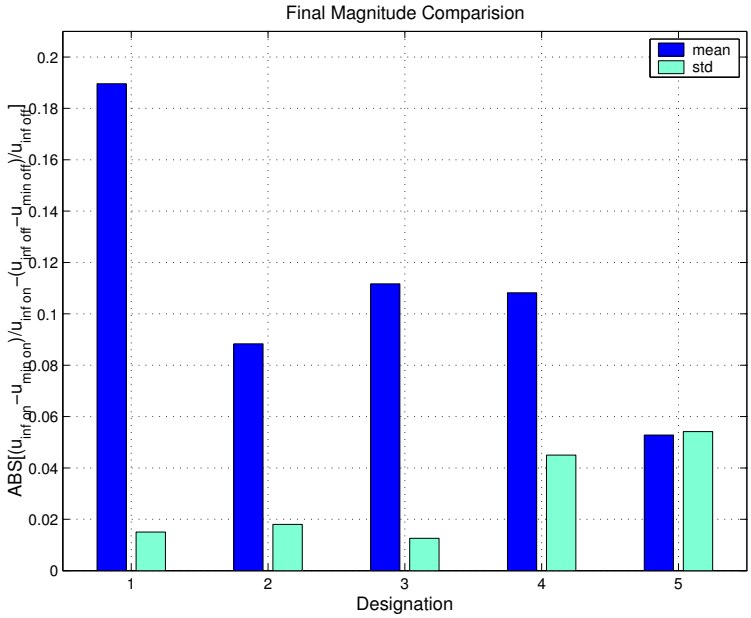

Desig.	Conf.	Angle (^{o})	Spacing (c)	V.P. (KV)	Master Desig.#'s Used in Average
1	3	-3	1/2	11.2	3,4,5
2	4	0	3/8	6.2	9,10
3	5	0	3/8	6.3	13,14,15,16
4	6	0	3/8	6.3	17,18,21,22
5	6	0	3/8	6.3	19,20,23,24

Figure 6.5. Comparison of similar results at the 5^{th} chord location to magnitude and repeatability of the actuator effect.

because while performing the flow visualization, it appeared to be the most effective. Referring back to Figure 6.4, the change from Configuration 3 to Configuration 4, is shown by Designation 6, illustrates approximately a 6 percent decrease in the actuator affect caused by the reduction of power and the addition of the third plate. However, it is unclear at this time the degree that the power reduction and third plate addition individually had. However, based on the differences in flow visualization results shown in Figure 4.7 and Figure 4.10, it seems that the reduction in the effect is primarily dependent on the change in voltage. Recall that the difference seen in the flow visualization occurred from increasing the voltage potential from 8.4 KV to 11.2 KV.

Of the remaining points, in Figure 6.5, Designation 3 is best configuration. It shows the highest velocity variation between the plasma actuator 'off' and 'on' cases, with the smallest standard deviation. This configuration has the advantage in that it requires less power, but as noted before, this may not be entirely the case when compared to Designation 1. Also, geometrically, a zero angle of attack setup would be easier to construct. However, the wider spacing angle of attack cases appear to be less sensitive to small geometrical variations.

Lastly, as pointed out before, Configuration 6, shown by Designations 4 and 5 in Figure 6.5, is the worst choice. This configuration had the highest standard deviation of the data points, which brings to question the repeatability of the results. Affects of the moving-wake generator on the flow have to be know and consistent to be used as a practical tool. These inconsistencies show that this configuration does not adhere to this requirement.

Given the original design constraint of 10.0 in. (25.4 cm), which for the plates was 5 chord lengths, the 1/2 chord, -3^o angle of attack, 11.2 KV potential of Configuration 3 and 6.3 KV potential case of Configuration 5 worked the best. These results are comparable to Doorly's setup which achieved 10 to 20 percent velocity fluctuations[6]

but lower than the 25 percent variation reported by Murawski and Vafai[15], which was based on results of Halstead et al.[12]. It is unclear whether the 25 percent estimate is based on the physical distance between the plain of the test blade leading edges and the plain of the cylinder motion or based on the distance in the wake path. The wake path distance is always greater than the physical distance between the plains, due to the geometry of the setup, and is dependent on the cylinder and free-stream velocities. The point being that the 25 percent could an over-estimate based on wake path distance. For the present work the wake path distance has not been considered because attempts at propagating the disturbance were not made.

The next section discusses the feasibility of positioning the moving-wake generator, based on current results presented in the this thesis, to distances on the order of one chord from the test blades.

6.3 Actuator Effect: At Other Chord Lengths Downstream

In this section, some of the results for the 1/2 and 1 chord downstream positions will be presented to illustrate some flexibility in the application of the unsteady turbulence generator. Up till now, the results shown have been restricted to the 5^{th} chord position design constraint. This constraint was placed on the design for the first intended application. Other researchers may have different design requirements.

The only data available for this investigation is from the stream profiles. As was done before, the magnitudes of the velocity deficits for the 1/2 and 1 chord location were collected and are presented in Figure 6.6. This bar graph shows that positioning the moving-wake generator closer to the test blades has no benefit. However, these data points where collected as the previous ones, that is, at a fixed position, in line with the minimum velocity of the actuator 'off' case for the 1/2 chord location profile, behind the actuated plate. For the cases of the -3^o angle of attack, if the

measurement location is shifted, there is an improvement.

The motivation for investigating the closer chord positions is due to the large difference between the plasma actuator 'off' and 'on' case at the 1 chord plate spacing, -3^o angle of attack, tests of Configuration 3 at the 1/2 chord downstream location. Select mean velocity profiles, from the stream profiles for that setup shown in Figure 4.13 of Section 4.2.2 were replotted, along with the difference between the 'off' an 'on' case shifted, by adding 1 to all the values. This was done so that all three sets of data could be on the same axis and the result of this is shown as Figure 6.7. Included in the first sub-plot is a sketch reflecting the plate orientation and location that the data was taken. The horizontal line indicated by the letter 'A' is the location of minimum velocity of the actuator 'off' case, and thus the y-location where the data was taken for comparison in the previous bar graphs. The horizontal line indicated by the letter 'B' is in line with the center of the plate. The line indicated by the letter 'C' represents the angle of attack of the plate and the projected area. The vertical distance between the ends of this line are drawn to scale with the actual width of the projected area of the plate. The length, angle, or the location of the line in no other way represent the actual location of the plate.

Obviously from Figure 6.7, the values used for comparison where not at the location of the maximum velocity deficit. This is due to the angle of attack of the plate. Since the angle of attack is small, the flow stays attached as it goes around the plates. This shifts the location of the minimum velocity above the physical location of the plate. When the plasma actuator is turned 'on', the induced velocity causes the flow to at least partially separate from the low pressure side of the plate. This in turn makes plate appear more like a bluff body. Which is why the wake shifts down towards the centerline of the plate. Recall that the flow visualization images shown in Figure 4.10 illustrated the large scale vortex shedding. For this case, the maximum

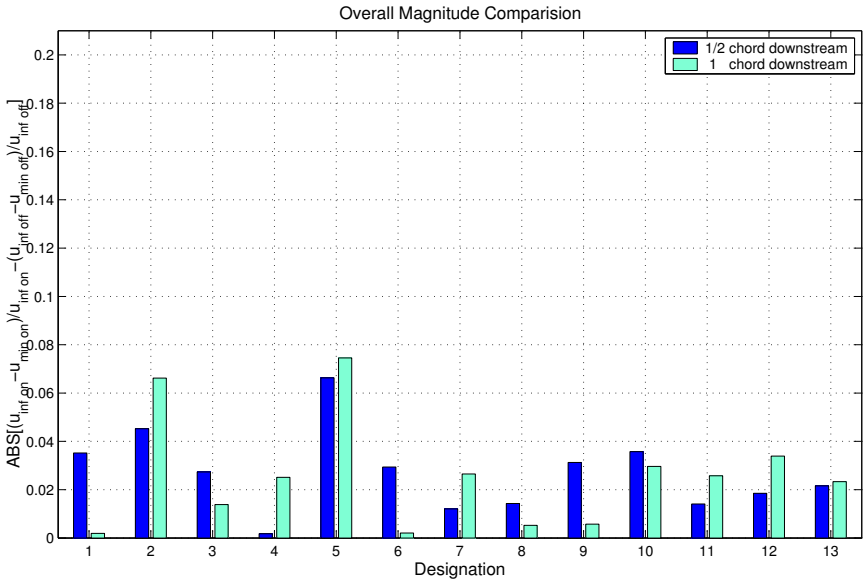

Desig.	Conf.	Angle (^{o})	Spacing (c)	Profile	V.P. (KV)	Note
1	3	−3	1	Stream	11.2	
2	3	−3	1/2	Stream	11.2	
3	3	−3	1/2	Stream	11.2	5.5 KHz
4	3	−3	1/2	Stream	11.2	5.5KHz sine wave
5	4	0	3/8	Stream	6.2	
6	5	0	3/8	Stream	6.3	Test 1
7	5	0	3/8	Stream	6.3	Test 2
8	-	0	-	Stream	6.2	S.P. 1/4 Elliptic LE
9	-	0	-	Stream	6.3	S.P. Round LE
10	6	0	3/8	Stream	6.3	Forcing Up Test 1
11	6	0	3/8	Stream	6.3	Forcing Down Test 1
12	6	0	3/8	Stream	6.3	Forcing Up Test 2
13	6	0	3/8	Stream	6.3	Forcing Down Test 2

Figure 6.6. Summary of actuator effect at the 1/2 and 1 chord locations for all of the stream profile cases.

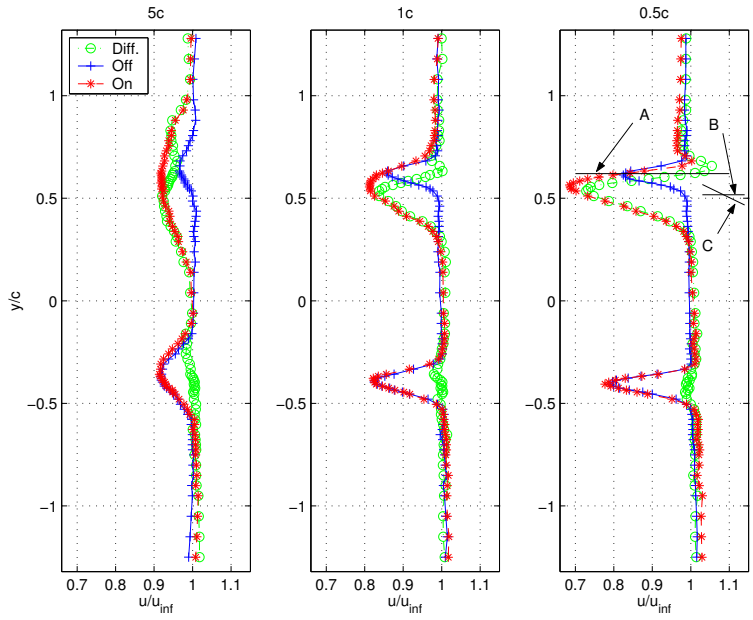

Figure 6.7. Select stream profiles of an actuator 'off' and 'on' case plotted with difference between them. A-Location minimum velocity of the actuator 'off' case. B-Indication of center of the plate area blockage. C-Represents the angle of attack of the plate and projected area.

fluctuation at the 1/2 chord location is 27 percent of the free-stream and drops to roughly 15 percent and 8 percent at the 1^{st} and 5^{th} chord location respectively.

Similarly, Figure 6.8, shows the same type of illustration for the -3^o, 1/2 chord spacing case of Configuration 3. This time only the difference is shown. Because of this, it did not have to be shifted. The corresponding stream profiles for this case were shown in Figure 4.14 in Section 4.2.2. This figure shows that the presented results for the -3^o, 1/2 chord spacing cases of Configuration 3, at the 5^th chord location, where close to there maximum amplitudes. The highest magnitude was approximately 31 percent at the 1/2 downstream position.

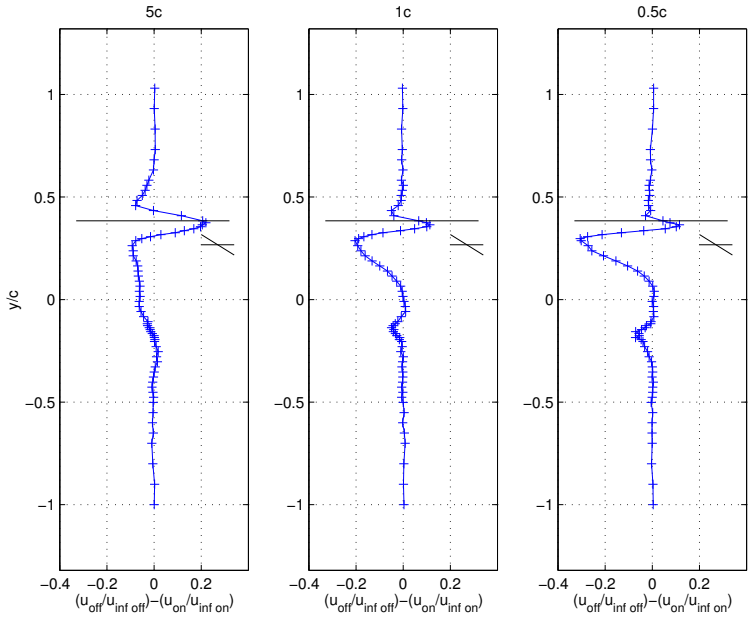

Figure 6.8. Difference between actuator 'off' and 'on' case for -3^o, 1/2 chord spacing case of configuration 3. A-Location minimum velocity of the actuator 'off' case. B-Indication of center of the plate area blockage. C-Represents the angle of attack of the plate and projected area.

Some additional remarks will be made in Chapter 7 discussing some recommendations that would investigate the possible versatility of the moving-wake generator as alluded to in Figures 6.7 and 6.8.

CHAPTER 7

CONCLUSIONS AND RECOMMENDATIONS

Presented in this chapter are some conclusions and recommendations for future work, both coupled with some final remarks. The chapter is broken down in to those two sub-sections.

7.1 Conclusions

The main objective of the work presented in this thesis was a proof of concept of the ability to use plasma actuators as an moving-wake generator. Many steps were taken to achieve this objective with promising results. The results of the experiments are concluded here.

Mean velocity profiles using a hot-wire were conducted in the wake of an unactuated NACA_0018 airfoil at the following downstream chord locations; 1/2, 1, 2, 3, 4, and 5 chord lengths. These tests were done at two velocities, namely 31 ft/s (9.45 m/s) and 54 ft/s (16.5 m/s). Similarity plots of the wake showed good agreement with theory in terms of the wake width and velocity deficit. The same tests were performed on two NACA_0018 airfoils to test the wake interactions relative to the airfoil spacing. It was shown that for a free-stream velocity of 31 ft/s (9.45 m/s) and a blade spacing of 1/3 chord that the airfoil wakes never act independently. For a spacing of 2/3 chord at the same velocity, the wakes started to interact 1 chord length downstream. At the last spacing, 1 chord length, the wakes were independent through

the 5 chord lengths. Similarly for the 54 ft/s (16.5 m/s) velocity, 1/3 chord spacing case, the wakes were never independent. For the 2/3 chord spacing, the wakes started to interact between 1 and 2 chord lengths downstream and for the 1 chord spacing case, the wakes were again independent throughout the 6 streamwise locations.

Plasma actuators with a 0.5 in. (1.27 cm) wide upper and lower electrode, were tested at three different chord positions on one of the two NACA_0018 airfoils at a voltage potential of 12.5 KV. The actuator was placed such that the active edge was at the 25 percent chord location and forcing the flow upstream. While the airfoil spacing was fixed at a 2/3 chord length, additional chord positions of 27 and 30 percent were tested with the 27 percent chord location, also the point of maximum thickness of the airfoil, being the most effective. This conclusion was based on flow visualization results. Also from these, the actuator/airfoil setup did not appear to have enough of an effect on the flow to use for the moving-wake generator.

Flow visualization techniques were also implemented for the study of two flat plates at zero angle of attack with plasma actuators that used Kapton tape as the dielectric material. Various actuator positions including the leading edge and 0.125 in. (0.318 cm) from the leading edge were tested, in addition to having multiple numbers of actuators in an array on both plates. Also, plate spacings of 1/4, 3/8, and 1/2 chord where tested. All these setups were tried at voltages levels of 1.9 and 6.8 KV potentials but showed no real affect.

The two plates were also tried at various angles of attack between 0 and 16 degrees with a plasma actuator positioned at the leading edge using a voltage potential of 11.2 KV. Flow visualization showed that the actuator could reattach the separated flow at the higher angle-of-attack cases, and thus be able to cause an unsteady disturbance by turning the actuator 'on' and 'off'. All of these tests were conducted at a plate spacing of 1 chord length. Limitations in the adhesive of the copper tape and the

robustness of the Kapton tape made it impossible to complete velocity profiles using a hot-wire due to the plasma actuator failing. Because of this, the dielectric material was changed to FR-4 printed circuit board material. Doing this also forced a change in the actuator location. The FR-4 printed circuit board material proved to be a much better dielectric material. The plasma actuators using it could be run intermittently for hours at a time and actuators could last for days of testing.

Tests with the active edge of the plasma actuator at the mid-chord of the plate, with the two plates at -3, -5, and -7 degrees angle of attack, at 1 chord spacing, with a voltage potential of 11.2 KV were very positive. For these tests, the actuator forced the flow upstream in the channel between the plates and downstream on the opposite side of the actuated plate. Flow visualization showed very high levels or turbulence in the wake, implying the ability of the plasma actuator to separate the flow from the low-pressure side of the plate. Based on the flow visualization, the -3^o angle of attack case was chosen for hot-wire measurements. The hot-wire measurements showed velocity fluctuations as large as 27, 16, and 8 percent of the free-stream velocity could be produced at the 1/2, 1, and 5 chord length downstream locations, respectively. Note that the plates used for these test had a 1/4 elliptical leading edge sloping away from the lower electrode. By reducing the spacing to 1/2 chord length, the possible velocity fluctuations were increased to as large as 31, 20, and 22 percent of the free-stream velocity at the respective 1/2, 1, and 5 chord downstream locations.

The combination of adding a third plate, one now on each side of the plate with the plasma actuator, and reducing the voltage potential across the actuator to 6.2 KV but maintaining the -3^o angle of attack and 1/2 chord spacing, caused an approximately 6 percent, of the free-stream velocity, decrease in the magnitude of the velocity fluctuation. Moving the plates closer together to 1/4 chord spacing caused an additional 7 percent decrease in effectiveness to approximately 5 percent of the

free-stream at the 5^{th} downstream chord location.

A non-uniform set of three plates and a uniform set of three plates were tested at zero angle of attack and 3/8 chord spacing. The uniform set of plates proved to give slightly better results, varying between approximately 9.7 to 12 percent, as opposed to 7.8 to 10 percent for the non-uniform plates, of the free-stream velocity at the 5^{th} downstream chord position. This was the location of the greatest affect for the zero angle of attack cases.

Tests with a sandwiched plate design that allowed the plasma actuator to force the flow upstream or downstream on both sides of the plate at a 3/8 chord spacing gave poor results. For the forcing upstream tests, the magnitude of the velocity fluctuation ranged from approximately 4.1 to 15 percent. For the downstream cases, the values ranged from close to zero to 12 percent at the 5^{th} downstream chord position.

In addition to these tests, single plate experiments were done for comparative purposes. Two single plates were tested at zero angle of attack; one had a round leading edge and the other had with a 1/4 elliptic leading edge. The plate with round leading was tested at a 6.3 KV voltage potential and proved to be 6 percent of the free-stream velocity better than the 4 percent velocity fluctuation possible with the plate with the 1/4 elliptic leading edge. This put the single plate with the round leading edge close to the values, in terms of the possible velocity fluctuation, seen with the zero angle of attack 3/8 chord uniform plate cases.

In conclusion, the two plate, -3^o angle of attack, 1/2 chord spacing, 11.2 KV voltage potential case with the 1/4 elliptic leading edges proved to be the most affective in terms of the magnitude fluctuations produced. The second most affective was the zero degree angle of attack, 3/8 chord spacing, 6.3 KV voltage potential case with the three uniform plates with the round leading edge.

The results presented in this thesis have shown the feasibility of the conceptual

design for the moving-wake generator. Results comparable to currently implemented designs have been achieved by two different test setups. Depending on design constraints and levels of turbulence desired, one of the two options could be better than the other, as such, further investigations should be done to pick one over the other.

7.2 Recommendations for Future Work

The work presented in this thesis has built a good foundation towards achieving a useful tool for turbine research. It has also raised some additional questions that could be addressed before making a final choice between the two existing options and finalizing a design. This section will present some of final comments on the two options and the questions they pose.

The -3^o, 1/2 chord spacing case that had the plates with the 1/4 elliptic leading edge has been shown to produce the largest velocity fluctuation. Based on this alone it would appear to be the best choice, but this effect was achieved at the 11.2 KV potential. If a better dielectric materials can be found that can hold up to the stress of these potentials this setup may be the better choice. In addition to the dielectric material needed, the plasma generating system must be able to maintain those power levels for extended periods of time, even for longer electrode lengths. Increasing the size and length of the plasma actuator increases the current required. This in turn increases the power required from the system. If system is not capable of outputting more power, then the maximum achievable voltage potential decreases with the size of the actuator which, for this setup, seems to decrease the magnitude of the achievable velocity fluctuation. During the course of this thesis, advancements in the area of power available by the system have been made but still need to be proven in this application. This could be done by doing what was referred to as power profiles behind this plate setup for voltage potentials over the range of 7 to 14 KV.

The zero angle of attack case has the advantage in that it was shown that increasing the voltage over the 6.3 KV did not improve the response of the flow. If the velocity fluctuations on the order of 12 percent of the free-stream velocity are acceptable, then the 3/8 chord zero angle of attack case with the uniform plates, that had the round leading edge seems to be the best choice. However, one has to keep in mind that because the cascade of turbine blades is going to be at an angle to the moving-wake generator, the 12 percent fluctuation is only going to be for the test blade that is 5 chord lengths from the moving-wake generator. Based on the results, the closer blades would experience turbulence fluctuations of a smaller magnitude. It is unclear at this point what the farther blades would experience, so the effect at farther downstream chords positions should be investigated.

One over shadowing question that remains is which of the plate styles, in terms of the leading edge, is the best. The answer to that question is lacking at least one test case. For the zero angle of attack, 3/8 chord spacing tests the rounded leading edge plates worked the best. The experiments at the -3^o angle of attack were only done with the plates with the 1/4 elliptic leading edge, so an angle of attack comparison, incorporating the different leading edge geometries could not be made. To do this, wake profiles need to be performed behind the plates with the round leading edge, at least for the -3^o angle of attack, 1/2 chord spacing, 11.2 KV test case.

An investigation that could remedy, in the event that it is a problem, the issue of the blades experiencing different levels of turbulence due to the varying distances of the blades from the moving-wake generator, would be to cant the array of the plates. If the array of plates where angled such that the array is parallel to the cascade of the turbine blades, while keeping the plates themselves parallel to the incoming flow, the distances from the plates to the airfoils would be constant. Experiments of this setup could prove to be beneficial, although, by canting the array, the amount of overlap of

the plates decreases. This in turn could reduce the close spacing effects seen in the results. It is worth investigating because canting the array would allow the plates to be positioned much closer to the turbine blades and allow more flexibility.

A potential advantage of the -3^o angled plate case is that the angle the plates make with the flow could actually aid in the propagation of the disturbance across the test section. This is because when the actuators are 'off', the flow is already turning around the plate. Coupled with the contiguous firing of the actuators on the different plates, this could prove to be very beneficial. In order to investigate this, some two-dimensional velocity experiments could be done using PIV or LDV technologies. As with the flat plates, putting these plates in a cascade of their own, parallel to the test cascade, so that they could be placed closer to the leading edge of the turbine blades could again prove to be beneficial, especially in being able to use the plasma actuators to vary the inlet flow angle to the turbine cascade.

Also, an additional investigation of the already obtained data into the area of the turbulence intensity between the plates needs to be done. The approach taken was to place the test plates or airfoils as close together as possible but still have the wakes act independently at 5 chord lengths downstream. As discussed earlier, the stochastic turbulence levels caused by the mixing of the upper stages of the turbine were on the order of 5 percent. It stands to reason then, instead of adding a turbulence grid to create the turbulence, move the plates closer together to have the minimum turbulence level between the wakes closer to 5 percent. The spacing required to do this could again prove to be useful for a final design.

The plate spacings chosen were artificially constrained to have the wakes interact as little as possible. This was done first intended application to minimize the affect of the passive unit while still keeping the discreetness of the moving-wake to a minimum, Doing this was also beneficial in that the closer spacings, which allowed the wakes

to interact, lessened the magnitude of the obtainable velocity difference between the actuator 'off' and 'no' case. A further investigation into the closer plate spacings however has been recommend to couple this work with other experimental and computational work being done at the University of Notre Dame. An advantage of the moving-wake generator over mechanical means is that it can produce purely vortical disturbances. All off the mechanical methods produce both vortical and potential disturbances. For computational work it is important to decouple these disturbances. This is because many computational programs utilize purely vortical disturbances as their input parameter [13]. Developing the moving-wake such that the vortical disturbance can be know and controlled would be greatly beneficial so comparisons between experimental and computational results could be made. This could be done because the same input could be used for the experiment and the computation. Once the computation is proven by the experimental result, it could then be used as a model in turbine machinery design. Some references into the experimental effort in this area by the University of Notre Dame are Fabian[8] and Falk[9, 10]. The computational effort being done at the University of Notre Dame is being done by Atassi[2, 1, 11].

During the course of this thesis additional knowledge has been gained about the role the electrode widths play. A study into the effect of shorting the upper electrode, to enable the chord length of the plate to be reduced could prove to be advantageous, especially if there is an intent to move the plates closer to the test blades of the turbine cascade. Reducing the plate's chord length could allow for shorter times scales for the vortex shedding. Shorter plates may also prove to be beneficial for an investigation of the closer spacings that may maybe needed for gearing the moving-wake generator to validate computational work.

Many suggestions have been made for future work. In terms of getting a workable piece of test equipment for the intended first application, many of them are not

necessary. To find the best design, to have confidence that it is the best, and have it catered specifically for a desired purpose then investigations into the suggested setups and additional data reduction should be done.

Lastly, the moving-wake generator is not meant to replace full rotating test rigs. It is a simulator meant to be used as an easy to implement tool to aid researchers in performing experiments in controllable, but closer to real world, wind tunnel applications.

BIBLIOGRAPHY

[1] Akai, T. J., and Atassi, H. M. "Aerodynamic and Aeroelastic Characteristics of Oscillating Loaded Cascades at Low Mach Number. Part I: Pressure Distribution, Forces and Moments". *Journal of Engineering Power 102* (1980), 344–351.

[2] Atassi, H. M., and Grzedzinski, J. "Unsteady Disturbances of Streaming Motions Around Bodies". *Journal of Fluid Mechanics 209* (1989), 385–403.

[3] Codner, D. I. "An Investigation of Combined Heat Exchanger/Turning Vanes For Wind Tunnels". Master's thesis, Illinois Insitute of Technology, December 1986.

[4] Corke, Thomas C. and He, Chuan and Mehul P. Patel. "Plasma Flaps and Slats: An Application of Weakly-Ionized Plasma Actuators". *AIAA paper* (2004-2127).

[5] Dibelius, G. H., and Ahlers, E. "Infulence of Periodically Unsteady Wake Folw on the Flow Separation in Blade Channels". *Journal of Turbomachinery 114* (January 1992), 108,113.

[6] Doorly, D. J. "Modeling the Flow in a Turbine Rotor Passage". *Journal of Turbomachinery 110* (January 1988), 27,37.

[7] Doorly, D. J., and Oldfield, M. L. G. "Simulation of Wake Passing in a Stationary Turbine Rotor Cascade". *Journal of Propulsion and Power 114* (1985), 316,318.

[8] Fabian, M. K., and Jumper, E. J. "Convected and Potential Unsteady Disturbances Interacting With an Unsteady Cascade". *AIAA paper*, 96-2627 (1996).

[9] Falk, E. A., Jumper, E. J., and Fabian, M. K. "An Experimental Study of Unsteady Forcing in the F109 Turbofan Engine". *AIAA paper*, 97-3286 (1997).

[10] Falk, E. A., Jumper, E. J., Fabian, M. K., and Stermer, J. "Upstream-Propagating Potential Disturbances Interacting with a Compressible Cascade". *Journal of Propulsion and Power* (2000).

[11] Fang, J., and Atassi, H. M. "Compressible Flows with Vortical Disturbances around a Cascade of Loaded Airfoils". In *Unsteady Aerodynamics, Aeroacoustics, and Aeroelasticity of Turbomachines and Propellers*, H. M. Atassi, Ed. Springer-Verlag, New York, NY, 1993, pp. 149–176.

[12] Halstead, D. E., Wisler, D. C., Okiishi, T. H., Walker, G. J., Hodson, H. P., and Shin, H.-W. "Boundary Layer Development in Axial Compressord and Turbines Part 4 of 4: Computations and Analysis". *ASME Paper No.*, 95-GT464 (1995).

[13] Jumper, E. "Internal collaboration at the University of Notre Dame", June 2004.

[14] Loehrke, R., and Nagib, H. M. "Experiments on Management of Free-Stream Turbulence". Tech. Rep. 598, AGARD-R, September 1972.

[15] Murawski, C. G., and Vafai, K. "Effect of Wake Disturbance Frequency on the Secondary Flow Vortex Structure in a Turbine Blade Cascade". *Journal of Fluids Engineering 122* (September 2000), 606,613.

[16] Pfeil, H., Herbst, R., and Schröder, T. "Investigation of the Laminar-Turbulent Transition of Boundary Layers Disturbed by Wakes". *Journal of Engineering Power 105* (January 1983), 130,137.

[17] Post, M. L. "Phased Plasma Actuators for Unsteady Flow Control". Master's thesis, University of Notre Dame, July 2001.

[18] Post, M. L. *"Plasma Actuators for Separation Control on Sationary and Oscillating Wings"*. PhD dissertation, University of Notre Dame, May 2004.

[19] Schobeiri, M. T., and Pappu, K. "Experimental Study on the Effect of Unsteadiness on Boundary Layer Development on a Linaer Turbine Cascade". *Engineering in Fluids 114* (February 1997), 306,316.

REPORT DOCUMENTATION PAGE

Form Approved
OMB No. 0704-0188

1. AGENCY USE ONLY (*Leave blank*)	2. REPORT DATE	3. REPORT TYPE AND DATES COVERED
	January 2007	Final Contractor Report

4. TITLE AND SUBTITLE

Use of Plasma Actuators as a Moving-Wake Generator

5. FUNDING NUMBERS

WBS–561581.02.08.03.21.02
NCC3–935

6. AUTHOR(S)

Thomas C. Corke, Flint O. Thomas, and Michael J. Klapetzky

7. PERFORMING ORGANIZATION NAME(S) AND ADDRESS(ES)

University of Notre Dame
Aerospace and Mechanical Engineering Department
Notre Dame, IN 46556

8. PERFORMING ORGANIZATION REPORT NUMBER

E–15812

9. SPONSORING/MONITORING AGENCY NAME(S) AND ADDRESS(ES)

National Aeronautics and Space Administration
Washington, DC 20546–0001

10. SPONSORING/MONITORING AGENCY REPORT NUMBER

NASA CR—2007-214676

11. SUPPLEMENTARY NOTES

Project manager, Dr. David Ashpis, Propulsion Systems Division, NASA Glenn Research Center, organization code RTT, e-mail: David.E.Ashpis@nasa.gov, 216–433–8317.

12a. DISTRIBUTION/AVAILABILITY STATEMENT

Unclassified - Unlimited
Subject Categories: 02, 07, and 34

Available electronically at http://gltrs.grc.nasa.gov

This publication is available from the NASA Center for AeroSpace Information, 301–621–0390.

12b. DISTRIBUTION CODE

13. ABSTRACT ***(Maximum 200 words)***

The work documented in this report tests the concept of using plasma actuators as a simple and easy way to generate a simulated moving-wake and the disturbances associated with it in turbines. This wake is caused by the blades of the upstream stages of the turbine. Two types of devices, one constructed of arrays of NACA 0018 airfoils, and the one constructed of flat plates were studied. The airfoils or plates were equipped with surface mounted dielectric barrier discharge (DBD) plasma actuators, which were used to generate flow disturbances resembling moving-wakes. CTA hot-wire anemometry and flow visualization using a smoke-wire were used to investigate the wake independence at various spacings and downstream locations. The flat plates were found to produce better results than the airfoils in creating large velocity fluctuations in the free-stream flow. Different dielectric materials, plasma actuator locations, leading edge contours, angles of attack and plate spacings were investigated, some with positive results. The magnitudes of the velocity fluctuations were found to be comparable to existing mechanical moving-wake generators, thus proving the feasibility of using plasma actuators as a moving-wake generator.

14. SUBJECT TERMS

Turbomachinery; Transition; Turbulence; Wakes; Boundary layers; Active flow control; Unsteady flow; Compressors; Turbines; Turbulence grid; Plasma; Dielectric barrier discharge; Glow discharge

15. NUMBER OF PAGES

172

16. PRICE CODE

17. SECURITY CLASSIFICATION OF REPORT	18. SECURITY CLASSIFICATION OF THIS PAGE	19. SECURITY CLASSIFICATION OF ABSTRACT	20. LIMITATION OF ABSTRACT
Unclassified	Unclassified	Unclassified	